CHIMIKA CHRONIKA

NEW SERIES

AN INTERNATIONAL EDITION
OF THE ASSOCIATION OF GREEK CHEMISTS

CMCRCZ 23(4), 179-189 (1994) ISSN 0366-693X

4/94

Volume 23, No 4 p.p. 179-189 October-December 1994

CHIMIKA CHRONIKA

NEW SERIES

AN INTERNATIONAL EDITION

Published by the Association of Greek Chemists (A.G.C.)
27 Kaningos str. Athens 106 82 Greece

Correspondence, submission of papers, subscriptions, renewals and changes of address should be sent to Chimika Chronika-New Series, 27 Kaningos street, Athens 106 82, Greece. The Guide to Authors is published in the first issue of each volume, or sent by request. Subscriptions are taken by volume at 2000 drachms for Corporations in Greece and 50 U.S. dollars to all other countries except Cyprus, where subscriptions are made on request.

Phototypesetted and Printed in Greece by EPTALOFOS S.A.

12, Arditou Str. 116 36 ATHENS Tel. 9217.513

Υπεύθυνος σύμφωνα με το νόμο: Ν. Κατσαρός, Κάνιγγος 27, Αθήνα 106 82.

Responsible under law: N. Katsaros, 27 Kaningos St., Athens 106 82, Greece.

Chimica Chronica, New Series, 23, 79-95 (1994)

SYNTHESES OF 4'-(9-ACRINIDINYLAMINO) METHANESULFONAMIDES AS POTENTIAL ANTITUMOR AGENTS - COMPOUNDS STRUCTURALLY RELATED TO m-AMSA.

GERASIMOS KAVADIAS*

(Received April 20 1988) (Revised March 18 1994)

SUMMARY

A series of 4'-(9-acrinidinylamino)methanesulfonamides were prepared by condensation of the appropriate 9-chloroacridine with 4-aminomethanesulfonanilide under acidic conditions and evaluated for antitumor activity.

Among them, the compounds 31, 39, 40, 42, and 46 showed the highest antitumor activity and were slightly more potent than m-AMSA.

KEY WORDS

4'-(9-acrinidinylamino)methanesulfonamides, 4'-substituted-AMSA, 3,5-disubstituted m-AMSA, substituted 9(1OH) Acridones

INTRODUCTION

Cain and co-workers[1] have prepared and tested a large number of 9-anilinoacridines for antitumor activity. A number of these agents, particularly the 4'-(9-acridinylamino) methanesulfonamide (AMSA) compounds, have shown a broad spectrum of action against a number of animal tumor systems. One member of this series, 4'-(9-acridinylamino) methanesulfon-m-anisidide (m-AMSA) is currently being evaluated clinically in the treatment of several human tumors[2].

**Director National Drug Organization*

Considerable knowledge of the SAR for the antitumor activity of 9-anilinoacridines has been accumulated during the last few years and portions of the molecule were identified where substitutes can be added which increase selectivity and/or antitumor activity[1,3-5]. In view of these findings and the need for more selective, more potent and less toxic agents, we[6] initiated a synthetic program on AMSA variants with substitutes at various positions of the acridine nucleus. In this paper, the synthesis and antitumor activities of several 4'-substituted AMSA and 3,5-disubstituted m-AMSA will be described.

CHEMISTRY

Preparation of the new agents listed in Table 2 followed the general procedure described by Cain et al.,[7,8] viz., by consideration of the appropriate 9-chloroacridine with 4-amino-methanesulfonanilide under acidic conditions.

The required 9-chloroacridines were synthesized from the corresponding 9(1OH) acridones (Table 2) by the sequence of reactions illustrated in Schemes 1 and 2. The starting materials in these syntheses were acids *1a-e* which were prepared according to our previous procedures[9] and were readily converted to their esters *2a-e* in high yields. The esters *2a-d* were subsequently reduced with lithium borohydrate in diglyme to the desired alcohols *3a-d* using conditions similar to those previously employed for the reduction of an analogous product[4]. In a similar manner, the ester *7a* was prepared from the known 5-methyl-9(1OH)acridone-3-carboxylic acid[10] and was reduced to the alcohol *7b*.

Treatment of the 9(1OH)acridone with $SOCl_2$ in the presence of a catalytic amount of DMF produced the 9-chloro-5-chloromethyl compounds *4a-d*. Simple 9(1OH)acridones *3b,c* afforded good yields of the corresponding 9-chloroacridines *4b,c* when refluxed in $SOCl_2$ under known conditions[8]. However, similar treatment of the bromo-analog *3a* and the methyl-analogs *3d* and *7b* gave erroneous results; compound *3a* produced the chloro-analog *4c* instead of *4a* by replacement of the aromatic bromine with a chlorine atom and compounds *3d* and *7b* gave mixtures of products. Conversions of *3a,d* to *4a,d* and of *7b* to the corresponding 9-chloro compounds were accomplished by reaction with $SOCl_2$ in $CHCl_3$ under controlled conditions (see Experimental).

Several attempts were made to selectively replace the benzylic chlorine in *4a-d* by an amino function and produce directly the 9-chloro-acridines *10a-k*. In all cases, however, the reaction of *4a-d* with aliphatic amines was selectively poor and mixtures of products were obtained. It was therefore necessary to convert *4a-d* to *5a-d* prior to reaction with amines. Simple refluxing of *4a-d* in 99% EtOH for a short period of time, selectively replaced the chlorine at C-9 and produced the 9(1OH)acridones *5a-d* which converted to the aminoalkyl analogs *8a-k* by treatment with the appropriate amine. Treatment of the hydrochloride salts of *8a-k* with $SOCl_2$ afforded the required 9-chloroacridines *10a-k*. Compounds *10, l,m* were prepared form *7b* by the same sequence of reactions.

It was also found difficult to convert *4b* directly to *9a-f* by a selective replacement of

the benzylic chlorine in *4b* with an alkoxy group due to the high reactivity of the chlorine atom at C-9. Reaction of *4b* with the appropriate alcohol in the presence of water afforded *6a-e* which on treatment with $SOCl_2$ produced the 9-chloroacridines *9a-d,f.*

9-Chloroacridines (*12a-i*) having a carbaxamido group in the molecule were prepared as shown in scheme 2. Treatment of the carboxylic acids *1a-e* with $SOCl_2$ produced compounds *11* which were then converted to the amides *12* by treatment with the appropriate amine. Alternatively, compounds *12* were prepared from the corresponding 9(1OH)acridones *13* by treatment with $POCl_3$ in nitrobenzene according to a described procedure[8].

The majority of the 9-anilinoacridines listed in Table 2 were prepared by direct coupling of 9-chloroacridines with the requisite aminosulfonanilide in anhydrous solvents. In the early stages of our experimentation, it was established that when EtOH-H_2O was used as the solvent[7] in the coupling reaction, low yields of products were obtained due to extensive hydrolysis of the 9-chloroacridine to acridone. Coupling in anhydrous EtOH (method A) or in anhydrous DMF (method B) provided acceptable yields. Anhydrous DMF was the preferred solvent since the formation of acridones in this solvent was at a minimum and the products which usually crystalized from the reaction mixture were in the pure state. In the preparation of the compounds containing the amide function, an equivalent amount of NaOAc was added in the coupling reaction to prevent hydrolysis of the amide group (method C).

Analogs *21* and *22* were prepared by reaction of *19* with the sodium salt of the corresponding thiol in DMF (method D). Oxidation of *21* and *22* with $NaIO_4$ afforded variants *23* and *24*, respectively (method E). Compound *20* was prepared by reaction with NaN_3 in DMF (method F).

The compounds *31*, *39*, *40*, *42* and *46* showed the highest antitumor activity and were slightly more potent (1.2 - 1.5 times) than m-AMSA.

EXPERIMENTAL

All melting points were determined in an open capillary tube on an Electrothermal melting point apparatus and are uncorrected. The microanalyses were performed by Micro-Tech Laboratories, Skokie, I11. When analyses are indicated only by symbols of elements, analytical results obtained for these elements were within ± 0.4% of the theoretical values. Preparative liquid chromatography was performed on Watters Associates Prep 500 LC system using PrepPak-500/silica column. Compounds were characterized by elemental analysis and by NMR (Varian CFT-20) and IR (Perkin-Elmer 267 grading spectrophotometer) spectra. All spectra and analyses of the elements, except where noted, were in accord with assigned structures. The progress of the reaction and product purity were determined by thin-layer chromatographies (TLC) on precoated silica gel plates (E. Merck F-254).

Ethyl esters of 9(1OH)acridone carboxylic acids (*2a-d* and *7a*)

Compounds *2a-d* and *7a* were prepared from the corresponding acids by a similar method to that described for *2a* below[9,14].

Ethyl 3-bromo-9(1OH)acridone-5-carboxylate (*2a*)

This product was prepared according to a general procedure described in the literature[11] which was modified as follows. To a suspension of 3-bromo-9(1OH)acridone-5-carboxylic acid[9] (20 g, 63 mmol) in acetone (63 mL) was added diisopropylethylamine (8.9 g, 69.3 mmol) and diethyl sulfate (18.8 g, 122 mmol) and the mixture was heated in an oil bath at 90 °C. After refluxing for 30 min, the condenser was removed and heating continued until the solvent had evaporated. The residue was cooled to room temperature and treated with 5% hydrochloric acid. The solids were collected, washed with water and dried to afford *2a* (19.6 g, 90%) which on recrystallization from EtOAc gave an analytical sample of *2a*, mp 214-216 °C: IR ($CHCl_3$) 3680, 3620, 1680, 1640, 1600, 1550 cm^{-1}; NMR ($CDCl_3$) δ 1.48 (t, 3H, CH_3), 4.49 (q, 2H, CH_2), 7.27 (t, 1H, H-7, $J_{6,7} = J_{7,8} = 8$ Hz), 7.37 (dd, 1H, H-2, $J_{1,2} = 9$, $J_{2,4} = 2$ Hz), 7.59 (d, 1H, H-4, $J_{2,4} = 2$ Hz), 8.29 (d, 1H, H-1, $J_{1,2} = 9$ Hz), 8.44 (dd, 1H, H-8, $J_{6,8} = 2$, $J_{7,8} = 8$ Hz), 8.70 (dd, $J_{6,7} = 8$, $J_{6,8} = 2$ Hz), 11.40 (bs, 1H, NH).

Propyl 3-nitro-9(1OH)acridone-5-carboxylate (*2e*)

A suspension of *1e*[9] (10 g, 35.2 mmol) in $SOCl_2$ (200 mL) and DMF catalyst (0.1 mL) was refluxed for 1.5 h while stirring. After removal of the excess $SOCl_2$ *in vacuo*, dry benzene was added and the mixture again evaporated to yield *11e* as a yellow solid. This product and dry 1-propanol (150 mL) was heated under reflux with stirring for 10 min, then water (0.65 mL, 36 mmol) was added and refluxing continued for 1 h. After cooling to room temperature, the solids were collected, washed with ether (35 mL) and dried. Recrystallization from DMF afforded 9.76 g (85%) of 2e, mp 223-224 °C.

Propyl 3-amino-9(1OH)acridone-5-carboxylate (*2f*)

This product was prepared according to the general procedure described by Atwell *et al*[12] as follows. To a suspension of *2e* (4.9 g, 15 mmol) in 70% EtOH-H_2O mixture (100 mL) was added under mechanical stirring iron powder (2.25 g), 0.3 mL of a solution of $FeCl_3$ (32.4 g) in water (100 mL) and glacial AcOH (0.9 mL) and the mixture was heated under reflex. The reaction was monitored by tcl (silica, 2% MeOH-CH_2Cl_2) and was completed after 1 h. The reaction mixture was concentrated under reduced pressure and the residue was extracted with hot (100 °C) DMF (75 mL). The mixture was filtered through a Celite pad, the cake washed with hot DMF (30 mL) and the washing was combined with the filtrate. The solution was concentrated *in vacuo* to a volume of about 50 mL, $CHCl_3$ (300 mL) was added and the resulting solution was washed with 5% $NaHCO_3$ solution (100 mL). After drying (Na_2SO4), the solvent was removed *in vacuo* to give 4 g (90%) of *2f* as a solid. Recrystallization from DMF (100 mL) -ether (30 mL) mixture gave the analytical sample, mp 223-225 °C.

Propyl 3-acetamido-9(1OH)acridone-5-carboxylate (2g)

To a suspension of *2f* (1g, 3.38 mmol) in CH_2Cl_2 (15 mL) and pyridine (15 mL) was added Ac_2O) (2 mL) and the mixture heated under reflux until all solids had dissolved (2 min). The resulting solution was stirred at 25°C for 20 h and then evaporated *in vacuo*. The solid residue was collected, washed successively with H_2O, EtOH (10 mL) and ether (10 mL) and dried. Recrystallization from DMF (5 mL) gave 1 g (88%) of *2g*, mp 289-290 °C.

Hydroxymethyl-9(1OH)acridones (*3a-d* and *7b*)

Compounds *3a-d* and *7b* were prepared from the corresponding esters by a similar method to that described below for *3a*.

3-Bromo-5-hydroxymethyl-9(1OH)acridone (*3a*)

A suspension of sodium borohydrate (2.59 g, 68.5 mmol) and lithium bromide (5.14 g, 59.2 mmol) in dry diglyme[4] (10 mL, dried over CaH_2) was blanketed with nitrogen and stirred at room temperature for 1 h, then *2a* (5 g, 14.4 mmol) was added. After stirring at room temperature for 24 h, the reaction mixture was poured into cold 5% hydrochloric acid. The solids were collected, washed with water and dried. This product was purified by preparative liquid chromatography using ethyl acetate-methylene chloride mixture (1:2) as eluent to provide 3.04 g (69.5%) of *3a* which showed a single spot on tlc (ethyl acetate-CH_2Cl_2, 1:2) of Rf 0.59. An analytical sample was obtained by recrystallization from dimethylformamide-ether mixture, mp 248-250 °C: NMR (DMSO-d_6) δ 4.89 (s 2H, CH_2), 7.28 (t, 1H, H-7, $J_{6,7} = J_{7,8} = 7$ Hz), 7.42 (dd, 1H, H-2, $J_{1,2} = 8$, $J_{2,4} = 2$ Hz), 7.8 (dd, 1H, H-6, $J_{6,7} = 7$, $J_{6,8} = 2$ Hz), 8.13 - 8.25 (m, 3H, H-1, H-4, H-8).

By the same procedure, *3d* and *7b* were prepared. Compounds *3b* and *3c* were prepared as in *3a* except that reduction was carried out at 25 °C for 18 h and at 90 °C for 1 h. Compound *3b* was purified by recrystallization from DMF-EtOH (1:1) mixture.

Chloromethyl-9(1OH)acridones (*5a-d* and *7c*)

Compounds *5a-d* and *7c* were prepared from the corresponding hydroxymethyl compounds by a similar method to that described for *5a* below.

3-Bromo-5-chloromethyl-9(1OH)acridone (*5a*)

To a suspension of *3a* (0.304 g, 1 mmol) in dry chloroform (10 mL) was added dry DMF (1 drop) and thionyl chloride (2 mL) and the mixture was heated under reflux with stirring until all solids had dissolved (5 min) and then for 20 min further. Removal of the solvent *in vacuo* gave 4a as a yellow solid. This product was suspended in 98% ethanol (20 mL) and the mixture was refluxed for 20 min. The reaction mixture was concentrated under reduced pressure on one half of the volume and the solids were collected by filtration to give 0.2 g (66%) of 5a, mp > 360 °C. This product showed on tlc (silica, CH_2Cl_2) a single spot of Rf 0.36.

When *3a* was refluxed in neat thionyl chloride, the bromine was replaced with chlorine affording 3-chloro-4-chloromethyl-9(1OH)acridone.

By the same procedure, *5d* and *7c* were prepared. Compounds *5b* and *5c* were prepared by the above process except that neat thionyl chloride (10 mL/g) was used in the chlorination step.

4-Alkoxy-9(1OH)acridones (*6a-e*)

Compounds *6a-e* were prepared from *3b* by a similar method to that described for *6b* below.

4-propoxymethyl-9(1OH)acridone (*6b*)

To a stirred suspension of *3b*, (2.0 g, 8.9 mmol) in $SOCl_2$ (30 mL) was added DMF catalyst (2 drops) and the mixture was refluxed for 1 h. After removal of excess $SOCl_2$ *in vacuo*, dry benzene was added and the mixture evaporated to give *4b*, as a yellow solid. This product was dissolved in 1-propanol-H_2O mixture (98:2, 60 mL) and the solution was heated in an oil bath at 120 °C. The reaction was monitored by TLC (silica, 2% MeOH-CH_2Cl_2). After 2 h, the reaction mixture was evaporated. The residue was dissolved in CH_2Cl_2 and the solution washed with 8% $NaHCO_3$, dried (Na_2SO_4) and filtered. Removal of the solvent under reduced pressure gave a solid residue which was chromatographed on a silica gel column using 1% MeOH-CH_2Cl_2 mixture as eluent to provide 2 g (84%) of *6b*. Recrystallization from EtOH gave the analytical sample, mp 162-164 °C: IR (Nujol) 3300, 1630, 1606, 1580, 1540 cm^{-1}; NMR ($CDCl_3$) δ 1.0 (m, 3H, CH_3), 1.73 (m, 2H, CH_2), 3.53 (t, 2H, OCH_2), 4.93 (s, 2H, CH_2O), 7.0-8.53 (m, 7H, ArH), 9.6 (s, 1H, NH).

4-(2-Dimethylaminoethoxymethyl)-9(1OH) acridone (*6f*)

To a solution of dimethylamine (1.9 g, 42 mmol) in dry dimethylformamide (10 mL) at 0°C was added *6e* (0.85 g, 2.55 mmol) and the resultant solution was stirred at 25 °C for 18 h. The solvent was removed by evaporation at reduced pressure (0.1 mm), xylene was added and the mixture evaporated to remove traces of dimethylformamide. The solid residue was partitioned between methylene chloride and 10% sodium bicarbonate, the organic phase separated, washed with water, dried and evaporated to give 0.8 g of solid material. This product showed on tlc (silica, 5% MeOH-CH_2Cl_2) a major spot of Rf 0.14 (*6f*) and some impurities (Rf 0.6, 0.48 and zero). The product was purified by chromatography on a wet column of silica (20 cm x 1.8 cm I.D) using 5% methanol in methylene chloride as eluent to provide 0.54 g (71.5%) of crystalline *6f*. The analytical sample was obtained by recrystallization from methylene chloride-ether solvent mixture, mp 128-130 °C: NMR ($CDCl_3$) δ 2.27 (s, 6H, $N(CH_3)_2$), 2.57 (m, 2H, $-CH_2N$), 3.63 (m, 2H, OCH_2), 4.73 (s, 2H, CH_2O), 7.0-8.55 (m, 7H, ArH), 10.2 (broad s, 1H, NH).

Alkylaminomethyl-9(1OH)acridones (*8a-m*)

Compounds *8a-m* were prepared by reaction of chloromethyl-9(1OH)acridones with the appropriate amine by a similar method to that described for *8g* below.

3-Chloro-5-propylaminomethyl-9(1OH)acridone (*8g*)

A solution of 3-chloro-5-chloromethyl-9(1OH)acridone (*5c*) (1.0 g, 3.59 mmol) and 1-

propylamine (1.77 g, 30 mmol) in dry DMF (10 mL) was stirred at 25°C for 24 h. The solvent was removed *in vacuo* and the residue was partitioned between CH_2Cl_2 and 5% NaOH solution. The organic phase was separated, was chromatographed on a silica gel column using 1% MeOH-$CHCl_3$ mixture as eluent to provide 0.95 g (88%) of title product as a solid. This product showed on tlc (silica, 5% MeOH-CH_2Cl_2) a single spot of Rf 0.35. Recrystallization from ethanol afforded the analytical sample, mp 159-169 °C.

Compounds *8l* and *8m* were purified by recrystallization of their hydrochloride salts. Unlike the other analogous amines in this series which form monohydrochlorides (e.q. *8b*), compounds *8l* and *8m* form dihydrochloride monohydrates. These salts gradually lose HCl on storage and therefore elemental analyses were not in accord with theoretical values.

9-Chloroacridines (*9a-d, f, 10a-m* and *12a-i*)

9-Chloro-4-propoxymethylacridine (*9b*)

To a suspension of *6b* (1.6 g, 6 mmol) in $SOCl_2$ (30 mL) was added DMF catalyst (2 drops) and the heterogenous mixture was heated under reflux until a clear solution resulted and then for 0.5 h longer. After removal of excess $SOCl_2$ *in vacuo*, dry benzene was added and the mixture was evaporated to remove traces of thionyl chloride. Compound *9b* thus obtained was a yellow solid and was used in the next reaction without delay.

By the same procedure compounds *9a,c,d* were prepared.

3-Bromo-9-chloro-5-methylaminomethylacridine hydrochloride (*10h*)

Acridone *8h* (3 mmol) was suspended in EtOH (20 mL) and the mixture was treated with hydrogen chloride. After removal of the solvent *in vacuo*, the hydrochloride salt of *8h* was suspended in $CHCl_3$ (30 mL), $SOCl_2$ (6 mL) and DMF (1 drop) were added and the mixture heated under reflux until evolution of gases had ceased (30 min). The reaction mixture was evaporated *in vacuo* to provide *10h* as a solid.

By the same procedure, *10f,g* and *10i-m* were prepared and used in the next reaction without delay. Compounds *9f* and *10a-e* were prepared by essentially the same procedure except that the reaction was carried out in neat $SOCl_2$.

9-Chloro-5-methylaminocarbonyl-3-nitroacridine (*12a*)

A suspension of *1e* (2 g, 7.05 mmol) in $SOCl_2$ (40 mL) and DMF catalyst (2 drops) was refluxed until a clear solution resulted (45 min) and then for 0.5 h further. Removal of $SOCl_2$ *in vacuo* gave *11e* as a yellow solid. This product was suspended in CH_2Cl_2 (45 mL) and the mixture cooled at 0 °C with stirring. To this mixture was added a solution of CH_3NH_2 (0.55 g, 18 mmol) in dioxane (14 mL) and the reaction mixture was stirred at 0 °C for 15 min and at 25 °C for 45 min. The solids were collected, washed with water and dried over P_2O_5 to give 1.65 (75%) of *12a* which on tlc (silica, 5% MeOH-CH_2Cl_2) showed a single spot of Rf 0.5. An analytical sample was obtained by recrystallization from DMF, mp 263 -264 °C: NMR (DMSO-d_6) δ 2.92 (d, 3H, CH_3, J = 5 Hz), 5.16 (s, 1H, H-2, $J_{1,2}$ = 9, $J_{2,4}$ = 2 Hz), 7.40 (t, 1H, H-7, $J_{6,7} = J_{7,8}$ = 8 Hz), 7.96 (dd, 1H, H-2, $J_{1,2}$ = 9, $J_{2,4}$ = 2 Hz), 8.22 (dd, 1H, H-6, $J_{6,8}$ = 2, $J_{6,7}$ = 8 Hz), 8.42 (m, 2H, H-1 and H-8), 8.77 (d, 1H, H-4, $J_{2,4}$ = 2 Hz), 11.21

(bs, 1H, NH) Anal. calcd for $C_{15}H_{10}N_3ClO_3$: C, 57.06; H, 3.19; N, 13.31; Cl, 11.23. found: C 56.93; H, 3.16;

By the same procedure, *12b-d* were prepared and were used without further purification. Compounds *12f,g* were prepared by the same procedure as in *12a* except that refluxing of 1a in $SOCl_2$ was limited to 15 min. Prolonged heating in $SOCl_2$ (1 h or more) resulted in replacement or bromine with chlorine. Compound *12e* was prepared from *11e* by treatment with EtOH (3 mol equivalent) in CH_2Cl_2 in presence of pyridine at 25 °C.

3-Acetamido-9-chloro-5-methylaminocarbonylacridine (*12 h*)

To a suspension of *13a* (0.9 g, 2.91 mmol) in nitrobenzene (10 mL) was added POCl3[8] (1.8 mL) and the mixture heated at 90 °C for 1 h. After removal of the solvent by evaporation *in vacuo* the residue was suspended into a mixture of ice and concentrated NH_4OH and stirred for 0.5 h. The orange colored solids were collected, washed with water and dried over P_2O_5 to give 0.9 g (95%) of *12 h.*

By the same procedure *12i* was prepared and used without delay.

3-Acetamido-5-methylaminocarbonyl-9(1OH)acridone (*13a*)

Into a solution of *2g* (1.5 g, 4.43 mmol) in $CHCl_3$-EtOH mixture (100 mL, 1:1) was bubbled CH_3NH_2 (gas) for 20 min. The resulting solution was left at 24 °C for 48 h and then evaporated. The solid residue was collected, washed with H_2O and dried. Recrystallization from DMF (30 mL) gave 1 g (73%) of *13a* mp > 360 °C.

5-Propylaminocarbonyl-3-nitro-9(1OH)acridone (*13b*)

A solution of *12b* (1.21 g, 3.52 mmol) in 99% EtOH (20 mL) was heated under reflux for 1 h. Removal of the solvent *in vacuo* and recrystallization of the solid residue from EtOH gave 0.93 g (81.5%) of *13b*, mp 233 -235 °C.

3-Acetamido-5-propylaminocarbonyl-9(1OH)acridone (*13c*)

Compound *13b* was reduced with powder Fe using the procedure described above in the preparation of *2f*. The resulting amine was treated with Ac_2O in pyridine using the process given in *2g* to provide an 80% yield of *13c*, mp 328-330 °C.

9-Anilinoacridines

Method A: Appropriate 9-chloroacridine (3 mmol) and 4-aminomethane-sulfonanilide hydrochloride[8] (3.3 mmol) were dissolved in absolute EtOH (10-15 mL), and the solution was heated under reflux for 45 min. In most cases product crystallized from the reaction mixture. In the cases where the product did not crystallize, the reaction mixture was evaporated and the residue was converted to the free base which was purified by column chromatography on silica gel using 2-5% MeOH-$CHCl_3$ mixtures as eluent. The free base was then dissolved in the appropriate solvent and converted to the hydrochloride salt by treatment with hydrogen chloride.

Method B: 9-Chloroacridine (3 mmol) and 4-amino-3-methoxysulfonaniline hydrochloride[3] (3.3 mmol) in dry DMF (10-15 mL) was heated in an oil bath at 85 °C for 45 min. In many cases product crystallized from the reaction mixture in the pure state. When purification was required, this was affected as in method A.

Method C: Essentially the same conditions were used as in method B with the following modification. The reaction mixture was heated for a short period (1-3 min) to initiate the reaction (appearance of red colour) and then an equivalent amount of anhydrous NaOAc was added to prevent hydrolysis of amide functions.

Method D: A solution of sodium mercaptide (3.6 mmol) in MeOH (5 mL) was added to a solution of 19 (3.6 mmol) in DMF. After stirring at 0 °C for 45 min. the reaction mixture was poured into 5% $NaHCO_3$ (100 mL) and the solids were collected and dried. The product was purified by column chromatography on silica gel using 3% MeOH-CH_2Cl_2 as eluent.

Method E: Alkylthio compounds were oxidized to sulfoxides by a literature procedure[12] as follows. A solution of $NaIO_4$ (0.28 g, 1.3 mmol) in H_2O (0.5 mL) was added slowly over a period of 3 min to a stirred solution of the thioether (0.65 mmol) in DMF (6 mL) at 23 °C. After stirring at room temperature for 4 h, the reaction mixture was poured into cold 5% $NaHCO_3$ solution (40 mL) and the mixture was extracted with CH_2Cl_2 (3x40 mL). The combined extracts were washed with water, dried and the solvent was removed *in vacuo*. The residue was chromatographed on silica gel using 3% MeOH-CH_2Cl_2 as eluent.

Method F: A mixture *19* (2.15 g, 5.23 mmol) and NaN_3 (2.15 g, 33 mmol) in DMF (40 mL) was stirred at 25 °C for 60 h. The reaction mixture was poured into cold H_2O and dried (150 mL) and the solids were collected, washed with H_2O and dried. The product was chromatographed on silica gel column using successively 2%, 5% and 10% MeOH-CH_2Cl_2 mixtures to provide 0.85 g (39%) of *20*. Recrystallization from CH_2Cl_2-ether mixture afforded the analytical sample, mp 182-184°C.

Method G: To a suspension of *8i* hydrochloride (1.15 g, 4 mmol) in $CHCl_3$ (40 mL) was added $SOCl_2$ (8 mL) and DMF (0.32 mL, 4.12 mmol) and the mixture was heated under reflux for 45 min. after removal of the solvent *in vacuo*, the residue was dissolved in dry DMF, 4-amino-3-methoxysulfonanilide hydrochloride (1.06 g, 4.02 mmol) was added and the mixture was heated at 85 °C for 1 h. After cooling to room temperature, the reaction solution was diluted with 1% $NaHCO_3$ (200 mL) and the mixture extracted with CH_2Cl_2 (3x80 mL). The organic extracts were combined, dried (Na_2SO_4) and evaporated *in vacuo*. The residue was chromatographed on a silica gel column using $CHCl_3$-EtOAc-MeOH (1:1:0.1) mixture as eluent to provide 0.9 g (41%) of *39* as an amorphous solid.

Method H: 3-Acetamido compound (1.0 g) was dissolved in AcOH-H_2O (2:1) mixture, concentrated hydrochloric acid (4 mL) was added and the mixture was heated under reflux until the removal of the N-acetyl group was complete. The reaction was monitored by tlc (silica, 20% MeOH-CH_2Cl_2), and was completed after 30 min. After cooling to room

temperature, the solids were collected and dried to provide the hydrochloride salt of the amine.

Method I: A solution of the nitro compound *42* (1.3 g, 2.63 mmol) in DMF and 10% Pd/C catalyst (0.2 g) was shaken under hydrogen in a Paar apparatus at room temperature and an initial pressure of 55 psi for 30 min. The catalyst was removed by filtration through a pad of Celite. The filtrate was concentrated under reduced pressure and the solid residue was recrystallized form DMF (2 mL)-EtOH (30 mL) mixture to provide 0.9 g (74%) of *50*, mp 240 °C (dec.).

ΠΕΡΙΛΗΨΗ

Στο άρθρο αυτό περιγράφεται η παρασκευή μιας σειράς 4′–(9–ακριδινυλαμινο)–μεθανοσουλφοναμιδίων με συμπύκνωση κατάλληλου 9–χλωροακριδόνης με 4–αμινομεθανοσουλφοναμίδιο υπό όξινες συνθήκες και στη συνέχεια εκτιμήθηκε στα εργαστήρια της Bristol η αντικαρκινική τους δράση.

Μεταξύ των παρασκευασθέντων ενώσεων, οι ενώσεις με αριθμό 31, 39, 40, 42 και 46 έδειξαν την υψηλότερη αντικαρκινική δραστικότητα και ήταν ελαφρώς δραστικότερες από το m–AMSA.

REFERENCES

1. W. A. Denny, B. F. Cain, G. J. Atwell, C. Hansch, A. Panthananickal and A. Leo, J. Med. Chem. *25*, 276 (1982) and references therein.
2. Drugs of the Future, *5*, 277 (1980).
3. B. F. Cain, G. J. Atwell and W. A. Denny, J. Med. Chem. *18*, 1110 (1975).
4. B. F. Cain, G. J. Atwell, J. Med. Chem. *19*, 1124 (1976).
5. B. F. Cain, G. J. Atwell, Eur. J. Cancer *10*, 539 (1974).
6. Bristol Laboratories Candiac Que., Canada.
7. G. J. Atwell, B. F. Cain and R. N. Seelye, J. Med. Chem. *15*, 611 (1972).
8. B. F. Cain, R. N. Seelye and G. J. Atwell, J. Med. Chem. *17*, 922 (1974).
9. Unpublished results.
10. B. F. Cain, G. J. Atwell, B. C. Baguley and W. A. Denny, South African Patent Application 80/5652, Sept. *12* (1980).
11. F. H. Stodola, J. Org. Chem. J. Med. *29*, 2490 (1964).
12. G. J. Atwell and B. F. Cain, J. Med. Chem. *11*, 295 (1968).
13. R. G. Hiskey and M. A. Harpold, J. Org. Chem. *32*, 3191 (1967).
14. N. S. Drosdov and A. F. Bekhli, J. Gen. Chem. (USSR) *8*, 1505 (1938); CA *33*, 4596.

Figure 1

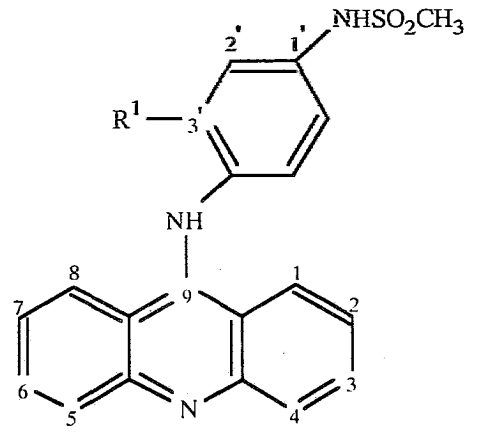

AMSA, $R^1 = H$
m-AMSA, $R^1 = OCH_3$

Scheme 1

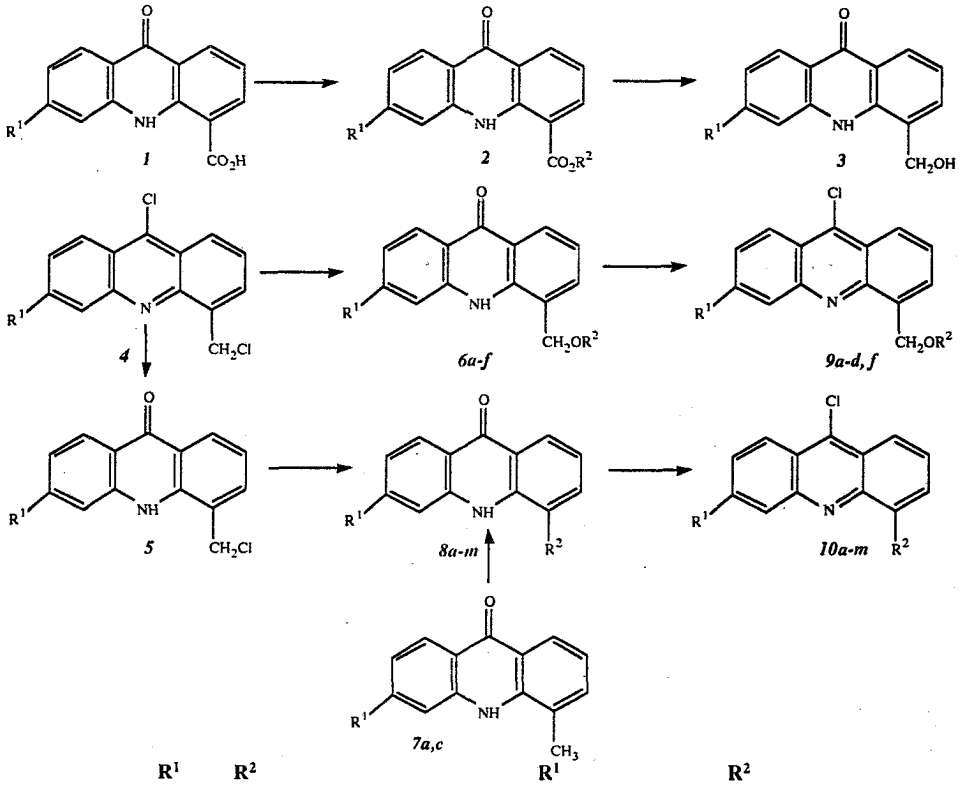

		R^1	R^2
1	a	Br	
	b	H	
	c	Cl	
	d	CH_3	
	e	NO_2	
2	a	Br	Et
	b	H	Et
	c	Cl	Et
	d	CH_3	Et
	e	NO_2	$(CH_2)_2CH_3$
	f	NH_2	
	g	NHAc	
3-5	a	Br	
	b	H	
	c	Cl	
	d	CH_3	

		R^1	R^2
7	a	CO_2Et	
	b	CH_2OH	
	c	CH_2Cl	
8,10	a	H	CH_2NHCH_3
	b	H	CH_2NMe_2
	c	H	$CH_2NH(CH_2)_2CH_3$
	d	H	$CH_2NH(CH_2)_2CH_3$
	e	H	$CH_2NH(CH_2)_2OCH_3$
	f	Cl	CH_2NHCH_3
	g	Cl	$CH_2NH(CH_2)_2CH_3$
	h	Br	CH_2NHCH_3
	i	CH_3	CH_2NHCH_3
	j	CH_3	$CH_2NHC_2H_5$
	k	CH_3	$CH_2NH(CH_2)_2CH_3$
	l	CH_2NHCH_3	CH_3
	m	$CH_2NH(CH_2)_2CH_3$	CH_3
6, 9	a	H	C_2H_5
	b	H	$(CH_2)_2CH_3$
	c	H	$(CH_2)_3CH_3$
	d	H	$CH_2CH_2OCH_3$
	e	H	CH_2CH_2Br
	f	H	$CH_2CH_2NMe_2$

Scheme 2

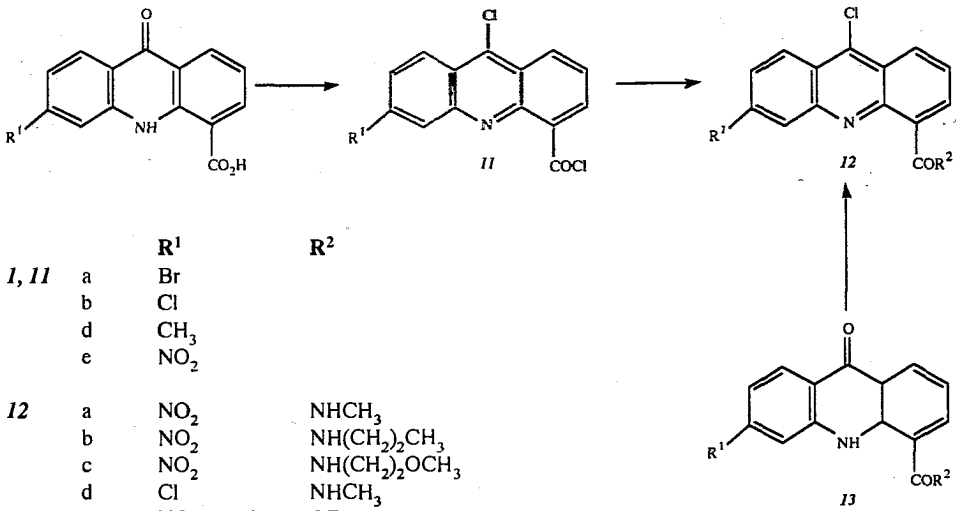

		R^1	R^2
1, 11	a	Br	
	b	Cl	
	d	CH_3	
	e	NO_2	
12	a	NO_2	$NHCH_3$
	b	NO_2	$NH(CH_2)_2CH_3$
	c	NO_2	$NH(CH_2)_2OCH_3$
	d	Cl	$NHCH_3$
	e	NO_2	OEt
	f	Br	$NH(CH_2)_2OCH_3$
	g	Br	$NHCH_3$
	h	NHAc	$NHCH_3$
	i	NHAc	$NH(CH_2)_2CH_3$
13	a	NHAc	$NHCH_3$
	b	NO_2	$NH(CH_2)_2CH_3$
	c	NHAc	$NH(CH_2)_2CH_3$

TABLE 1

PHYSICAL AND ANALYTICAL DATA FOR SUBSTITUTED 9(1OH) ACRIDONES

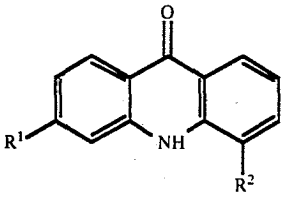

Cpd No.	R^1	R^2	Yield %	mp, C°	recrystallization solvent
2a	Br	CO_2Et	90	214-216	EtOAc
2b	H	CO_2Et	86	155-156[a]	EtOH-H_2O (5:1)
2c	Cl	CO_2Et	90	197-199	EtOAc
2d	CH_3	CO_2Et	95.4	158-159	EtOH
2e	NO_2	$CO_2(CH_2)_2CH_3$	85	223-224	DMF
2f	NH_2	$CO_2(CH_2)_2CH_3$	90	223-225	DMF-ether (1:1.5)
2g	NHAc	$CO_2(CH_2)_2CH_3$	88	289-290	DMF
3a	Br	CH_2OH	69.4	248-250	DMF-ether
3b	H	CH_2OH	60.5	283-285	DMF-EtOH (1:1)
3c	Cl	CH_2OH	79	276-278	DMF-ether
3d	CH_3	CH_2OH	93	236-238	MeOH-CH_2Cl_2 (1:1)
5a	Br	CH_2Cl	66	>360	EtOH
5b	H	CH_2Cl	87	>360	EtOH
5c	Cl	CH_2Cl	82	>360	EtOH
5d	CH_3	CH_2Cl	63.5	>360	EtOH
6a	H	$CH_2OC_2H_5$	75	178-179	EtOH
6b	H	$CH_2O(CH_2)_2CH_3$	84	162-164	EtOH
6c	H	$CH_2O(CH_2)_2CH_3$	75	138-140	EtOH
6d	H	$CH_2O(CH_2)_2CH_3$	56	132-133	EtOH-ether
6e	H	$CH_2OCH_2CH_2Br$	30	148-150	EtOH-ether
6f	H	$CH_2OCH_2CH_2NM$	71.5	128-130	CH_2Cl_2-ether

TABLE 1 (continued)

PHYSICAL AND ANALYTICAL DATA FOR SUBSTITUTED 9(1OH) ACRIDONES

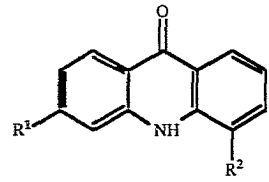

Cpd No.	R^1	R^2	Yield %	mp, C°	recrystallization solvent
7a	CO_2Et	CH_3	83	256-258	EtOH
7b	CH_2OH	CH_3	87	275-277	EtOH
7c	$ClCH_2$	CH_3	83	272-274	1-propanol
8a	H	CH_2NHCH_3	65	161-163	EtOH
8b	H	CH_2NMe_2	67	268-270[b]	EtOH-ether
8c	H	$CH_2NH(CH_2)_2CH_3$	64	syrup	
8d	H	$CH_2NH(CH_2)_2CH_3$	60	126-128	CH_2Cl_2-hexane
8e	H	$CH_2NH(CH_2)_2CH_3$	77.5	124-126	MeOH-CH_2Cl_2 (1:1)
8f	Cl	CH_2NHCH_3	74	193-195	EtOH
8g	Cl	$CH_2NH(CH_2)_2CH_3$	88	159-160	EtOH
8h	H	CH_2NHCH_3	75	205-207	EtOH
8i	CH_3	CH_2NHCH_3	69	154-157	$CHCl_3$-ether
8j	CH_3	$CH_2NHC_2H_5$	90	109-111	EtOH
8k	CH_3	$CH_2NH(CH_2)_2CH_3$	80	108-109	ether
8l	CH_2NHCH_3	CH_3	88	258-262[c]	EtOH
8m	$CH_2NH(CH_2)_2CH_3$	CH_3	87	275-280[d]	EtOH
13a	AcNH	$CONHCH_3$	73	>360	DMF
13b	NO_2	$CONH(CH_2)_2CH_3$	81.5	233-235	EtOH
13c	AcNH	$CONH(CH_2)_2CH_3$	80	328-330	EtOH

Footnotes:

[a]Literature[4] mp 162-163°C

[b]Hydrochloride salt

[c]Decomp., decomposition started at 170°C

[d]Decomp., decomposition started at 230°C

Elemental Analysis for every compound were found to be within ± 0,3 % the calculated values

TABLE 2

PHYSICAL AND ANALYTICAL DATA FOR SUBSTITUTED 9(10H) ACRIDONES

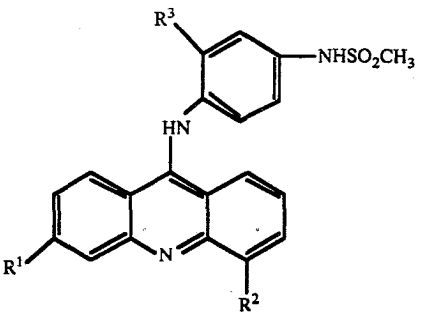

No.	R^1	R^2	R^3	Yield %	mp, C°	recrystallization solvent	Method
14	H	$CH_3OC_2H_5$	H	45	a		A
15	H	$CH_2O(CH_2)_2CH_3$	H	62	229-230[b]	EtOH-ether	A
16	H	$CH_2O(CH_2)_3CH_3$	H	55	230-233[b]	EtOH	A
17	H	$CH_2OCH_2CH_2OCH_3$	H	69	138-141	EtOH	A
18	H	$CH_2OCH_2CH_2NMe_2$	H	64	192-193	EtOH	A
19[c]	H	CH_2Cl	H	88	>360	acetone-ether	B
20[d]	H	CH_2N_3	H	40	182-184	CH_2Cl_2-ether	F
21	H	CH_2SCH_3	H	52	234-237	CH_2Cl_2-ether	D
22	H	$CH_2S(CH_2)_2CH_3$	H	54	182-184	CH_2Cl_2-hexane	D
23[e]	H	CH_2SOH_3	H	76	224-229	CH_2Cl_2-ether	E
24	H	$CH_2SO(CH_2)_2CH_3$	H	52	198-200	CH_2Cl_2-ether	E
25	Br	CH_2Cl	OCH_3	77	238-240[b]	DMF-ether	B
26	H	CH_2NHCH_3	H	55	283-285[b]	EtOH	A
27	H	$CH_2N(CH_3)_2$	H	41	280-282[b]	EtOH	A
28	H	$CH_2NH(CH_2)_2CH_3$	H	50	280[b]	EtOH	A
29	H	$CH_2NH(CH_2)_2OCH_3$	H	47	273-275[b]	EtOH	A
30	H	$CH_2NH(CH_2)_2CH_3$	OCH_3	45	254-258	CH_2Cl_2-ether	A
31	Cl	CH_2NHCH_3	OCH_3	46	225[b]	DMF	B
32	Cl	$CH_2NH(CH_2)_2CH_3$	OCH_3	54	245-247[b]	DMF	B
33	Br	CH_2NHCH_3	OCH_3	57	a		B
34	CH_3	CH_2NHCH_3	OCH_3	30	>360[f]	EtOH	B

TABLE 2 (continued)

PHYSICAL AND ANALYTICAL DATA FOR SUBSTITUTED 9(1OH) ACRIDONES

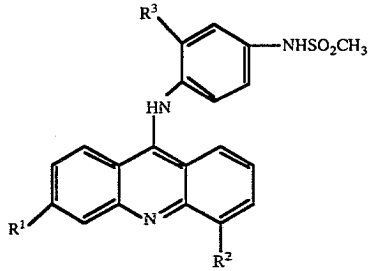

No.	R^1	R^2	R^3	Yield %	mp, C°	recrystn solvent	Method
35	CH_3	$CH_2NHC_2H_5$	OCH_3	42	>360[g]	DMF	B
36	CH_3	$CH_2NH(CH_2)_2CH_3$	OCH_3	44	268-270	DMF	B
37[h]	CH_3NHCH_2	CH_3	OCH_3	24	260-265[b]	DMF	B
38	$CH_3(CH_2)_2NHCH_2$	CH_3	OCH_3	52	250[i]	DMF	B
39	CH_3	$CH_2NCHOCH_3$	OCH_3		a		G
40[j]	Br	$CONHCH_3$	OCH_3	60	279-284[b]	DMF	B
41	Br	$CONHCH_2CH_2OCH_3$	OCH_3	25	228-231	$CHCl_3$-EtOH	C
42	NO_2	$CONHCH_3$	OCH_3	60	265-267	DMF	C
43	NO_2	$CONH(CH_2)_2OCH_3$	OCH_3	76	243-245	DMF	C
44	NO_2	$CONH(CH_2)_2OCH_3$	OCH_3	70	194-196	DMF	C
45k	NHAc	$CONHCH_3$	OCH_3	74	282-285	DMF	C
46	NH_2	$CONHCH_3$	OCH_3		325[l]	EtOH	C
47	NHAc	$CONH(CH_2)_2CH_3$	OCH_3	67	303-305	EtOH	C
48	NH_2	$CONH(CH_2)_2CH_3$	OCH_3	70	274-276	DMF-ether	H
49	NH_2	$CONH(CH_2)_2OCH_3$	OCH_3	30	268-270	EtOH	H
50	HONH	$CONHCH_3$	OCH_3	74	240[b]	EtOH	I
51	Cl	$CONHCH_3$	OCH_3	81	285-287	DMF	B
52	NO_2	$CO_2C_2H_5$	OCH_3	56	225-228	EtOH	C

Footnotes:

[a]Amorphous solid. [b]Decomposes. [c]N: calcd, 10.21: found, 9.66. [d]N: calcd, 19.25; found, 18.82. [e]C: calcd, 60.12; found, 59.17 [f] Decomp., decomposition started at 280 °C. [g]Decomp., decomposition started at 250 °C. [h]C: calcd, 53.23; found, 53.83. [i] Decomp., decomposition started at 210 °C. [j]N: calcd, 9.90; found, 10.25. [k]H: calcd, 15.28; found, 4.76. [l]Decomp., decomposition started at 290 °C. Elemental Analysis for every compound (except h, j. k) were found to be within ± 0,3 % the calculated values

Chimica Chronica, New Series, 23, 97-101 (1994)

CYANO-DERIVATIVES OF 2-PIPERAZINONES[1] VIA STRECKER REACTION

MINAS P. GEORGIADIS

Chemical Laboratory Agricultural University of Athens, Iera Odos 75, Athens, Greece 11855.

(Received Augoust 30 1993)

SUMMARY : Strecker type reaction of *N*-Acetonyl glycinate results in cyclization yielding 2-piperazinone derivatives.

KEY WORDS : Piperazinone derivatives, novel ring closure, 4-benzyl-2-methyl-6-oxo-2-piperazine carbonitrile, 4-benzyl-6-hydroxy-6-methyl-2-piperazinone.

INTRODUCTION

The preparation of α-amino nitriles can be achieved via the Strecker synthesis[2,3]. This reaction has not been applied heretoforth on *N*-acetonyl-*N*-benzylglycinates which contain a keto and an ester functionality in the same molecule. We have recognized that the latter type of compounds when subjected to Strecker conditions would provide a facile method for preparing a broad range of piperazinone derivatives. The more reactive keto group would react first yielding an intermediate which would, upon subsequent intramolecular cyclization, yield the desired piperazinone derivatives. The applicability of our idea is exemplified here.

Treatment of *N*-acetonyl-*N*-benzylglycine ester 1 with potassium cyanide and ammonium carbonate in methanol yielded 4-benzyl-2-methyl-6-oxo-2-piperazinone carbonitrile 2. When gaseous ammonia was passed through a methanolic solution of 1 however, 4-benzyl-6-hydroxy-6-methyl-2-piperazinone 3 was formed. We have assumed that in the described reaction , the carbonyl group of the keto ester 1 was first converted to an amino nitrile or to an amino alcohol (intermediate 2a or 3a) which subsequently yielded 2 or 3, respectively, as shown in Scheme I.

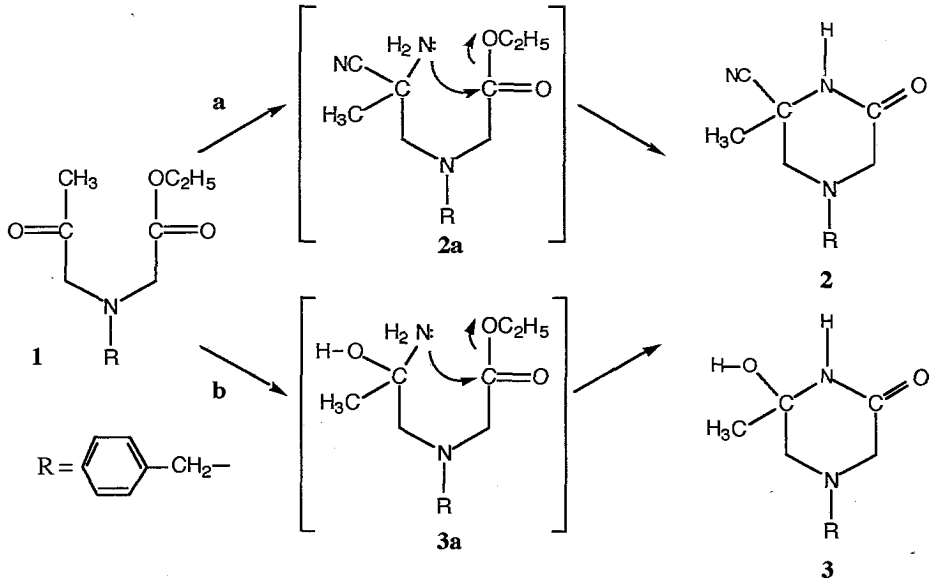

Scheme I a: KCN, $(NH_4)_2CO$, H_2O, EtOH b: NH_3, MeOH

A variety of alkyl or aralkyl substituents may be introduced to the piperazinone ring by the proper choice of an analogous starting material[4]. In addition, the benzyl group may be easily removed by hydrogenolysis[5]. Thus, the described procedure may be useful for preparing a variety of piperazinone derivatives for biological screening or synthons for further syntheses[6]. The preparation of diketopiperazines with similar ring system may be found in the literature[7].

EXPERIMENTAL

Melting points were determined on a Thomas-Hoover apparatus and are uncorrected. Infrared spectra were recorded on a Perkin-Elmer Model 225 spectrophotometer. ^1H NMR spectra were recorded on a Varian A-60A spectrometer and the chemical shifts (δ) in ppm are reported relative to internal tetramethylsilane. Elemental analyses were done with a Perkin-Elmer Model 240 C,H,N analyzer.

N-Acetonyl-*N*-benzylglycine ethyl ester 1.

A solution of *N*-benzylglycine ethyl ester (43g, 0.25 mol), sodium bicarbonate (21 g, 0.25 mol), and chloroacetone (0.25 mol) in tetrahydrofuran (200 ml, containing 2-3% water) was heated at 55-60° C under stirring for 6 hours. The solution was allowed to stand at room temperature for 2 hours and it was then filtered. Sodium hydroxide (2.5 g, 0.25 mol)

was dissolved in 100 ml of water and it was slowly added to the filtrate. The solution was cooled in an ice-bath and benzylchloride (8.75 g, 0.625 mol) was slowly added, under vigorous stirtring. The reaction mixture was subsequently stirred for 20 min. at 5-6° C and an additional 20 min. at room temperature. The reaction mixture was then carefully acidified with dilute hydrochloric acid. The unreacted benzylating agent was removed with ethyl ether (3 x 200 ml). Sodium hydroxide (10%) was subsequently added to the aqueous layer until basic pH, and the product was extracted with ethyl ether. The ethereal layer was washed with water, was dried ($MgSO_4$), and evaporated to dryness yielding a brownish residue which upon distillation under reduced pressure, yielded 42.4 g (68%) of 1, b.p. 151-152°C (2mm/Hg). In a second run the yield was increased to 75%. Spectral data were consistent with the proposed structure. I.R.($CHCl_3$): ν_{max} (cm^{-1}) 1718 (carbonyl), 1594, 1576, 1486, 693 (arom.); ^1H NMR ($CDCl_3$): δ 7.36 (m, 5H, phenyl), 4.17 (q, 2H, *J*=7 Hz, -C*H*$_2$OCO-), 3.86 (s, 2H, -NC*H*$_2$COO), 3.52 (s, 2H, -NC*H*$_2$CO-), 3.46 (s, 2H, Ph-C*H*$_2$-N), 2.12 (s, 3H, C*H*$_3$CO-), 1.25 (t, 3H, *J*= 7 Hz, -CH$_2$C*H*$_3$).

4-Benzyl-2-methyl-6-oxo-piperazinecarbonitrile 2

A mixture of *N*-acetonyl-*N*-benzylglycine ethyl ester (22.44 g, 0.09 mol), ammonium carbonate (41.9 g, about 0.35 mol) and potassium cyanate (16.5 g , about 0.25 mol), in ethanol/water (1:1, 100 ml) were stirred and heated at 55-60° C for about 10 hours (overnight). Heating was stopped and water was slowly added over a 2h period, under vigorous stirring until the total volume was gradually increased to one liter. After 10 hours of additional stirring at room temperature the reaction mixture was cooled and filtered, yielding 12.51 g (60.6%) of 2 which was recrystallized from ethanol/water (2:8) or ethanol/hexane yielding white crystals m.p. 147-148° C. I.R.($CHCl_3$): ν_{max} (cm^{-1}) 3380, 3190 (NH), 2230 (weak, CN), 1670 (carbonyl),1590, 1575, 1485 (weak arom.), 690 (strong, arom.); ^1H NMR ($CDCl_3$): δ 8.25 (s, lH, N*H*), 7.34 (m, 5H, phenyl), 3.66 (s 2H, -NC*H*$_2$-Ph), 3.50 (d, 1H, *J*= 17.0 Hz, -NC*H*CO-), 2.92 (d, 1H, *J*=17.0 Hz, NC*H*CO-), 3.13 (d, 1H, *J*=12.0 Hz, NC*H*-), 2.32 (d, 1H, *J*=12.0 Hz, NC*H*C-), 1.54 (s, 3H, -C*H*$_3$). Anal. Calcd. for $C_{13}H_{15}NO_3$: C, 68.10; H, 6.59; N, 18 33. Found: C, 67.92; H, 6.69; N, 18.45.

4-Benzyl-6-hydroxy-6-methyl-2-piperazinone 3

To a solution of 25 g *N*-acetonyl-*N*-benzylglycine ethyl ester (0.1 mol) in a small amount of methanol, placed in a round bottom flask equipped with a dry ice condenser, gaseous ammonia was bubbled for three hours. Then bubbling was stopped and the condensed ammonia was allowed to evaporate at room temperature overnight. The methanol was evaporated under reduced pressure leaving a residue which upon crystallization from

methanol-hexane yielded 19.8 g (90%) of **3** as white crystalline material m.p. 140-141° C. Spectral and analytical data supported the proposed structure. I.R.($CHCl_3$): ν_{max} (cm^{-1}) 3660, 3500 (OH), 3380, 3210 (NH), 1665 (carbonyl), 690 (arom.); ^1H NMR ($CDCl_3$): δ 7.30 (m, 6H, phenyl and N*H*), 4.10 (s, 1H, -OH), 3.62 (s, 2H, Ph-CH_2N), 3.43 (d, 1H, *J*=17.0 Hz, -COC*H*N-), 2.85 (d, 1H, *J*=17.0 Hz, -COC*H*N), 2.82 (d, 1H, *J*=11.5 Hz, -C*H*N), 2.38 (d, 1H, *J*=11.5 Hz, -C*H*N), 1.38 (s, 3H, -CH_3). Anal. Calcd. for $C_{12}H_{16}N_2O_2$: C, 65.43; H, 7.32; N, 12.72. Found: C, 65.42; H, 7.35; N, 12.72.

ΠΕΡΙΛΗΨΙΣ

ΠΑΡΑΣΚΕΥΗ ΚΥΑΝΟ-ΠΑΡΑΓΩΓΩΝ ΤΩΝ 2-ΠΙΠΕΡΑΖΙΝΟΝΩΝ ΜΕΣΩ ΤΗΣ ΑΝΤΙΔΡΑΣΕΩΣ STRECKER.

Κατεργασία του αιθυλεστέρος της N-ακετονυλο-N-βενζυλογλυκίνης **1** με κυανισύχον κάλιον και ανθρακικόν αμμώνιον εις μεθανόλην έδωσεν το 2-καρβονιτρίλιον της 4-βενζυλο-2-μεθυλο-6-οξο-πιπεραζίνης **2**. Η διαβίβασις αερίου αμμωνίας εις μεθανολικόν διάλυμα της ενώσεως **1** οδήγησεν ως ανεμένετο εις κυκλοποίησιν και σχηματισμόν της 4-βενζυλο-6-υδροξυ-6-μεθυλο-2-πιπεραζινόνης **3**. Προτείνεται μηχανισμός της κυκλοποιήσεως κατά τον οποίον η κετονομάς του κετο-εστέρος **1** μετατρέπεται αρχικώς εις αμινονιτρίλιον ή αμινοαλκοόλην (ενδιάμεσα **2α** και **3α**, αντιστοίχως), τα οποία εν συνεχεία δίδουν τας ενώσεις **2** και **3**, αντιστοίχως (βλ. σχήμα Ι). Δεδομένου ότι η βενζυλο-ομάς απομακρύνεται ευκόλως με υδρογονόλυσιν, η περιγραφείσα μέθοδος δύναται και γενικώτερον να χρησιμεύσει διά την παρασκευήν παραγώγων πιπεραζινονών διά βιολογικάς δοκιμάς ή ενδιαμέσων διά περαιτέρω συνθέσεις.

REFERENCES

1. a) Alternatively named as 6-oxo-2-piperazine carbonitriles b) This work preliminary performed long ago at Ayest Laboratories in Mondreal Canada and repeated and improved by the author at the Agricultural University of Athens.
2. a) R.M. Williams *"Synthesis of Optically Active a-Amino Acids" Organic Chemistry Series*, J.E. Baldwin, P.D. Magnus Ed.; *Pergamon Press, Oxford 1989, pp. 208-299.* b) A.J. Fadiadi *"Preparation and Synthetic Applications of Cyano Compounds, in the*

was allowed to evaporate at room temperature overnight. The methanol was evaporated under reduced pressure leaving a residue which upon crystallization from methanol-hexane yielded 19.8 g (90%) of 3 as white crystalline material m.p. 140-141° C. Spectral and analytical data supported the proposed structure. I.R.($CHCl_3$): ν_{max} (cm^{-1}) 3660, 3500 (OH), 3380, 3210 (NH), 1665 (carbonyl), 690 (arom.); ^1H NMR ($CDCl_3$): δ 7.30 (m, 6H, phenyl and N*H*), 4.10 (s, -OH), 3.62 (s, 2H, phenyl-C*H*$_2$N), 3.43 (d, *J*=17 Hz, 1H, -COC*H*N), 2.85 (d, *J*=17 Hz, 1H, -COC*H*N), 2.82 (d, *J*=11.5 Hz, -C*H*N), 2.38 (d,*J*=11.5 Hz, 1H, -C*H*N), 1.38 (s, 3H, -C*H*$_3$). Anal. Calcd. for $C_{12}H_{16}N_2O_2$: C, 65.43; H, 7.32; N, 12.72. Found: C, 65.42; H, 7.35; N, 12.72.

REFERENCES

1. a) Alternatively named as 6-oxo-2-piperazine carbonitriles b) This work preliminary performed long ago at Ayest Laboratories in Mondreal Canada and repeated and improved by the author at the Agricultural University of Athens.
2. a) R.M. Williams *"Synthesis of Optically Active a-Amino Acids" Organic Chemistry Series*, J.E. Baldwin, P.D. Magnus Ed.; *Pergamon Press, Oxford 1989, pp. 208-299.* b) A.J. Fadiadi *"Preparation and Synthetic Applications of Cyano Compounds, in the Chemistry of Functional Groups Suppl. C"* S. Patai, Z. Rappaport ed., *J. Wiley & Sons Ltd; N.York, 1983 pp. 1067-1303.*
3. For related papers on Strecker Reaction published recently see:
   a) M.S. Dapper, R. Pellicciari, B. Natalini, J.B. Monahan, C.Chiorri, A.A. Cordi *J. Med. Chem 34 161(1991)* b) N. Dekimpe, P. Sulmon, C. Stevens *Tetrahedron 47, 4723(1991)*
   c) T. Inaba, M. Fujita, K. Ogura *J. Org. Chem. 56, 1274 (1991)* ; d) T.K. Chakraborty, G.V. Reddy, K.Azhar-Hussain *Tetrahedron Lett., 32 7597 (1991).*
4. F. Zymalkowski and P. Messinger , *Arch.Pharm. 300, 91 (1967).*
5. Fr. E. Ziegler and Gr. B. Bennet *Tetrahedron Lett, 2545-2547 (1970).*
6. L. T. Webster, *The Pharmacological Basis of Therapeutics, Chapt. 44, pp 1017-19.* A. Goodman Gilman, L. S. Googman, T. W.: Rall, and F. Murid, Eds., *Seventh Edition. McMillan Publ. Co., New York, 1985.* See also *Annual Reports in Med. Chem. Vols. 8 (1973), 9 (1374), 12 (1977), 13 (1978), 15 (1980) 16 (1981) for Antiparasitic compounds.*
7. a) B.W. Bycroft, G.R. Lee, *J.C.S. Chem. Comm. p. 988, (1975)* ; b) J.Haesler and M. Schimdt *Chem. Ber. 107, 28044-2815 (1974)*; c) J.W. ApSimon, R.P. Sequin *Tetrahedron 35, 2797,(1979)*.

Chimica Chronica, New Series, 23, 103-113 (1994)

POTASSIUM EXCHANGE IN SOILS

M.DOULA[1] , A.IOANNOU[2*], A.DIMIRKOU[1]

1. National Agricultural Research Foundation of Greece, Institute of Soil Science, 1 S. Venizelou St. Lycovrissi, 14123, Attiki, Greece.
2. University of Athens, Department of Chemistry, Panepistimiopolis-Zografou, 15771 Attiki, Greece.

(Received May 14, 1993)

SUMMARY

In this review are reported the theories derived from experimental procedures in order to describe the potassium adsorption-desorption by soils and soil components.
Potassium is an essential element for plant and animals and this is the reason why the knowledge of adsorption-desorption processes is of great importance, in order to prevent the potassium pollution caused by the use of fertilizers.

Keywords: potassium exchange , soils.

INTRODUCTION

The potassium content of the lithosphere is 2,6% whereas the average content of soils is estimated to be 0,83%. Potassium is an essential element for animals and one of the three major fertilizer nutrients required by plants, adsorbed by clays and organic materials as it presented in geochemical cycles of the element.(Fig.1). [1]

The clay minerals are hydrous aluminium silicates (Al,Si,O and OH) of small size with a layered structure made up of sheets of either tetrahedral [SiO_4] units or octahedral [AlO_6] units. (Fig.2)[1] .

The simplest of the clay structures is shown by Kaolinite [$Al_4Si_4O_{10}(OH)_8$] with one octahedral sheet and one tetrahedral sheet forming a 1:1 clay mineral.

*Postal address of the corresponding author: A.Ioannou , 14 Thermopillon st , 15344, Pallini Attiki, Greece.

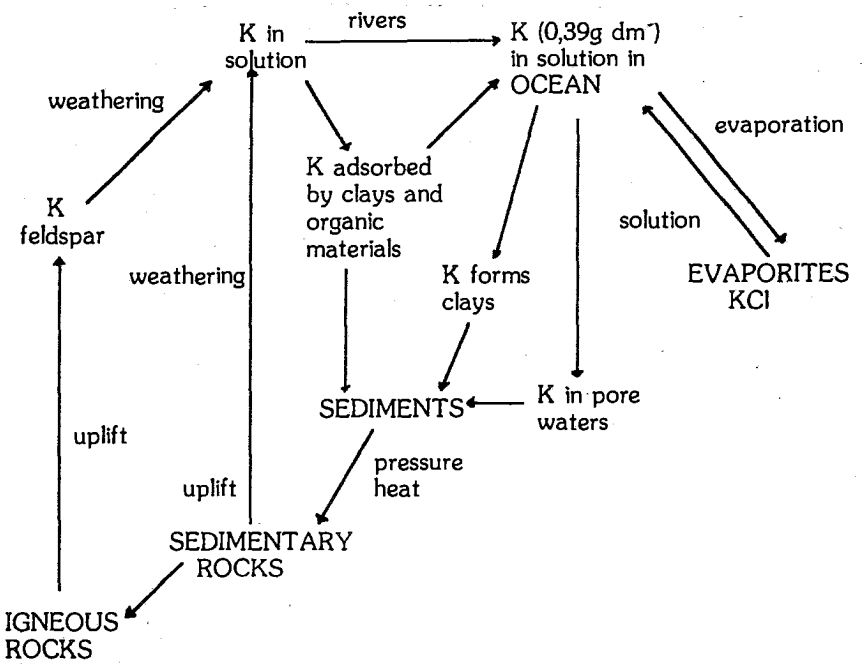

FIG. 1: Geochemical cycle of potassium.

The 1:1 layers are stocked above each other and held together by hydrogen bonds between the oxygen in one layer and the hydroxyl groups in the next layer.

The hydrogen bonds prevent other groups (K^+,H_2O) from entering between the individual layers and keep the structure relatively rigid.

Kaolinite shows only a limited amount of isomorphous replacement of the Al, and Si.

Members of the other major group of clay minerals, the smectites, each consist of one octahedral sheet sandwiched between two tetrahedral sheets.

Montmorillonite $[Al_4(Si_4O_{10})_2(OH)_4]$ and illite $[K_{0-2}Al_4(Si_{8-6}Al_{0-2})O_{20}(OH)_4]$ are the most common of the 2:1 clays. In each case the oxygens of one 2:1 layer always face the oxygens of the next layer,therefore no hydrogen bond can take place.The layers are not so strongly held together and ions such as K^+ in illite and small molecules such as water in montmorillonite can enter between the layers.

Montmorillonite-containing clays are described as expanding clays because when water enters between the layers the repeat distance can increase from 0,96nm to 2,14 nm .The entry of potassium between the layers to form illite is only reversed with difficulty.The potassium ions tend to hold the layers together,at a fixed distance apart and make the entry of water difficult.Kaolinite and illite are described as non-expanding clays.

Organic materials exchange cations mainly due to the presence of the carboxylate group - COO^-.

Kaolinite has a relatively low C.E.C. (cation exchange capacity) which is due to the exchange of H^+ ions from the hydroxyl-groups on the clay surface.The hydroxyl groups of montmorillonite react similarly,but the greater degree of isomorphous substitution and the consequent excess negative charges lead to a higher C.E.C.

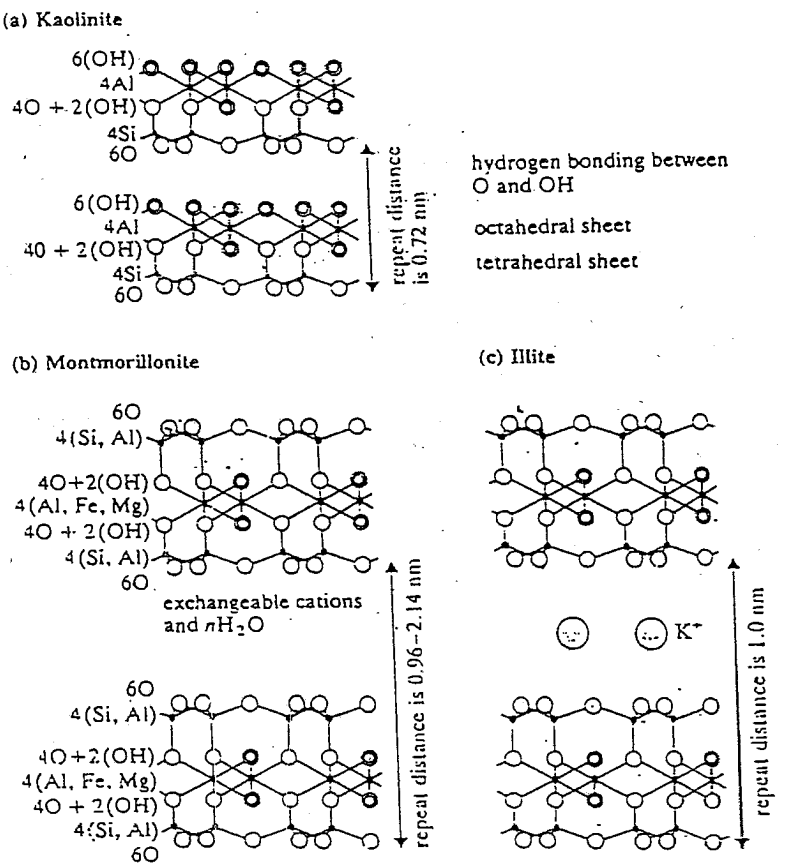

FIG. 2: Representations of the structures of a) Kaolinite b) montmorillonite and c) illite.

Kinetic and thermodynamic of potassium exchange in soils

The kinetic and thermodynamic of potassium exchange was investigated in Ca-satured and Al - satured soil samples , by adding KCl and measured the amount of potassium excisted at the solution after specific period of time.

Many researchers concur that soil K exists in soil solution exchangeable, non exchangeable and mineral phases.The soil solution and exchangeable phases are regarded as readily available forms of K^+ [2] , and also named assimilable.

The non exchangeable K is generally considered as a slowly available from occurring in "illitic" clay and other 2:1 types minerals [2-4] and the mineral phases of K is relatively unavailable.Kinetic reactions exist between the various phases of K.

Sparks et al [5] found that K adsorption and desorption in soils conformed to first order kinetics.

a. Estimation of adsorption rate coefficient (k_{ad})

By considering the following simplified process for potassium adsorption and desorption, we can express the kinetic for the element,[6]

$$K_{adsorption} \underset{k_{des}}{\overset{k_{ad}}{\rightleftharpoons}} K_{desorption}$$

$$\text{Rate} = \frac{-d\,C_{ad}}{dt} = k_{ad}\,C_{adsorbed} - k_{des}\,C_{desorbed} \Rightarrow$$

$$\frac{-d\,C_{ad}}{dt} = k_{ad}\,(C^o - C_t) - k_{des}\,C_t \Rightarrow \frac{-d\,C_{ad}}{dt} = k_{ad}\,C^o - k_{ad}\,Ct - k_{des}\,Ct \quad (1)$$

where C_{ad} is the amount of adsorbed K at time t, C_{des} is the amount of K desorbed at time t, k_{ad} is the rate coefficient for the adsorption process, k_{des} is the rate coefficient for the desorption process ,C_t is the amount of K at the solution at time t and C^o the initial potassium concentration.

At the equilibrium stage :

$$R = \frac{dC_{ad}}{dt} = 0 \Rightarrow k_{ad}C^o - k_{ad}C_\infty - k_{des}C_\infty = 0 \Rightarrow k_{des} = \frac{k_{ad}(C^o - C_\infty)}{C_\infty} \quad (2)$$

By replacing k_{des} coefficient on the kinetic equation (1) results :

$$R = \frac{-dC_{ad}}{dt} = k_{ad}(C^o - C_t) - \frac{k_{ad}(C^o - C_\infty)}{C_\infty} C_t \Rightarrow$$

$$\frac{-d(C^o - C_t)}{dt} = k_{ad}C^o - k_{ad}C_t - \frac{k_{ad}C_tC^o}{C_\infty} - k_{ad}C_t \xrightarrow{\frac{dC^o}{dt}=0}$$

$$\frac{-dC_t}{dt} = k_{ad}C^o - \frac{k_{ad}C_tC^o}{C_\infty} \Rightarrow \frac{-dC_t}{dt} = k_{ad}C^o(1 - \frac{C_t}{C_\infty}) \Rightarrow$$

$$\frac{-d\frac{C_t}{C_\infty}}{dt} = \frac{k_{ad}C^o}{C_\infty}(1 - \frac{C_t}{C_\infty}) \Rightarrow \frac{d(1 - \frac{C_t}{C_\infty})}{dt} = k'_{ad}(1 - \frac{C_t}{C_\infty})$$

where $k'_{ad} = \frac{k_{ad}C^o}{C_\infty}$

and $C\infty$ is the amount of K on the soil at equilibrium.

$$\int_o^{Ct} \frac{1}{1 - Ct/C_\infty} d(1 - Ct/C_\infty) = \int_o^t K'_{ad}dt \Leftrightarrow \ln(1 - \frac{Ct}{C\infty}) = -K'_{ad}dt \quad (3)$$

The plot of ln(1-Ct/C∞) as function of time t is a straight line with slope K'ad (Fig.3).

b. Estimation of desorption rate coefficient (k_{des}) for the solid surface phase.

$$dCt = -k_{des}(Ct)dt$$

where Ct is the amount of K on the exchange sites of the soil at time t.
The plot of the quantity of adsorbed potassium vs time is presented at the following figure 4.

$$\frac{d\,Ct/Co}{Ct\,/\,Co} = -k_{des}dt \Leftrightarrow \int_{Co}^{\phi} \frac{d\,(Ct/Co)}{Ct/Co} = -\int_o^t k_{des}dt \Leftrightarrow \ln\frac{Ct}{Co} = k_{des}dt \Leftrightarrow \ln\frac{Ct}{Co} = k_{des}dt$$

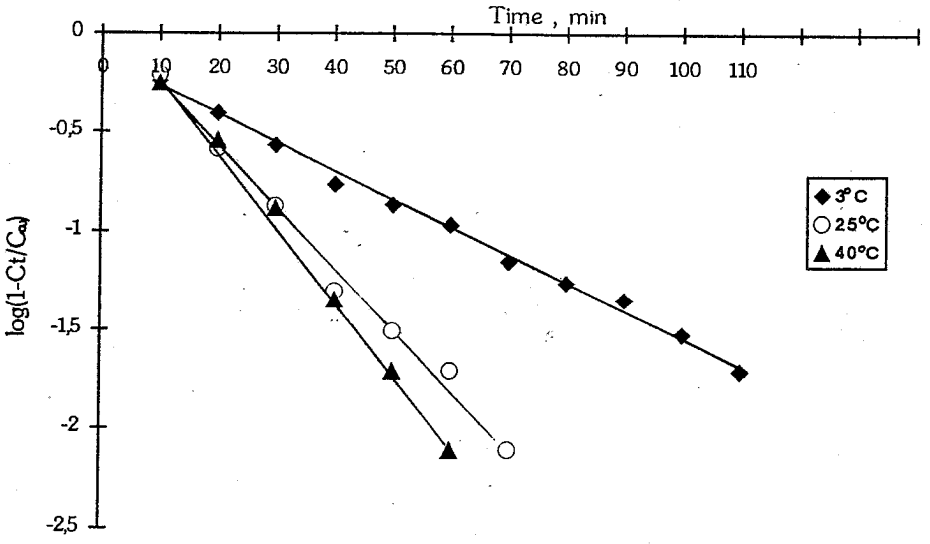

FIG. 3: Log(1-Ct/C∞) vs. time at 3,25 and 40°C. [6]

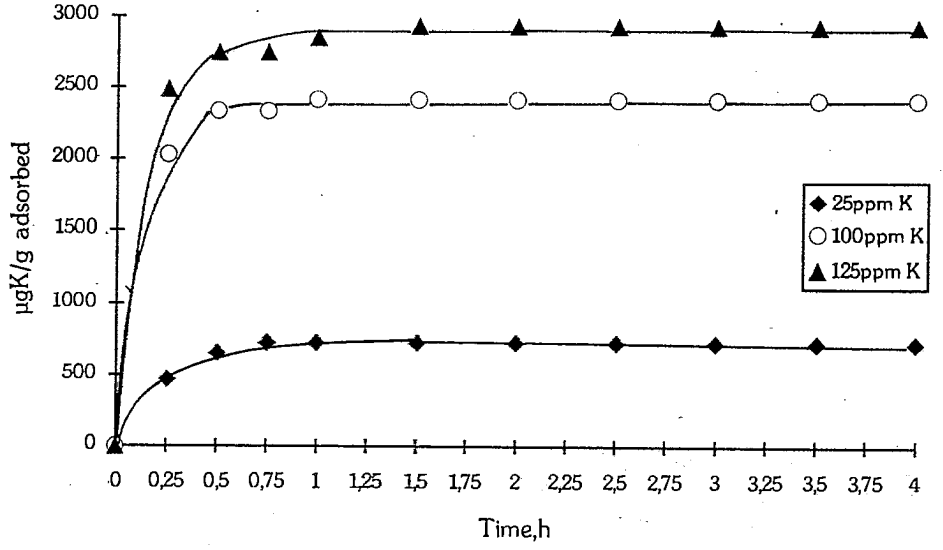

FIG. 4: Plot of adsorbed potassium as function of time. [17]

where, Co is the amount of K on the exchange sites of the soil at zero time,
The plot of ln(Ct/Co) as function of time t is a straight line with slope k_d.
By considering the K^+ exchange as the following process,we can estimate the apparent equilibrium constant K,

$$K_{adsorption} \underset{k_{des}}{\overset{k_{ad}}{\rightleftharpoons}} K_{desorption}$$

From the mass action law (7),

$$K = \frac{kad}{kdes}$$

The plot of the quantity of desorbed potassium vs time is presented at the following figure 5.(10)

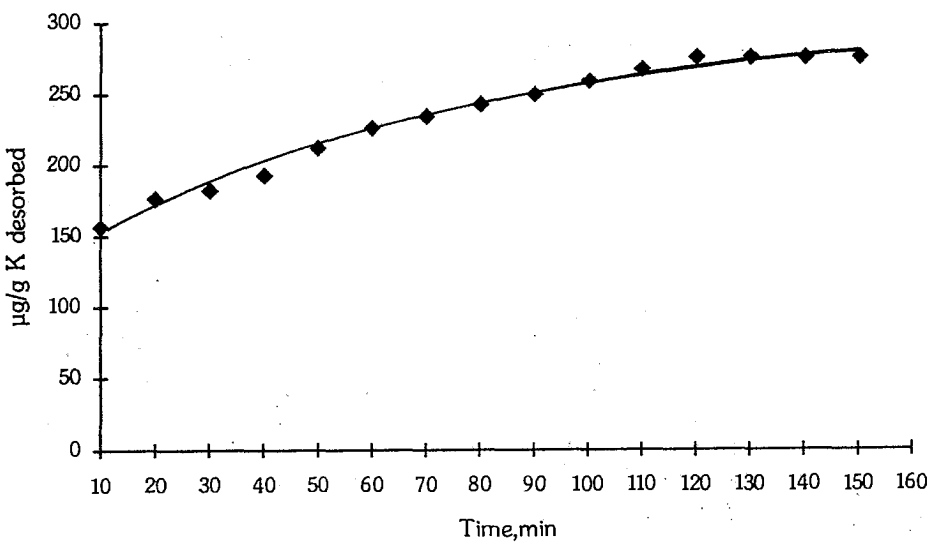

FIG. 5: Plot of desorbed potassium as function of time.

The adsorption rate coefficient k_{ad} can also calculated from a modification of the Freundlich equation (5,8)

$$k_{ad} = \frac{x}{Co\,t^{1/m}} \Leftrightarrow \log\frac{x}{Co} = \log k_{ad} + \frac{1}{m}\log t$$

where k_{ad} the adsorption rate coefficient in h^{-1}, x the amount of K adsorbed in μg/g, Co the initial K concentration in ppm and t reaction time in hours and 1/m constant .The parameter 1/m and k_{ad} calculated from the slope and intercept of the linear portion of the plots respectively.

We can also estimate from the equilibrium constant the free energy for potassium adsorption and desorption

$$\Delta G^{o} = -RT\ln K \Rightarrow \Delta G^{o} = -RT\ln\frac{k_{ad}}{k_{des}}$$

Energies of activation for potassium adsorption (E_{ad}) and desorption (E_{des}) estimated by Arrhenius and Van't Hoff equations [7] ,

$$\frac{d\ln k_{ad}}{dT} = \frac{Ead}{RT^2} \quad \text{and} \quad \frac{d\ln k_{des}}{dT} = \frac{Edes}{RT^2}$$

The enthalpy for potassium exchange (ΔH^{o}) can be determined from Van't Hoff's equation,

$$\frac{d\ln K}{dT} = \frac{\Delta H^{o}}{RT^2} \quad \text{or} \quad Ead - Edes = \Delta H^{o}$$

From the third law of thermodynamics, the entropy for potassium exchange (ΔS^{o}) can be estimated,

$$\Delta S^{o} = \frac{(\Delta H^{o} - \Delta G^{o})}{T}$$

The first-order kinetic equations [9]

$$\ln\frac{Ct}{Co} = -k_{ad}dt \quad \text{and} \quad \ln\frac{Ct'}{Co'} = -k_{des}t$$

where Ct, Ct' the amount of K on soil exchange sites at time t of adsorption and desorption respectively, Co' the amount of K on exchange sites at zero time of desorption, Co the initial concentration of K at zero time of adsorption. (10) can also express the potassium exchange when the adsorption of the element is assumed to be negligible.

The log(Ct/Co) v.s (t) relationship is linear and k_{des} and k_{ad} calculated by line's slope.(Fig.6). Instead of the above data other researchers (Selim et al,1976) proposed that the adsorption reaction (k_{ad}) is the nth order although the desorption reaction (k_{des}) is first order.

The k_{ad} and k_{des} values increased with increasing temperature (11) although the amount of potassium desorbed by soil decreased.

The k_{des} values are lower than the k_{ad} values,and this result indicates that desorption rate is slower than the adsorption rate.This is due to the partial collapse of the vermiculitic clay minerals upon K adsorption.

The energies of activation for desorption (Ed) (7,12) are greater than those for adsorption (Ea). So that is needed greater amount of energy for potassium desorption than for adsorption and this is probably due to the partial collapse of the vermiculitic clay minerals upon K adsorption.

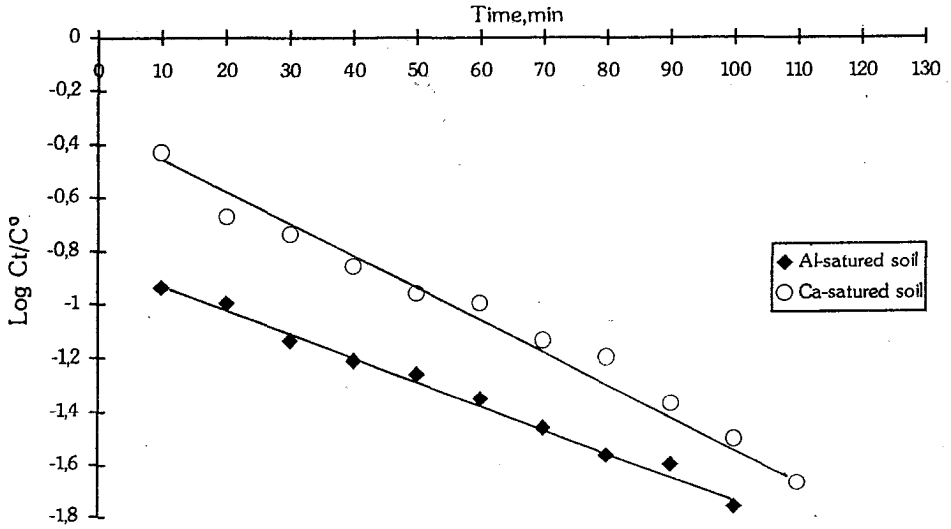

FIG. 6: Log(Ct/C°) vs time for four Al-satured and Ca-satured soil systems

The adsorption-desorption of potassium is a reversible process.The amount of adsorbed K is at 95-98% desorbed.The rest of 2-5% of the adsorbed K could not be desorbed because is adsorbed on specific sites.(13)

The thermodynamics parameters can be calculated as it is already discussed, although there are some uncertainties in the results [14].

Those uncertainties caused by ions present in small amounts on the exchanger.Another difficulty arises in connection with ΔH^o whose values includes the enthalpies of hydration, dilution, mixing and exchange.

Because of uncertainties about the energy of hydration of adsorbed ions, most of these parameters cannot be calculated with high degree of accuracy.

The ΔG^o values for K exchange are negative and increased with increasing temperature [6,15]. ΔG^o become more negative with a decrease in particle size,and this implied that K selectivity increased as the clay content increased [16,17].

The enthalpy ΔH^o values are exothermic and indicated stronger binding of K^+ ions .

ΠΕΡΙΛΗΨΗ

Στην παρούσα εργασία ανασκόπησης εξετάζονται και αναφέρονται εκείνες οι θεωρίες που εχουν προκύγει, μετά από πειραματικά δεδομένα, με σκοπό να ερμηνεύσουν την προσρόφηση και εκρόφηση του καλίου από τα εδάφη καθώς και τα συστατικά αυτών.

Το κάλιο είναι ένα από το πλέον σημαντικά στοιχεία τόσο για τα φυτά ,όσο και για τα ζώα,και αυτός είναι ο λόγος που η γνώση των διαδικασιών προσρόφησης-εκρόφησης είναι τόσο σημαντική, ώστε να περιορισθεί η ρύπανση από το κάλιο μέσω της χρήσης λιπασμάτων.

REFERENCES.

1. Peter O' Neil ,"Enviromental Chemistry", 1985.
2. Reitemeier R.F., 1951. The chemistry of potassium. *Adv.Agron.* 3:113-114
3. Wood.L.K. and E.E. De Tunk ,1940. The adsorption of potassium in soil in non-replaceable forms. *Soil Sci.Soc.Am.Proc.* 5:152-161
4. Rich,C.I. ,1968, Minerology of soil potassium ,p.79-108. In V.J.Kilmer. , S.E.Younts and N.C.Brady (ed).The role of potassium in agriculture. *Am. Soc. of Agron.*,Madison,Wis.
5. Sparks, D. L. ,L.W., Zelazny, and D.C.Martens ,1980a ,Kinetics of potassium exchange in a Paleudult from the Virginia Coastal Plain.*Soil Sci.Soc.Am.J.* 44:37-40

6. Sparks,D.L., and P.M.Jardine ,1981, Thermodynamics of potassium exchange in Soil using a kinetics approach. *Soil Sci.Soc.Am.J.* 45 : 1094-1099
7. Denbigh,K.G., 1966.The principles of chemical equilibrium with applications in chemistry and chemical engineering.2nd ed. Cambridge Univ.Press.N.Y.
8. Kuo S., and E.G.Lotse ,1974 ,Kinetics of phosphate adsorption and desorption by Lake sediments. *Soil Sci.Soc.Am.Proc.* 38 : 50-54
9. Sparks,D.L., L.W.,Zelazny,and D.C.Martens ,1980 ,Kinetics of potassium desorption in soil using miscible displacement.*Soil Sci.Soc.Am.J.* 44 : 1205-1208
10. Sivasubramanian ,S.,and O.Talibudeen ,1972 ,Potassium,aluminium exchange in acid soils I.Kinetics. *J.Soil Sci.* 23 : 163-176
11. Adamson,A.W., 1973.A textbook of physical chemistry. Academic Press.N.Y.
12. Laidler,K.J.,1965,Chemical kinetics,2nd Ed. ,McCraw-Hill,N.Y.
13. Udo,E.J., 1978. Thermodynamics of potassium-calsium and magnessium-calsium exchange reactions on a kaolinitic soil clay.*Soil Sci.Soc.Am.J.* 42 : 556-560
14. Deist, J. and O.Talibudeen, 1967,Thermodynamics of K-Ca exchange in soils, *J.Soil Sci.* 18 : 138-148
15. Goulding,K.W.T, 1981.Potassium retention and release in Rothamsted and Saxmundhum *Soils.J.Sci.Food Agric.* 32 : 667-670
16. Jardine P.M., and D.L.,Sparks, 1984. Potassium-Calcium Exchange in a multi reactive soil system II.Thermodynamics.*Soil Sci.Soc.Am.J.* 48 : 45-49
17. Doula,M., Ioannou A., Dimirkou A., Mitsios J. 1994. Potassium sorption by Calcium-Bentonite (Ca-b) *Commun. in Soil Sci. Plant Anal.* 25 (9&10), 1378-1401

Chimica Chronica, New Series, 23, 115-135 (1994)

A STUDY OF THE ELECTROLYTIC REDUCTION OF U^{VI} ON A Ti CATHODE

Y. TYROVOLAS

Dpt of Chemical and Process Engineering, University of Newcastle upon Tyne, Newcastle upon Tyne, NE1 7RU, England, U.K.

(Received April 18, 1994)

ABSTRACT

The electrolytic reduction of U^{VI} has been studied in a nitric acid / hydrazine solution in conjunction to the electrochemical behaviour of Ti used as cathode. The presence of an oxide and a hydride film covering the Ti surface has been confirmed. The nature of the film has been found to be dependent on the concentration of uranyl nitrate and on the cathode potential. High concentrations of uranyl nitrate and / or low cathode potentials favour the formation of an oxide film, the reverse conditions apply for the hydride film. The nature of the electrode surface affects the electrolytic reduction of U^{VI}. A reaction model has been proposed describing the performance of the primary and of the secondary reactions of the system on the two states of a Ti electrode.

Key words: Electrolytic reduction of U^{VI}, electrolytic behaviour of Ti, Purex process.

INTRODUCTION

The Purex process [1,2,3,4] is the prime reprocessing method of spent nuclear fuels throughout the world. An important step in this process is the separation of U from Pu by reducing Pu^{IV} to Pu^{III}. This can be achieved by using U^{IV} ions (5, 6), an in situ reduction is also under investigation (1, 2, 7). U^{IV} is prepared by electrochemical means from U^{VI}; the feasibility of the method has been demonstrated by pilot plant experiments (8, 9, 10).

The scope of the present work is to study the electrolytic reduction of U^{VI} in conjunction to the electrochemical behaviour of Ti, used as cathode material. A model will be proposed describing quantitatively the electrolytic behaviour of U^{VI} on the two states of a Ti electrode. The electrochemical environment and experimental conditions in the present study were similar to those used in industry.

THEORETICAL PART

Electrochemical Reactions

In a uranyl nitrate/nitric acid / hydrazine system three groups of electrochemical reactions take place at the cathode.

a) Hydrogen evolution. The mechanism can be found in any electrochemical textbook.
b) Electrolytic reduction of nitric acid. This reaction proceeds via intermediates with the possibility of further reduction of the intermediates. A number of products, such as HNO_2, NO, N_2O, NH_4^+ have been reported (11), according to the applied experimental conditions.
c) Electrolytic reduction of U^{VI} to U^{IV} to be discussed below.

$$UO_2^{2+} + 4H^+ + 2e \longrightarrow U^{4+} + 2H_2O$$

d) Hydrazine is expected to be stable.

At the anode the oxygen evolution and the oxidation of hydrazine take place. U^{IV} is expected to be stable (7, 12, 13, 14).

In this section the electrolytic behaviour of U^{VI} will be discussed briefly. The reduction rate of U^{VI} has been found to be proportional to the concentration of U^{VI} (15, 16) and dependent on the acidity of the solution (15, 16, 17). The mechanism of the electrolytic reduction of U^{VI} has been studied extensively (18, 19, 20, 21). Hexavalent uranyl ion, UO_2^{2+}, is reduced initially to the pentavalent ion, UO_2^+, via a reversible or a quasi-reversible single electron step. On the following U^{IV} is produced (18) either by an E.C.E. mechanism or by a disproportionation step, according to the applied experimental conditions. In practice both mechanisms may occur.

Electrochemical behaviour of Ti electrode

Kelly (22) studied the mechanism of Ti dissolution extensively in acidic media (HCl, H_2SO_4). According to Kelly, Ti exists in three different states. The active state, where the metal dissolution takes place. The passive state, where the substrate metal is oxidised to form an oxide. The transition state, where a transformation is taking place from one state to the other. When the metal is in the passive state it is covered by an oxide film, mainly TiO_2, the existence of other oxides has also been reported (23). When the metal is in the active or in the transition state the metal surface is covered by a monolayer adsorbed species (22). The presence of TiH_2 on the Ti surface has also been reported (24, 25, 26). In nitric acid solution, no metal dissolution was observed (26), the formation of TiH_2 was reported at - 0.55 V (S.C.E.) (26).

The presence of oxidising agents in solution seems to passivate metals exhibiting active-passive behaviour like Ti. The mechanism of passivation is well-understood (27, 28) and has been applied on Ti in the presence of certain oxiding agents in solution such as Ti^{IV}, Fe^{3+}, Cu^{2+}, Pt^{4+}, NO_3^- , NO_2^- , quinone, H_2O_2, (27-32). The reduction of the oxidising species on the metal surface is responsible for the passivation of the metal, as the mixed potential produced shifts to more noble values (27, 28). This occurs, as the current produced by the reduction of the corrosion inhibitor, has to balance the currents produced by the oxidation of the metal and the oxidation of the reduced form of the inhibitor. It has been found (27) that there is a critical concentration of the inhibitor above which the metal remains in the passive state and below which in the active one. At the critical concentration the metal surface is at an unstable situation which may lead to an oscillation between the two states before settling down to either state.

Choice of electrode material

There are two main criteria for the choice of an acceptable cathode material: resistivity against corrosion, high hydrogen overvoltage / good current efficiency.

Mercury, a metal with a high hydrogen overvoltage, showed excellent current efficiencies (12, 33). It was rejected from a possible cathode material on the grounds of its dissolution under mild oxidising conditions and its liquid nature creating waste disposal / recovery problems.

At present there are two metals used worldwide for the electrolytic reduction of U^{VI}: Ti is the preferred cathode material in Germany (2, 7), China (17) and Britain (34, 35) and Pt in America (36) and Belgium (12).

Pt is preferred on the grounds of the lower reaction overpotential and the smaller amount of gases evolved. The feasibility of the reaction of U^{VI} has been demonstrated (12, 36) and the role of metal impurities has been discussed (37). Combining the advantages of Pt and Hg, a platinum amalgam cathode was prepared and the feasibility of the U^{VI} reduction has been studied (15).

Ti is preferred for its relatively low price, high strength and resistivity against corrosion. The poor performance of Ti metal obtained by Nichols (38) is not very convincing. Current densities above 100 A/m^2 must be avoided as hydrogen embrittlement may take place (2). This can be avoided by the deposition of metal impurities existing in the electrolyte on the Ti surface shifting the U^{VI} reduction to more noble potentials (39). The presence of U^{VI} seems to have a stabilising effect on the metal against corrosion (2). Ti is expected to exhibit a weight loss of the order of 1mm per annum in the absence of U^{VI} (40); this figure is reduced to 0.05 mm per annum in the presence of U^{VI} (2).

PROCEDURE

A typical three compartment "rotating disc electrode" (R.D.E.) was used, the catholyte was separated from the anolyte chamber by a cation permeable Nafion membrane. The cathode was a Ti cylinder (area = 1.26×10^{-5} m^2) encased in a P.T.F.E. sheath connected to the motor via a stainless steel bar and a spring. The working electrode, the R.D.E. cell and the saturated calomel electrode (S.C.E.) were manufactured according to the instructions found in the literature (41). A platinum wire was used as anode. The IR_{drop} was measured by an interrupter technique (34). All chemicals were of "Anala R" grade prepared with double distilled water. The electrolyte was a solution of uranyl nitrate (0.1-1.0 M) in nitric acid (2.0 M) / hydrazine (0.2 M). The role of hydrazine in the solution is to protect U^{IV} from oxidation acting as a NO_2^- scavenger (42). All experiments were carried out at room temperature. The potential, being corrected for the IR_{drop}, was measured versus a saturated calomel electrode.

Before each run, the electrode was polished with a P600 wet and dry emery paper, rinsed thoroughly with double distilled water and treated electrochemically. During the electrochemical treatment the electrode was immersed in the solution to be examined and a certain current density was applied for a specified time according to the experimental demands.

All polarisation curves were obtained galvanostatically by sweeping manually at an approximate rate 50 mV / min at 1000 r.p.m. The electrode was previously matured at 660 A/m^2 for 24 hrs (overnight). The examined region of interest was 200-1000 A/m^2. To examine the effect of possible excursions of a plant towards lower or higher current densities on the region of interest a further treatment was applied on the electrode at 20 A/m^2 and 2000 A/m^2 for a certain period. After the electrode treatment polarisation curves were obtained in the region 20-2000 A/m^2. To check the reproducibility of the curves, the electrode was treated further at 660 A/m^2 for an extra day and all curves were repeated as before. Using this method different concentrations of uranyl nitrate were examined in the range 0.1-1.0 M including the one of the background solution in the absence of U^{VI}; ie 0.0 M. Before quoting the potential sufficient time was allowed, usually 0.5-1.0 min, for the potential to settle down.

For the current efficiency curves preparative runs were performed at 1000 r.p.m. for the concentration range and potentials similar to those examined by the polarisation curves. The runs were performed galvanostatically, usually overnight, the quoted potential was the one measured at the end of each run. Allocates of electrolyte were withdrawn before and after each run and were analysed quantitatively for U^{IV} (34) by a Pye SP600 U.V. spectrophotometer at 650 nm. The charge passing through the cell was measured by a rotating electrical integrator. The electrode was polished on an occasional basis between the runs.

RESULTS - DISCUSSION

Nature of films covering the Ti surface

An examination of the electrode surface with an electron microscope electrochemically treated at the potential region 0.0V to - 0.8V (S.C.E.) revealed that certain physical and chemical changes occur on the electrode surface during the electrolytic process according to the photographs in Fig (1). The roughness of the electrode surface, Fig (1a), caused by polishing, disappears during the electrochemical treatment of the electrode, Fig (1 b, c, d, e). Furthermore, an oxide film is found covering the Ti surface at potentials positive to - 0.45V (S.C.E.), Fig (1 b, c), and a hydride film at potentials negative to - 0.65V (S.C.E.), Fig (1 d, e). These observations are in agreement with the evidence found in literature. Straumanis (23) has reviewed the presence of the oxide film on Ti. Kelly (22, 30) found that the passive state of Ti in HCl, H_2SO_4 solutions starts at potentials positive to - 0.3V (S.C.E.). Evidence for the presence of a hydride film is given by Harrison (26), Kelly (22) and other research workers (24-25). The presence of the hydride film on Ti in nitric acid solution has been reported at -0.55V (S.C.E.) (26). The inability to obtain steady-state Tafel behaviour (22) and changes in double layer capacity with time (26) were attributed to the unstable nature of Ti surface.

Further evidence for the presence of the oxide and the hydride film covering the Ti surface and the role of U^{VI} ions in the formation of an oxide film is given in Fig (2). At the begining of the electrode treatment all potentials corresponding to various concentrations of U^{VI}, 0.0-1.0 M, lie in a wide potential band (-0.5V to - 0.7V) (S.C.E.) in the hydride region, Fig (2). As the treatment of the electrode proceeds overnight, the electrode potentials gradually deviate from the initial band. After 24 hours at the end of the electrode treatment the electrode potentials lie into two distinct narrow potential bands. The one at approx. -0.3V (S.C.E.) corresponds to the oxide region and the other at approx. -0.55V (S.C.E.) corresponds to the hydride region. On a closer examination it is seen that all electrode potentials corresponding to low concentrations of uranyl nitrate, 0.0-0.6 M, lie in the hydride region. Electrode potentials of higher concentrations, 0.7-1.0M U^{VI}, lie in the oxide region. The presence, therefore, of uranyl nitrate in a 2.0 M nitric acid solution seems to be responsible for the formation of the oxide film for concentrations higher than 0.7 M. These observations are in agreement with the model proposed by Stern (27, 28) for metals exhibiting active-passive state in the presence of an oxidising agent. The concentration of 0.7 M uranyl nitrate is the critical concentration, above which an oxide film is formed. At this proposed critical concentration the Ti surface has been found unstable oscillating between the oxide and the hydride potential region, in a similar way to the one reported in the literature (27, 43). Incidentally after an electrolytic treatment of 48 hours, the electrode potential of 0.7 M U^{VI} was found in the hydride region at -0.52V (S.C.E.).

In the present system there are two oxidising agents, NO_3^- and U^{VI} ions, in the solution. There is evidence in the literature of the corrosion inhibiting role of NO_3^- (27) and of metal ions (32) such as Pt^{4+}, Cu^{2+}, Fe^{3+} and ions of Au, Hg, Zn, Co. At

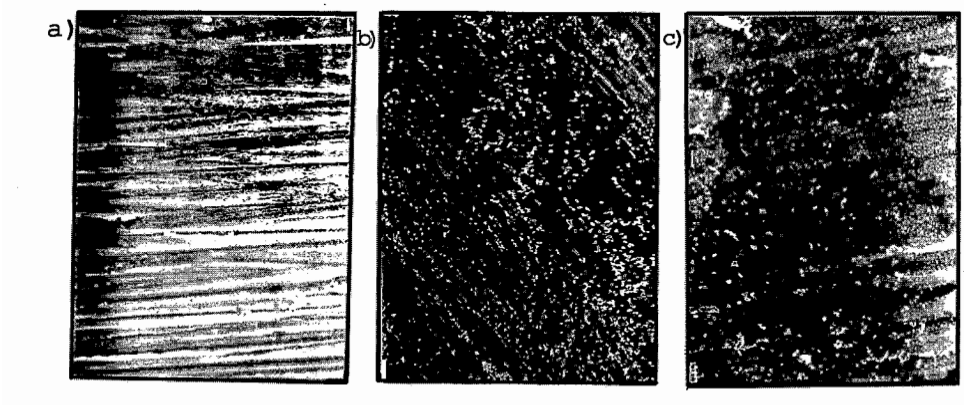

Fig (1)

Photographs of the films covering the surface of a Ti electrode taken by an electrone microscope. The electrode was treated electrochemically in a 2.0 M HNO_3 solution.

a) x1500 magnification. Polished electrode without electrochemical treatment.
b) x1000 magnification. Overnight treatment at -0.01 V (S.C.E.) OXIDE FILM.
c) x3500 magnification. Treatment for 4 hrs at -0.45 V (S.C.E.) OXIDE FILM.
d) x5000 magnification. Treatment for 5 hrs at -0.65 V (S.C.E.) HYDRIDE FILM.
e) x1500 magnification. Treatment for 5 hrs at -0.80 V (S.C.E.) HYDRIDE FILM.

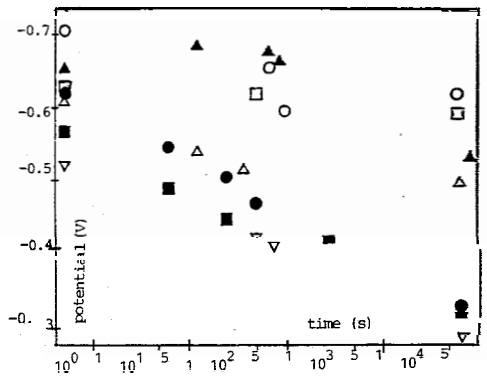

Fig (2)

The variation of the cathode potential with time during an overnight treatment of a Ti electrode at 660 A/m² for different concentrations of U(VI) (0.0 - 1.0M).

$[U^{VI}]$ = 0.0M, 0.1M, 0.6M, 0.8M, 1.0M

this stage there is no evidence to tell which of the two ions, NO_3^- or U^{VI} is responsible for the formation of the oxide film. Most probable, the formation of an oxide film is caused by the combined action of both oxidising agents.

Due to the absence of information in the literature concerning the active / passive states of Ti in nitric acid solutions, no reference to an active state of Ti, if it exists, can be made in the present work. The reference to an oxide and to a hydride state is made only to denote the existence of an oxide and of a hydride film covering the electrode surface at the potential region discussed above. Research on the active / passive states of Ti was not the scope of the present work.

Polarisation curves

As it has been discussed before, the electrode treatment at 660 A/m^2 in low concentrations of uranyl nitrate is responsible for the formation of the hydride film. The polarisation curves of 0.0, 0.1, 0.3 M U^{VI}, Fig (3 a, b ,c), were, therefore, obtained on a hydride surface. The region of interest, 200-1000 A/m^2, lies well in the hydride potential region. Excursions of short time intervals towards a lower current density, 20 A/m^2, fall into the oxide potential region, without affecting the system. Similar excursions towards a higher current density, 2000 A/m^2, doesn't affect the system either. The reproducibility of the curves when repeated on the following day (second day of the electrode treatment) is excellent.

A similar treatment of the electrode in high concentrations of uranyl nitrate is responsible for the formation of an oxide film. Polarisation curves of 0.8M and 1.0M U^{VI} were, therefore, obtained on an oxide surface, Fig (3 f, g.) The region of interest, 200-1000 A/m^2, lies well into the oxide potential region. Similar excursions to the hydride case towards higher or lower current densities don't seem to affect the system either. Repeating the polarisation curves on the second day of the electrode treatment, the curves were shifted by 50-100 mV retaining their shape. The poor reproducibility of the curves may be attributed to certain physical (dimensional) changes on the electrode surface or to changes of the stoichiometry of the oxide film (23).

Concentrations of uranyl nitrate close to the critical concentration create an unstable electrode surface which may oscillate between the oxide and the hydride state. The unstable nature of the electrode surface seems to affect the polarisation curves of U^{VI}, Fig (3 d, e). The curves of 0.6 M U^{VI}, Fig (3d), shift towards more negative potentials on the second day of the electrode treatment, followed by a change of their shape. On the second day the system appears to be more stable than the first day. The second day polarisation curves of 0.6M U^{VI} have obtained a shape similar to the ones of 0.1M and 0.3M U^{VI}, Fig (3 b, c), on a hydride surface. The surface has, therefore, been fully developed after 48 hours. The polarisation curves of 0.7 M U^{VI} were obtained on an oxide surface on the first day and on a hydride surface on the following day. The different shape of the "second day's" curves with those obtained on a stable hydride surface, Fig (3 b, c), indicates that

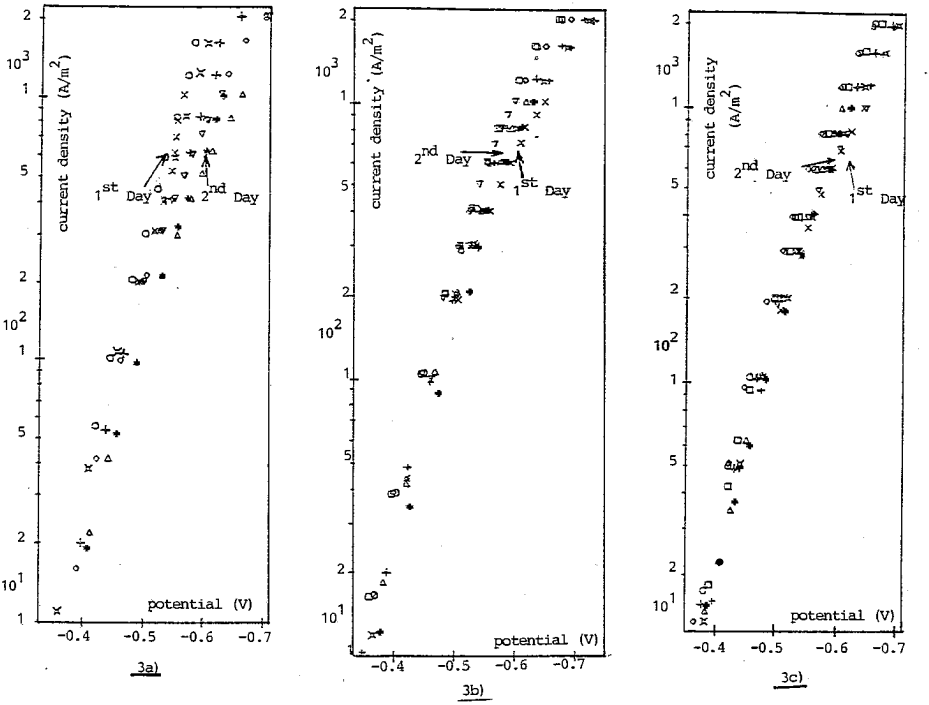

Fig (3) Polarisation curves of U^{VI} for concentrations 0.0 - 1.0M U^{VI}. The electrode was treated overnight in the solution to be examined at 660 A/m^2. The curves were obtained in the following order: × immediately, after a further treatment at ✠ 20 A/m^2 for 10 mins, ✧ 2000 A/m^2 for 5 mins, ⧓ 2000 A/m^2 for 15 mins, + 2000 A/m^2 for 1 hr. The electrode was further treated overnight at 660 A/m^2 and the curves were repeated: ▽ immediately, after a further treatment at Δ 20 A/m^2 for 10 mins, ◇ 2000 A/m^2 for 5 mins, ○ 2000 A/m^2 for 15 mins, □ 2000 A/m^2 for 1 hr. ⟶ Electrode potential at the end of the overnight treatment.

3a) Polarisation curves of 0.0M U^{VI}. Hydride surface.

3b) Polarisation curves of 0.1M U(VI). Hydride surface.

3c) Polarisation curves of 0.3M U^{VI}. Hydride surface.

3d) Polarisation curves of 0.6 M U^{VI}. Hydride surface.

3e) Polarisation curves of 0.7 M U^{VI}.

3f) Polarisation curves of 0.8 M U^{VI}. Oxide surface.

3g) Polarisation curves of 1.0M U^{VI}. Oxide surface.

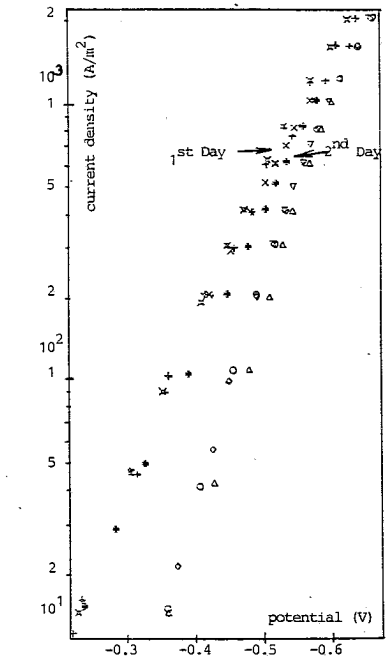
current density (A/m²)
1st Day
2nd Day
potential (V)
-0.3
-0.4
-0.5
-0.6

3d)

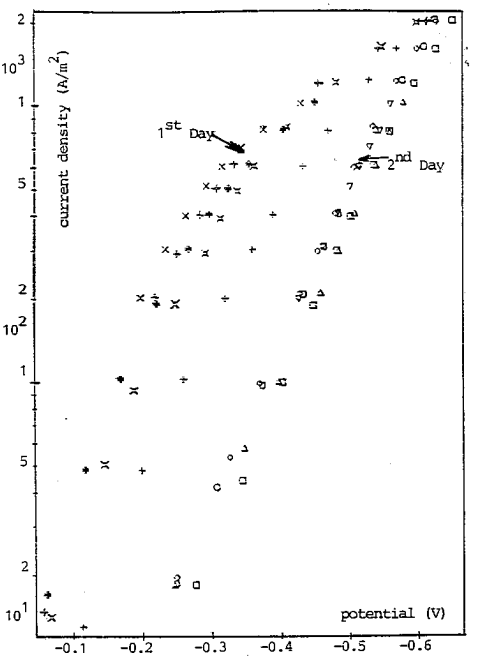
current density (A/m²)
1st Day
2nd Day
potential (V)
-0.1
-0.2
-0.3
-0.4
-0.5
-0.6

3e)

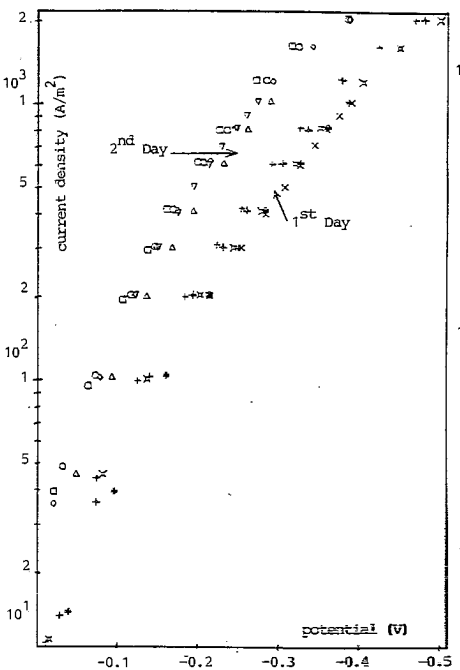
current density (A/m²)
2nd Day
1st Day
potential (V)
-0.1
-0.2
-0.3
-0.4
-0.5

3f)

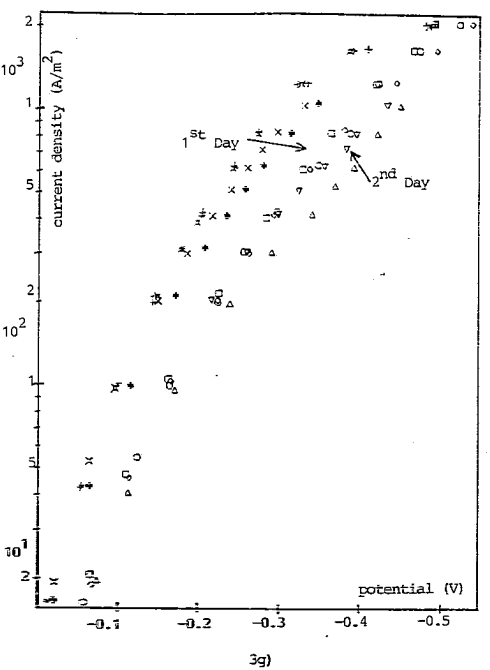
current density (A/m²)
1st Day
2nd Day
potential (V)
-0.1
-0.2
-0.3
-0.4
-0.5

3g)

the surface has not been fully developed even on the second day of the electrode treatment.

A similar shift of the polarisation curves of 1.0 M U^{VI} on a Ti/TiO_2 electrode towards more positive potentials was observed by Schultze and Borgerding (39). They attributed this phenomenon to the existence of certain metal impurities of Pb^{2+}, Pd^{2+}, Cu^{2+} in the electrolyte. These metal impurities deposit at the cathode during the electrolysis modifying gradually the electrode surface. In the present work no metal impurities were detected at the electrode surface, besides the Stern model (27, 28) explains adequately the experimental results.

Reversible establishment of the oxide-hydride film

After an overnight treatment of the electrode at 0.1 M U^{VI} a hydride film is formed on Ti. The examination of the behaviour of 0.8 M U^{VI} at that surface revealed that initially the polarisation curves, Fig (4a), were obtained at potentials similar to those of 0.1 M U^{VI}, Fig (3b). Gradually as the electrode is treated in a 0.8 M U^{VI} solution, it starts gaining the oxide character, the polarisation curves being shifted to less negative potentials, Fig (4a), approaching the potential region of the polarisation curves of 0.8 M U^{VI} obtained on an oxide surface, Fig (3f). Apparently an oxide film is formed slowly replacing the hydride one. On examining the polarisation curves of 0.1 M and 0.0 M U^{VI} obtained on the developed oxide surface, Fig (4 a), revealed that these curves appear in the same potential region with those curves obtained on a hydride surface, Fig 3 (a, b, c). The hydride film seems to be established immediately when the electrode is found in the appropriate environment, in contrast to the slow establishment of the oxide film. After a further treatment of the electrode, all curves were repeated on the following day to check the reproducibility. The reproducibility was confirmed revealing a reversible establishment of the film from one state to the other, as Fig (4b) demonstrates.

Current efficiency curves

Current efficiency curves of U^{VI} in the concentration range 0.3 - 1.0M U^{VI} are shown in Fig (5 a, b, c, d). The curves seem to be dependent on the concentration of U^{VI}, high current efficiency values are obtained on high concentrations of U^{VI}. All curves are undergoing a maximum at approx - 0.4V (S.C.E), turning point between the oxide - hydride potential region.

Partial polarisation curves

The primary current density, i_p, will refer to the primary reaction of the system, namely the electrolytic reduction of U^{VI} to U^{IV}. The secondary reactions of the system, namely the hydrogen evolution and the electrolytic reduction of nitric acid, will be represented lumped together by one parameter which is the current density of the secondary reactions, i_{sec}. The total current density, i_T, is the sum of all the individual current densities according to equation (1).

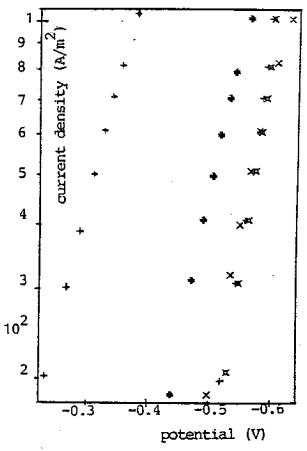

4a) Electrode matured overnight at 660 A/m^2 in a 0.1M U(VI) solution. Polarisation curves of 0.8M U(VI) taken ✕ immediately, after a further treatment of ⊠ 3 hrs, ⊹ 20 hrs at 660 A/m^2. The polarisation curves of + 0.1M U(VI), ⋈ 0.0M U(VI) were taken straight after.

Fig (4) Reversible establishment of the oxide/hydride film.

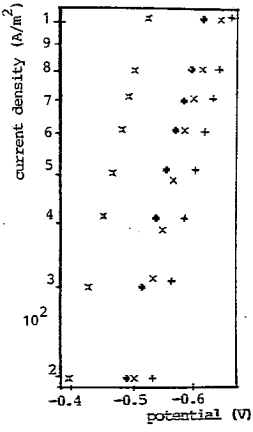

4b) After the polarisation curves Fig 4a, the electrode was treated overnight at 660 A/m^2 in a 0.1M U(VI) solution. Polarisation curves of ✕ 0.1M, ⊹ 0.0M, ⊠ 0.8M U(VI) were taken straight after. After a 4 hrs treatment at the same current density in a 0.8M U(VI) solution, the pol. curve of ⋈ 0.8M U(VI) was repeated.

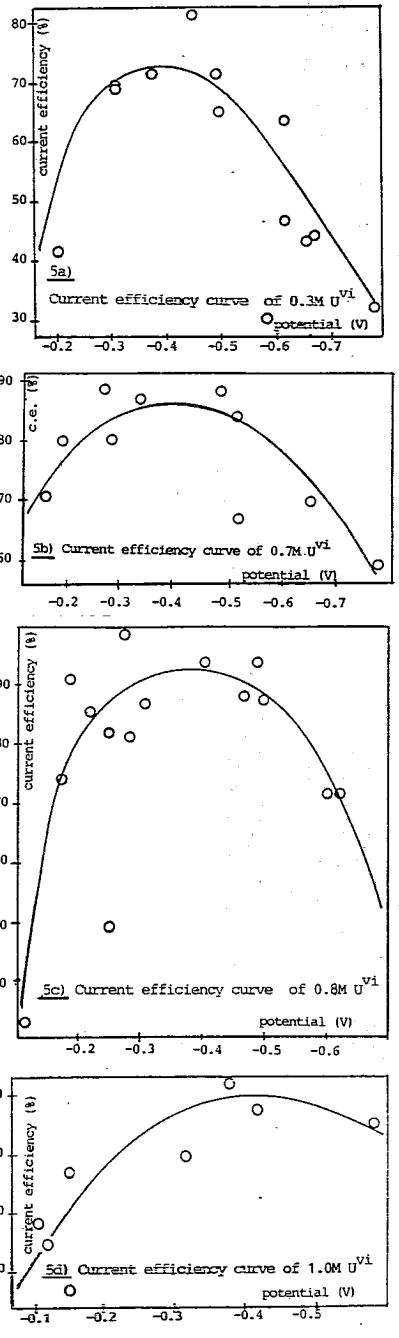

Fig (5) Current efficiency curves of U^{vi} for different concentrations of U(VI) (0.3 - 1.0M)

$$i_T = i_p + i_{sec} \qquad \text{eq (1)}$$

Current efficiency, c.e., is defined by eq (2)

$$\text{c.e.} = 100 \times \frac{i_p}{i_T} \qquad \text{eq (2)}$$

From equations (1), (2), expressions of i_p and i_{sec} are obtained

$$i_p = \frac{i_T \times \text{c.e.}}{100} \qquad \text{eq (3)}$$

$$i_{sec} = \frac{i_T \times (100 - \text{c.e.})}{100} \qquad \text{eq (4)}$$

Linking the polarisation with the current efficiency curves for the same concentration of U^{VI} through equations (3) and (4) the partial polarisation curves of the primary and the secondary reactions can be obtained, shown in Fig (6 a, b, c, d, 7, 8).

The primary polarisation curves were compared with the primary current densities obtained by overnight preparative runs of the same concentration of U^{VI}, Fig (6 a, b, c, d). The close agreement between the curves and the current densities indicates that both results were obtained on a chemically compatible electrode surface. The curves, therefore, represent the correct quantities and are suitable for quantitative interpretation. The disagreement between certain current densities and the polarisation curves of 0.3 M and 0.8 M U^{VI}, Fig (6 a, c), were outside the potential region examined by the polarisation curves. Most probable the data were obtained on different states of Ti electrode.

The electrolytic behaviour of the secondary reactions is very different on the two states of Ti, Fig (7, 8). The partial polarisation curves of the secondary reactions of 0.3 M and 0.7 M U^{VI}, obtained on a hydride surface, seem to be linear reproducible and independent on the initial concentration of U^{VI}, Fig (7). A comparison between the curves of the secondary reactions and those of the background solution (in the absence of U^{VI}) reveals that the secondary reactions are suppressed in the presence of U^{VI}. On the oxide surface, Fig (8), the poor reproducibility of the polarisation curves of U^{VI}, Fig (3 f, g), is reflected on the curves of the secondary reactions. Both secondary polarisation curves of 0.8 M and 1.0 M U^{VI} are shifted when being repeated on the second day of the electrode treatment. The shift of the curves doesn't merit prediction on any possible U^{VI} concentration dependence. The shape of these curves is different from the ones of the hydride surface. The curves on the oxide state undergo a maximum at approx - 0.25 V (S.C.E.). The different behaviour of the secondary reactions on the two states of Ti has to be taken into account for any quantitative interpretation of the results.

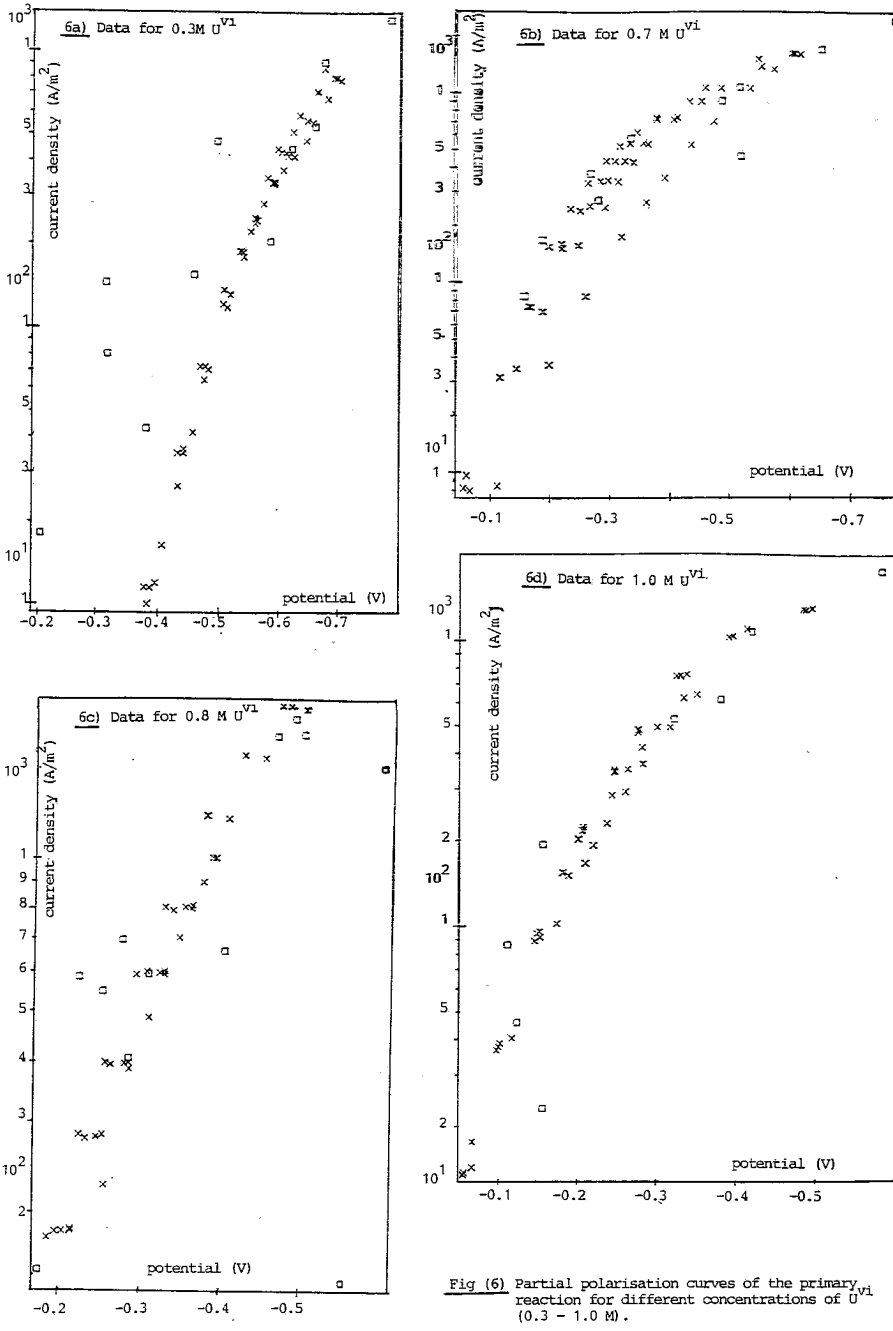

Fig (6) Partial polarisation curves of the primary U^{VI} reaction for different concentrations of U^{VI} (0.3 - 1.0 M).

× partial polarisation curves
⊡ primary current density from preparative runs.

REACTION MODEL

Reaction model of primary reaction

The object of a reaction model is to express the rate of a reaction as a function of relevant independent variables. Goodridge (45) demonstrated that the reaction model of an electrochemical reaction can be represented as the partial current density of the reaction expressed as a function of the mass transfer contribution and the reaction kinetics, shown in equation (5) modified for the present reaction.

$$i_u = \frac{1000\ c_u}{\frac{1}{2F\ k_L} + \frac{1}{2\ Fk\ e^{-bE}}} \qquad \text{eq (5)}$$

i_u = partial current density of the reduction of U^{VI}
c_u = concentration of U^{VI} in the bulk electrolyte
F = Faraday constant, 96,500 C/mol
k_L = mass transfer coefficient, 4.0×10^{-5} m/s proposed by Yoon [44] at 1000 r.p.m
k,b = kinetic parameters of the reaction
E = cathode potential

A rearrangement of the above equation into equation (6), represents the primary current density free from any contribution of the concentration of U^{VI} and of the mass transfer :

$$\lg\left[\frac{c_u}{i_u} - \frac{10^{-3}}{2Fk_L}\right] = -\lg[2000\ Fk] + \frac{bE}{2.303} \qquad \text{eq (6)}$$

An application of equation (6) on the data of the primary polarisation curves of U^{VI} for the hydride and the oxide state of Ti electrode is shown in Fig (9). The obtained linear relationship indicates that equation (6) is applicable on both states of Ti with different kinetic paramenters for each state. The electrolytic reduction of U^{VI} seems to be favoured by the presence of the oxide film. The different behaviour of the reaction on the two states of Ti has to be taken into account for the derivation of the reaction model.

Because of the stable character of the hydride film and the reproducible behaviour of the curves on it, the polarisation curves of 0.3 M U^{VI} have been found adequate for the derivation of the reaction model on the hydride surface. A plot of $\lg [c_u/i_u - 1/2000\ F\ k_L]$ vs E for the data of 0.3 M U^{VI}, was found linear, Fig (10). A regression analysis of the data, excluding those negative to -0.65 V (S.C.E.), proposed the following set of values for the kinetic paramenters of the reaction on the hydride state :

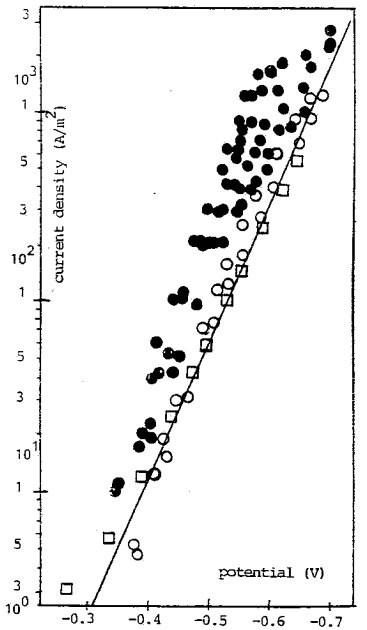

Fig (7) Partial polarisation curves of the secondary reactions on the hydride surface.
○ curves of 0.3M U(VI)
□ curves of 0.7M U(VI)
● background polarisation curves (0.0M U(VI))

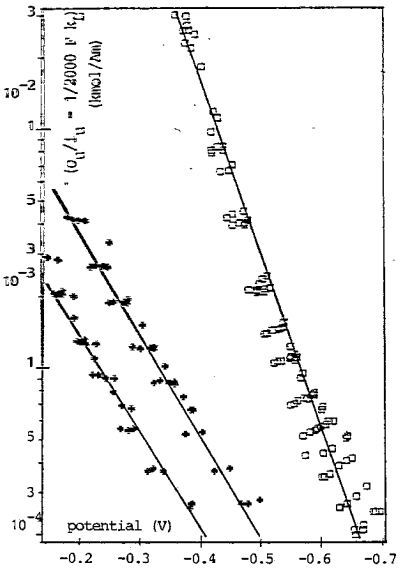

Fig (9) Application of the equation of the reaction model on the electrolytic reduction of U(VI) for the two states of Ti.
✱ [U(VI)] = 0.8M
□ [U(VI)] = 0.3M

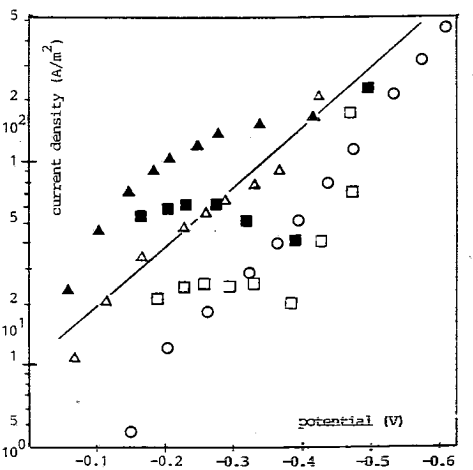

Fig (8) Partial polarisation curves of the secondary reactions on the oxide surface.
○ curves of 0.7 M U(VI)
△ ▲ curves of 1.0 M U(VI)
□ ■ curves of 0.8 M U(VI)

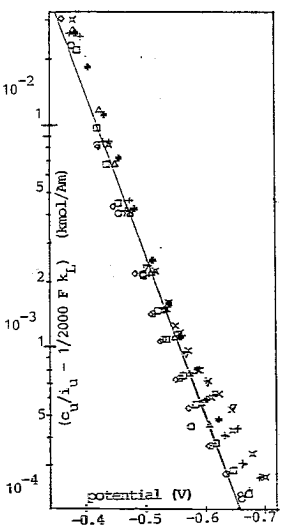

Fig (10) Modelling the electrolytic reduction of U(VI) on the hydride state of Ti, based on the data of 0.3M U(VI). Symbols as in Fig(3).

$b = 16.6\ V^{-1}$

$k = 4.84 \times 10^{-10}$ m/s

Substituting the set of kinetic parameters into equation (6) the reaction model of the electrolytic reduction of U^{VI} on the hydride state of Ti is represented below :

$$i_{u,hyd} = \frac{2000\ F c_u}{1/k_L + 1/4.84 \times 10^{-10} \exp(-16.6\ E)} \qquad \text{eq (7)}$$

The derivation of the reaction model on the oxide surface will be based on the primary polarisation curves of 0.8 M and 1.0 M U^{VI}. A plot of lg $[c_u/i_u - 1/2000\ F\ k_L]$ vs E for the two sets of data define a wide band of points, Fig (11), with an area in common where the two sets of data are overlapping. The overlapping area define the most probable operating region of a plant. The reaction model must refer mainly to this region.

A regression analysis of the data, excluding those positive to - 0.05 /V (S.C.E.), proposes a straight line passing from the common area, Fig (11). A set of kinetic parameters derived from the slope and intercept of the line is given below :

$b = 7.46\ V^{-1}$

$k = 3.75 \times 10^{-7}$ m/s

Substituting these values into equation (6) the reaction model of the electrolytic reduction of U^{VI} on the oxide state of Ti is represented below :

$$i_{u,ox} = \frac{2000\ F c_u}{1/k_L + 1/3.75 \times 10^{-7} \exp(-7.46\ E)} \qquad \text{eq (8)}$$

The validity of the proposed model is confirmed by overnight preparative runs, Fig (12), for a wide range of operating conditions concerning current density (50-6000 A/m^2) and concentration of U^{VI} (0.1 - 1.0 M). The performance of all points irrespective of their concentration origin is predicted by the oxide model for potentials positive to - 0.4 V (S.C.E.) - region of existence of the oxide film. Similarly the performance of all points irrespective of their concentration origin is better explained by the hydride model for potentials negative to -0.5 V (S.C.E) - region of existence of the hydride film. It is interesting to notice that in the potential range -0.4 V to -0.5 V (S.C.E.) there is a gradual deviation of the points from one model towards the other indicating possibly the transformation of the surface from one state to the other.

Reaction model of secondary reactions

The partial polarisation curves of the secondary reactions showed a different electrochemical behaviour according to the state of the electrode surface. This leads to the proposal of two different models one for each state.

For the hydride state, the model will be based on the data of 0.3 M and 0.7 M U^{VI}, Fig (7). The fact of the suppression of the secondary reactions in the presence of U^{VI}, Fig (7), excludes the backgound polarisation curves from the set of data on which the derivation of the model will be based. The reason is that normally a plant is expected to operate in the presence of U^{VI}. As the partial polarisation curves of 0.3 M and 0.7 M U^{VI}, Fig (7), seem to be independent on the concentration of U^{VI}, a concentration factor is not included in the proposed model. A regression analysis of the partial polarisation curves of the secondary reactions of 0.3 M and 0.7 M U^{VI}, Fig (7), showed a linear relationship leading to equation (9).

$$i_{sec,\,hyd} = 10^{(-7.34\,E\,-\,1.95)} \qquad \text{eq (9)}$$

Equation (9) is the model of the secondary reactions on the hydride electrode surface.

The presence of a maximum combined with the observed shift of the polarisation curves of the secondary reactions on an oxide surface doesn't lead to a simple quantitative description of the performance of the secondary reactions, Fig (8). Absence of background polarisation curves on an oxide surface doesn't allow for any reference guideline. To overcome all these problems, all the data on the oxide surface (0.8 M and 1.0 M U^{VI}) can be considered lumped together as points disregarding their concentration origin. A wide band of points is, therefore, obtained representing the operating area of a plant. A regression analysis of the data suggests a number of the best fitting curves. The one with the linear form, if rearranged, is given below :

$$i_{sec,\,ox} = 10^{(-2.97E+1)} \qquad \text{eq (10)}$$

Equation (10) represents the model of the secondary reactions on an oxide Ti surface.

The validity of the proposed models is confirmed for the two states of Ti by overnight preparative runs, Fig (13). The runs were performed on a wide range of operating conditions; current density : 10-6000 A/m^2, concentration of U^{VI} 0.0-1.0M. The observations are similar to those of the primary reaction. For potentials negative of -0.5 V (S.C.E.) the hydride model seems to describe better the experimental data. For potentials positive of - 0.4 V (S.C.E.) the oxide model is preferred. For potentials between - 0.4 V and - 0.5 V (S.C.E.) the points diverge

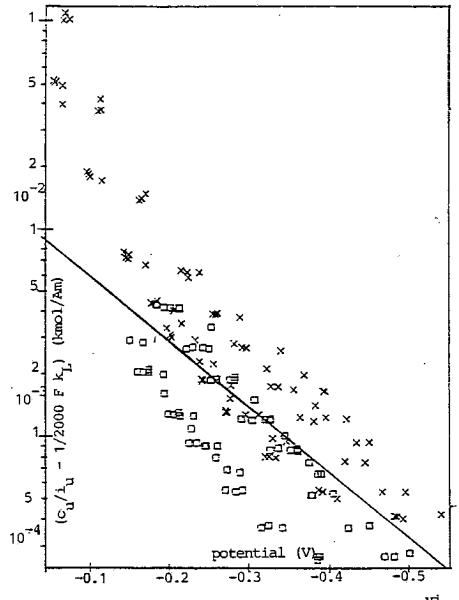

Fig (11) Modelling the electrolytic reduction of U^{VI} on the oxide surface of Ti, based on the data of 0.8M, 1.0M U(VI).

× [U(VI)] = 1.0M
□ [U(VI)] = 0.8M

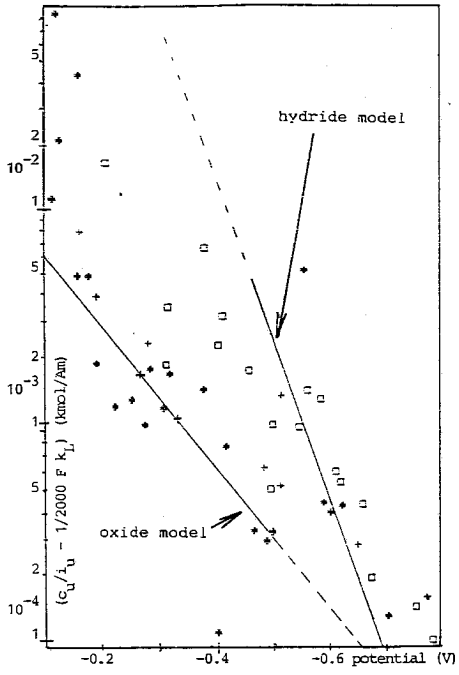

Fig (12) Comparison between the experimental data from the preparative runs and the predictions of the model of the primary reaction for the oxide and the hydride surface of Ti.

✱ [U(VI)] = 1.0M, 0.8M
+ [U(VI)] = 0.7M
□ [U(VI)] = 0.6M, 0.3M, 0.1M

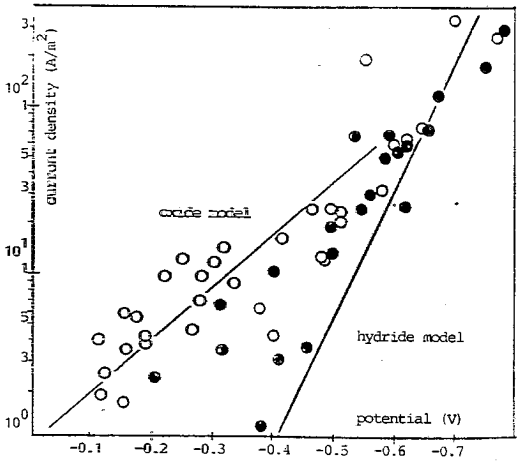

Fig (13) Comparison of the experimental data of the preparative runs with the predictions of the model of the secondary reactions for the oxide and the hydride surface.

○ secondary current densities for [U(VI)] = 0.7 - 1.0M
● secondary current densities for [U(VI)] = 0.3 - 0.6M

gradually from one model to the other demonstrating the transformation of the electrode surface from one state to the other. It has to be emphasised that the predictions of the models of the primary and of the secondary reactions are in perfect agreement on the potential region concerning the presence of the oxide and of the hydride film. The perfect agreement applies also on the transformation region between the two films.

Proposed reaction model

Substituting the equations of the derived models on an oxide and on a hydride surface into equation (1), the proposed reaction model of all reactions will be derived for an oxide, equation (12), and for a hydride surface, equation (11).

$$i_{T,hyd} = \frac{2000\ F c_u}{1/k_L + 1/4.84 \times 10^{-10} \exp(-16.6\ E)} + 10^{(-7.34\ E - 1.95)} \qquad \text{eq (11)}$$

$$i_{T,ox} = \frac{2000\ F c_u}{1/k_L + 1/3.75 \times 10^{-7} \exp(-7.46\ E)} + 10^{(-2.97\ E + 1)} \qquad \text{eq (12)}$$

CONCLUSIONS

The surface of Ti undergoes a number of physical and chemical changes during an electrolytic process. Very long time intervals up to 24 hours are usually required for the electrode surface to become fully developed. An oxide and a hydride film are covering the Ti electrode surface according to the applied experimental conditions. The cathode potential plays a decisive role on the nature of the film. Potentials below approx. -0.5V (S.C.E.) favour the formation of an oxide film, while at higher potentials a hydride film covers the electrode surface. The existence of a transition potential region between -0.5 V and -0.4 V (S.C.E) is also possible, where a transformation takes place of one state to the other. The reduction of uranyl nitrate in nitric acid solution plays also a very important role on the formation of the oxide film, according to a mechanism proposed by Stern for metal passivation.

The electrolytic reduction of U^{VI} is possible on both states of Ti. The current efficiency has been found good for a rather narrow potential region. The mechanism and the kinetics of the examined reaction seems to be affected by the state of Ti electrode on which it takes place. The oxide state seems to favour the electrolytic reduction of U^{VI}. The performance of the secondary reactions, namely the hydrogen evolution and the reduction of nitric acid, is also affected by the state of the electrode surface. The primary and the secondary reactions were modelled separately on each state of Ti. A reaction model proposed by Goodridge was found applicable for the modelling of the primary reaction. For this reason two sets of kinetic parameters were proposed one for each state. A complicated electrochemical system can, therefore, adequately be described by a simple reaction model.

ΠΕΡΙΛΗΨΗ

ΗΛΕΚΤΡΟΧΗΜΙΚΗ ΑΝΑΓΩΓΗ ΤΟΥ U^{VI} ΣΕ ΚΑΘΟΔΟ Ti

Η ηλεκτροχημική αναγωγή του U^{VI} μελετήθηκε σε διάλυμα νιτρικού οξέος/υδραζίνης σε συνδυασμό με την ηλεκτροχημική συμπεριφορά του Ti χρησιμοποιημένου ως καθόδου. Τα πειραματικά δεδομένα πιστοποιούν την ύπαρξη δύο διαφορετικών στρωμάτων που καλύπτουν την επιφάνεια του ηλεκτροδίου και δημιουργούνται κατά την ηλεκτρόλυση ανάλογα με τις πειραματικές συνθήκες. Ειδικότερα, διαφορές δυναμικού κάτω των -0.5 V (S.C.E.) και υψηλές πυκνότητες του νιτρικού ουρανίου ευνοούν την ανάπτυξη του οξειδίου του Ti, ενώ αντίθετες συνθήκες ευνοούν την ανάπτυξη του υδριδίου του Ti. Η ύπαρξη των δύο αυτών στρωμάτων, επιδρά με τη σειρά της στο μηχανισμό και στην κινητική της ηλεκτροχημικής αναγωγής του U^{VI} καθώς επίσης και στις δευτερεύουσες αντιδράσεις του συστήματος. Σε μαθηματικές εξισώσεις που προτείνονται, περιγράφεται η ηλεκτροχημική αναγωγή του U^{VI} στο Ti και πιο συγκεκριμένα η εξίσωση (8) για την οξείδια φάση του Ti και η εξίσωση (7) όταν το Ti καλύπτεται απο στρώμα TiH_2. Ανάλογες εξισώσεις έχουν προταθεί και για τις δευτερεύουσες αντιδράσεις, δηλαδή οι εξισώσεις (10) και (9) για το οξείδιο και το υδρίδιο αντίστοιχα. Οι εξισώσεις συμφωνούν με τα πειραματικά δεδομένα, σχήματα (12, 13).

ACKNOWLEDGEMENTS

I would like to express my sincere gratitude to Prof. F. Goodrigde and Dr. R.E. Plimley for their help and advice during the experimental work. I would like also to thank Mr. E. Hosley and his team for their technical support and Mr. H. Sargent for the examination of the specimens and the photographs by the electron microscope. My acknowledgements are extended to B.N.F.L. for the financial support of the present work.

REFERENCES

1. Schneider, A. Wahlig, B.G., *Actinide Separations A.C.S. Symp. Ser. No 117* (1980) 279.
2. Baumgartner, F., Schmieder, H., *Radiochimica Acta,* 25 (1978) 191.
3. Regnaut, P., *Proceedings of the 2nd United Nations, International Conference on the Peaceful Uses of Atomic Energy*, Geneva, 1958, Vol 17, p 73.
4. Baumgartner, F., Ertel, D., *J. Radional. Chem.* 58 (1980) 11.
5. Rydberg, J, *Acta Chem. Scand.* 11 (1957) 201.
6. Rydberg, J, *J. Inorg. Nucl. Chem.* 5 (1957) 79.
7. Schmieder, H., et.al., *KFK-2082, ORNL-tr-2999* (1974).
8. Schlea, C.S., et.al., *Du Pont de Nemours (E.I.) and Co, Savannah River Lab AIKEN, S.C.*, Apr. 1963, DP-808.
9. McKay H.A.C., Edwall, B., De Leone, R., Aqueous of Reprocessing Chemistry of Irradiated Fuels, Brussels, Symposium 1963, *European Company for the chemical processing of the Irradiated Fuels*, p 281-298.
10. Mc Kay, H.A.C., Streeton, R.J.W., Wain, A.G., *Atomic Energy Research Establishment*, Harwell, Berkshire (1963), AERE - R4381.
11. Kreysa, G., Breidenback, G., Muller, K.J., *Ber. Bunsenges. Phys. Chem.* 87 (1983) 66.
12. Lopez-Menchero, E., et.al., ETR-180 (1966), *Industrial Development Division, Eurochemic*, Mol, Belgium.
13. Araujo, B.F., et.al., *Instituto de Pesquisas Energeticas e Nucleares,* Sao Paolo (Brazil). Centro de Engesharia Quimica, May 1981, IPEN-PUB-24.
14. Buckingham, J.S., Colvin, C.A., Goodall, C.A., *HW-59283* (1959).
15. Orebaugh, E.G., Propst,R.C., DP - 1549 (1980), *E.I. du Pont de Nemours and Co, Savannah River Laboratory*, Aiken, SC 29808.
16. Hsiang, C.C., Chang, C.T., *J. Inorg. Nucl. Chem.* 37 (1975) 1949.
17. He, J., Zhang, Q., Lo, L., *J. Am. Chem. Soc.* (1980) 317.

18. Mastragostino, M., Saveant, J.M., *Electrochim. Acta* 13 (1968) 751.
19. Bansal, N.P., Plambeck, J.A., *Can. J. Chem.* 59 (1981) 1515.
20. Casadio, S., Lorenzini, L., *Anal. Lett.* 6 (1973) 809.
21. Sipos, L., et.al., *J. Electroanal. Chem.* 32 (1971) 35.
22. Kelly, E.J., *"MODERN ASPECTS OF ELECTROCHEMISTRY"* No 14 Ed., J.O'. M. Bockris, B.E. Conway,R.E. White.
23. James, W.J., Straumanis, M.E., *Encyclopedia of Electrochemistry of the Elements*, Vol V (1976) by Bard, A.J.
24. Phillips, I.I., Poole, P., Shreir, L.L., *Corrosion Science*, 12 (1972) 855.
25. Sukhotin, A.M., Tungusova, L.I., *Prot. Met.* 4 (1968) 5.
26. Harrison, J.A., Plimley, R.E., Tyrovolas, J., *J. Electroanal. Chem.* 225 (1987) 139.
27. Stern, M., *J. Electrochem. Soc.,* 105 (1958) 638.
28. Greene, N.D., *Corrosion*, 18 (1962) 136t.
29. Tomashov. N.D., Matveeva,T.V., *Prot. Met.* 7 (1971) 515.
30. Kelly, E.J., *J. Electrochem. Soc.* 123 (1976) 162.
31. Andreeva, V.V., Yakovleva, E.A., *Protective metallic and oxide coating, metal corrosion and electrochemistry*, Ed. Fedot' ev., N.P.
32. Tomashov, N.D., Al'Tovskii, R.M., *Corrosion*, 19 (1963) 217.
33. Finlayson, N.B., Wowat, J.A.S., *Electrochem. Technol.*, 3 (1964) 148.
34. Tyrovolas, Y., *Ph. D. Thesis*, (1989), University of Newcastle upon Tyne, U.K.
35. Dafana, R., *Ph.D. Thesis* (1988), University of Newcastle upon Tyne, U.K.
36. Miller, F.C., et.al., *Atomic Energy of Canada Ltd, Chalk River, Ontario, Chalk River Nuclear Labs*, AECL - 8256 (1984).
37. Davies, W., *Talanta* 17 (1970) 937.
38. Nichols, G., Du Pont de Nemours (E.I.) and Co., *Savannah River Lab.* AIKEN, S.C., DP - 1065 (1966).
39. Schulze, J.W., Borgerding, A., *Dechema Monographien Band 109, VCH Verlagspesdeschaft* (1987) p23.
40. Poczyajlo, A., Zolnierczuk, M., *Nucleonika*, 25 (5) 1980, 635.
41. Goodridge, F., King, C.J.H., *"Techniques of Electroorganic Synthesis"* Part 1, Ed. Weinburg, L., Wiley Interscience (1974).
42. Ondrejcin, R.S., *AEC Research and Development Report, Du Pont de Nemours (E.I.) and Co, Savannah River Lab*, AIKEN, S.C., July 1961, DP-602.
43. Ward, J.W., Waber, J.T., *J. Electrochem. Soc.* 109 (1962) 76.
44. Yoon, J., *Ph. D. Thesis* (1987), University of Newcastle upon Tyne, U.K.
45. Goodridge, F., *J. Chem. Tech. Biotechnol,* 38(1987) 127-42.

Chimica Chronica, New Series, 23, 137-153 (1994)

DAIRY LACTIC ACID BACTERIA PHYSIOLOGY AND GROWTH

I.G. ROUSSIS

Laboratory of Food Chemistry, Department of Chemistry, University of Ioannina, 451 10 Ioannina, Greece

(Received July 17 1993)

SUMMARY

Dairy lactic acid bacteria, *Lactobacillus, Lactococcus, Leuconostoc, Pediococcus* and *Streptococcus salivarius* ssp *thermophilus*, are divided into homofermentatives and heterofermentatives.

Lactococci utilize lactose by phosphenolpyruvate-dependent phosphotransferase system (PEP/PTS) and metabolize both monosaccharide moieties while *Str. salivarius* ssp *thermophilus* and *Lb. delbruckii* ssp *bulgaricus* transport lactose via a permease and can not metabolize the released galactose.

Lactococcus lactis ssp *diacetylactis* and leuconostocs metabolize citrate producing flavour compounds, diacetyl and acetoin.

Casein is essential for growth of lactic acid bacteria in milk in high cell densities, which is limited by the caseinolytic activity of cell-wall associated proteinase.

Starter bacteria possess amino acid and peptide transport systems which work in concert with starter peptidases (cell wall bound, cell membrane and mainly intracellular) for growth in milk.

Lactic bacteria are only weakly lipolytic. Lipase and esterase activities have been detected in cell free extracts of numerous *Lactococcus* and *Lactobacillus* species, while extracellular lipases have also been reported.

In mixed starter cultures, e.g. *Str. salivarius* ssp *thermophilus* and *Lb. delbruckii* ssp *bulgaricus*, the organisms have a favourable interaction.

Growth of mesophilic cultures in milk is limited at pH 4.5 while the thermophilic starters are more acid tolerant and reduce pH to 4.1-3.8. However the cytoplasmic pH seems to have the greater effect on cellular metabolism.

Key words: Lactic acid bacteria, physiology, growth

INTRODUCTION

Lactic acid bacteria (LAB) represents a heterogeneous group of microorganisms with a long and outstanding record as starters in the dairy industry.

These organisms are not only regarded as safe (GRAS), but also considered to be beneficial to health[1].

The main lactic acid bacteria can be classified as follow:

Lactobacillus

The genus *Lactobacillus* comprises about 50 species that can be arranged in three groups.

The obligately homofermentative lactobacilli form the first group (thermobacteria). They ferment hexoses almost exclusively to lactic acid, whereas pentoses not fermented. Typical representatives are *Ld. delbruckii* ssp. *bulgaricus*, *Lb. delbruckii* ssp. lactis, *Lb. acidophilus* and *Lb. helveticus* . The second group (streptobacteria) contains facultatively heterofermentative lactobacilli. They also ferment hexoses almost exclusively to lactic acid, but in addition, they are able to form lactic acid and acetic acid from pentoses. Typical representatives are *Lb. casei*, *Lb. plantarum* and *Lb. sake*. The third group (betabacteria) consists of obligately heterofermentative lactobacilli that ferment hexoses to lactic acid, acetic acid, ethanol and carbon dioxide. The production of gas from hexoses is a characteristic feature of these organisms. Typical representatives are, *Lb. brevis*, and *Lb.fermentum* [2,3].

Lactococcus

All group N "streptococci" form the recently proposed genus *Lactococcus* .

The lactococci are not-motile and usually non-haemolytic. They usually grow in 4% (w/v) NaCl, the exception is *Lc. lactis* ssp. *cremoris* that tolerates only 2% (w/v) NaCl. The ability of lactococci to grow at 10°C but not at 45°C is a characteristic feature that distinguishes them from both streptococci and enterococci. Most lactococci react with group N antisera. However, not all strains reacting with group N antisera are members of the genus *Lactococcus* .

The most common starters are *Lc. lactis* ssp. *lactis*, *Lc. lactis* ssp *cremoris* and *Lc. lactis* ssp *diacetylactis*. The main difference between *Lc. lactis* and *Lc. lactis* ssp. *diacetylactis* is the ability of the latter to metabolize citrate which property is carried on a plasmid. The main character which distinguishes *"lactis"* from *"cremoris"* is the inability of the latter to produce ammonia from arginine[2,3].

Leuconostoc

Leuconostocs can be divided into two groups: (a) the acidophilic *Leuc.oenos* which does not occur in milk and milk products and (b) non acidophilic species which comprise the three sub-species of *Leuc. mesenteroides*, i.e. *mesenteroides*, *dextranicum* and *cremoris*, *Leuc.paramesenteroides* and *Leuc.lactis* .

Leuconostocs are found in dairy starter cultures and may be important in flavour formation because they break down citrate, forming diacetyl from the pyruvate produced. The two organisms for aroma production *Leuc.mesenteroides* ssp. *cremoris* and *Leuc.lactis*. The subspecies *cremoris* ferments few sugars and will only grow in milk if supplemented with yeast extract or amino acids. *Leuc. lactis* ferments lactose more readily than do the other species but only about 50% will grow in unsupplemented milk. Any leuconostoc strains used in the dairy should be screened for their ability to utilize citrate (at pH values below 5.0) as only strains able to do so are of use in starter cultures. Occasional checking is necessary because citrate utilization may be an unstable property[2,3].

Pediococcus

Pediococci are not used in any dairy starters, though they may grow in maturing cheese and ferment residual lactose over a long period. They can also occur in milk and will grow in media selective for lactobacilli.

Morphologically pediococci are ture cocci dividing in two planes and can be mistaken form micrococci. However, they do not possess catalase and are homofermentative, producing large amounts of lactic acid when fermenting glucose.

Only two species, *Ped. pentasaccus* and *Ped. acidilactici* are found in dairy products, neither ferment lactose actively, and milk is a deficient medium for a number of strains of the former species which have a requirement for folinic acid[4].

Streptococcus salivarius* ssp. *thermophilus

Streptococcus salivarius ssp. *thermophilus*, which was formerly known as *"Streptococcus thermophilus"*, is a member of the genus *Streptococcus sensu stricto*, which consists mainly of the pyogenic and the oral or viridans streptococci. On the other hand enterococci and group N lactic streptococci have been assigned to separate genera, namely *Enterococcus* and *Lactococcus* , respectively.

Although lactose is readily fermented, growth in milk may be slow because casein is not readily hydrolysed. It is for this reason that *Str. salivarius* ssp. *thermophilus* is paired with proteolytic partners, e.g., *Lb. delbruckii* ssp. *bulgaricus* for milk fermentrations[2,5].

CARBOHYDRATE CITRATE AND PROTEIN METABOLISM

Dairy lactic acid bacteria have complex nutritional requirements, since they are unable to synthesize many amino acids and vitamins. They grow in milk where there are rich carbon and nitrogen sources. This fact indicates that it can supply them with all essential nutrients such as vitamins, metals and nucleic acid bases.

On the other hand detailed information on the mechanisms of nutrient utilization are confined only to carbohydrates, citrate and proteins (reflecting the relative importance of carbohydrates and proteins to the growth of the organisms in milk and fermented dairy products). Carbohydrate metabolism is particularly well documented, but protein utilization has not sufficiently clarified[6].

Carbohydrate

The lactic acid bacteria can be divided into two groups depending whether their main pathway of glucose fermentation is the Embden-Meyerhof (EM) glycolytic pathway (homofermentative) or a combination of the hexose monophosphate (HMP) followed by the phosphoketolase pathways (heterofermentative) [Fig.1, Table 1][4].

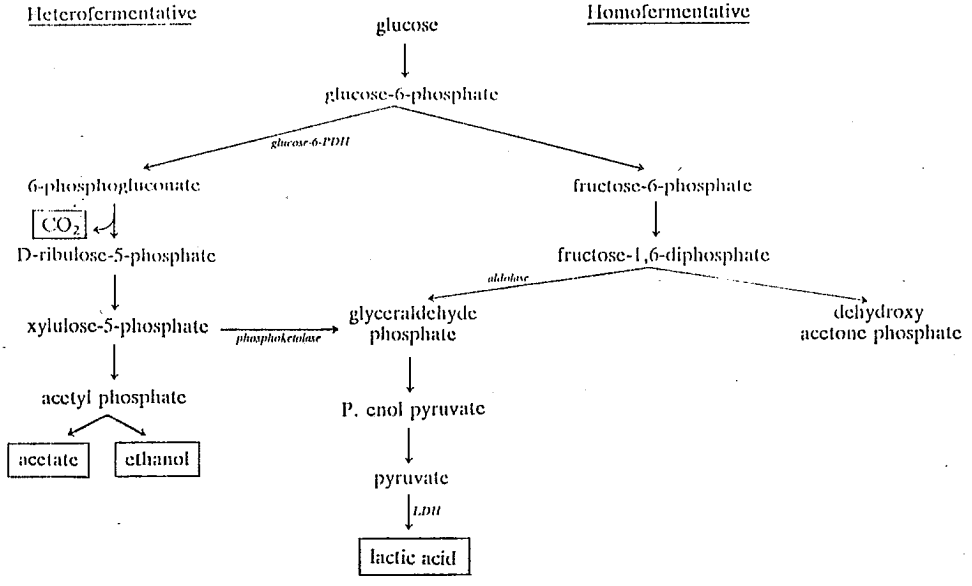

FIG. 1. *Glycolytic pathways in lactic acid bacteria.*

However, some species normally forming only lactic acid also have enzymes associated with heterofermentative pathways. When substrates other than glucose are fermented or glucose is fermented in conditions of stress, metabolism can be affected and other end products may be formed.

In the lactic acid bacteria the pathway of glucose fermentation can be ascertained by the end products formed: CO_2, acetate, ethanol and lactic acid. The fermentation route can also be established by detecting key enzymes. The presence of fructose -

1,6 - diphosphate (FDP) aldolase shows that strains have the EM pathway while glucose - 6 - phosphate dehydrogenase (G-6-PDH) indicates heterofermentative species.

TABLE I. Metabolic pathways in lactic acid bacteria

Genus	Sub-genus	Metabolic pathway		
		Embden-Meyerhof	Hexose-monophosphate	Phospho-Ketolase.
Lactococcus	all species	+	-	-
Leuconostoc	all species	-	+	+
Pediococcus	all species	+(probably)	-	-
Streptococcus salivarius ssp thermophilus		+	-	-
Lactobacillus	thermobacteria	+	-	-
	streptobactera	+	(+)	(+)
	betabacteria	-	+	+

+, present; (+), present but used only under special conditions; -, not present

Lactate dehydrogenases (LDH_S) are found in all lactic acid bacteria, and catalyse the final step in their energy - producing metabolism. The types of lactate formed by lactic acid bacteria important in dairying are given in Table 2 [4].

The ability to utilize lactose is essential for starter growth in milk

In lactococci this is mediated by a phosphenolpyruvate - dependent phosphotransferase system (PEP/PTS) which catalyses the transport and concomitant phosphorylation of this sugar resulting in its intracellular accumulation in a phosphorylated form. The PEP/PTS consists of four components, enzyme I (EI), enzyme II(EII), heat stable protein (HPr) and factor III (FIII). The phosphate group is donated by phosphoenolpyruvate which is converted to pyruvate and is transferred to lactose during its transport via the lactose-specific components FIII and EII which are located at the cytoplasmic membrane.

Lactose - 6 - phosphate is then hydrolyzed by phospho -β - D - galactosidase (β-P gal) to yield glucose and galactose - 6 - phosphate.

The galactose phosphate is metabolized to triose phosphate directly via the tagatose phosphate pathway, analogous to the fructose phosphate pathway from glucose[7].

TABLE II. Isomer of lactate formed by dairy lactic acid bacteria

D(-)	L(+)	DL
All leuconostocs	All lactococci	*Lb. helveticus*
		plantarum
Lb. lactis	*Lactobacillus casei*	*Lb. fermentum*
Lb. delbruckii ssp	(a trace of D(-)	*brenis*
bulgaricus	is also found)	
		Ped. pentosaccus
		acidilactici

Some lactic acid bacteria transport lactose via an ATP energized permease as the free sugar and use their β-D-galactosidase (β-gal) to cleave it into two unphosphorylated monosaccharides.

The reaction catalysed by β-Pgal differs from that of β-gal in that one of the monosaccharide (galactose) is already phosphotylated[6]. *Str. salivarius* ssp *thermophilus*, *Lb.delbruckii* ssp *bulgaricus* and *Lb. helveticus* use the permease transport system and hydrolyse the lactose with intracellular β-gal.

Str. salivarius ssp *thermophilus* and *Lb. delbruckii* ssp *bulgaricus* can not metabolize the released galactose and excrete it from the cells (into the external medium)[6].

Some strains phosphorylate the galactose at the carbon 1 position with a galactokinase. This sugar then enters the Leloir pathway and galactose - 1 - P is converted first to glucose 1 - P and then to glucose - 6 - P [6].

Citrate

In lactic acid bacteria, diacetyl and acetoin are not produced from carbohydrate unless an additional source of pyruvate is present. This is because in homofermentative organisms there is a need to reduce all the pyruvate derived from the carbohydrate to lactate to regenerate oxidized pyridine nucleotides. Those bacteria which use the heterofermentative pathway have greater versality, but the enzymes leading to production of diacetyl and acetoin are often repressed. Citrate metabolism provides a means of producing "surplus" pyruvate[3].

Neither *Lc. lactis* ssp. *diacetylactis* nor the leuconostocs can use citrate as an energy source, but both will utilize citrate in the presence of a metabolizable carbon source [3,6,7]. Metabolism of citrate by *Lc. lactis* ssp *diacetylactis* and *Leuconostoc* species results in the production of diacetyl and acetoin[6,7].. Citrate enters the cell via a citrate permease which has been shown to be encoded on a plasmid in all *Lc. lactis*

ssp. *diacetylactis* strains examined. Loss of this plasmid leads to the inability of the cell to transport citrate but citritase activity is maintained[7]. Once inside the cell, citrate is converted to oxaloacetate and acetate by citricase (citrase lyase). This enzyme is constitutive in *Lc. Lactis* ssp. *diacetylactis* but inducible in *Leuconostoc* . Oxaloacetate is decarboxylated via pyruvate to acetaldehyde - TPP (thiamine pyrophosphate) which condenses either with acetylo - CoA to form diacetyl or with another molecule of pyruvate to form acetolactate, which is decarboxylated to acetoin[3,7].

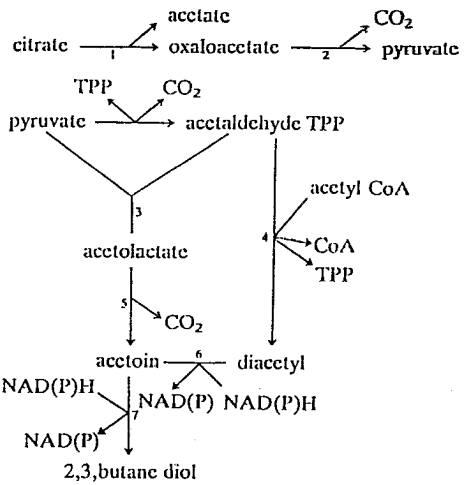

FIG.2. *Pathway of citrate metabolism: 1, citrase lyase; 2, oxaloacetate decarboxylase; 3, acetolactate synthase; 4, diacetyl synthase; 5, acetolactate decarboxylase; 6, diacetyl reductase; 7, acetoin reductase.*[7]

The pathway of citrate utilization is shown in Fig. 2[6].. The four enzymes, citrate lyase, acetolactate synthase, diaxetyl reductase and acetoin reductase have been characterized in *Lc. lactis* ssp. *diacetylactis, Leuc: lactis* and *Lb. plantarum*[6].

Diacetyl and acetoin accumulate because citrate represses synthesis of diacetyl reductase and acetoin reductase, the necessary regenaration of oxidized pyridine nucleotides being provided by reduction of pyruvate to lactate[3,7].

It is clear that production of intracellular acetoin exceeds diacetyl because there are two pathways leading to its synthesis from citrate. There are some reports of acetoin: diacetyl ratios being as high as 43:1 [3].

Protein

Starter bacteria are considered as the organisms added to milk whose basic function is the fermentation of lactose to lactic acid. For most purposes these selected

organisms must produce acid rapidly, which requires rapid growth to high cell densities in milk[9].

Growth of typical lactococcal strains in milk results in maximum cell densities of ~500μg (dry weight) bacteria/ml (or about 10^9 cfu/ml). This growth requires the synthesis of ~260μg bacterial protein/ml. The concentration of essential amino acids (in free form) in milk is usually well below the minimum required for this cell protein synthesis. Even if all the amino acids in the non-protein nitrogen fraction were readily available, the levels of most essential amino acids in low molecular weight form would still limit starter growth in milk. With respect to amino acid requirements, *Streptococcus salivarius* ssp *thermophilus* and lactobacilli (*Lb.helveticus*) appear to be at least as fastidious as the lactococci[10].

The potential sources of nitrogen for starter growth in milk are casein, whey proteins and low molecular weight compounds.

Experimental data indicate that the free amino acids initially present in milk are an important nitrogen source for growth at low cell densities. The decline in specific activity of bacterial protein after two or three generations indicates that as the cell density reaches 8 to 16% of the maximum (i.e. that found in coagulated milk), then amino acids are supplied increasingly from other sources.

The low molecular weight peptides in milk are a significant potential source of nitrogen. Experimental data suggest that the peptides originally present in the milk supplied an almost constant proportion of the nitrogen used for cell growth. However, the contribution of these peptides to the total nitrogen requirement must be small[9].

The use of milk protein as a nitrogen source has been clearly demonstrated. Experimental data indicate that milk protein becomes an increasingly important source of nitrogen as the cell densities increases[9].

It is known that caseins (mainly αs1 - αs2, - β - and k - caseins, 4:1:3:1), which occur as micelles, have an open, rargely random structure which makes them readily susceptible to proteolysis. In contrast, the principal whey proteins (β-lactoglobulin and α-lactalbumin) are globular molecules with a high degree of secondary and tertiary structure. In undenatured form steric factors make whey proteins remarkably resistant to proteolysis[10].

The presence of casein in milk is clearly important in nitrogen nutrition since its removal necessitates supplementation of whey with hydrolysed protein to obtain adequate growth of starters[9].

Casein degradation by starter bacteria yields free amino acids, as well as low - and high - molecular - weight peptides. These are the sources of essential and growth -

stimulating amino acids for starter bacteria. On the basis of casein hydrolysis studies with several *Lactococcus* strains, β-casein seems to be the most readily utilized milk protein. Growth studies with different caseins alone and in combinations (as the sole source of organic nitrogen) revealed that β-casein in combination with a relatively low concentration of κ-casein supported maximal growth. Therefore, the soluble β-casein fraction, which is in equilibrium with micellar β-casein, and the easily accessible hydrophilic part of micellar κ-casein are most likely the major sources of essential and growth - stimulating amino acid for lactococci [11].

Since lactic acid bacteria have complex amino acid requirements, the efficient operation of proteolytic enzymes coupled to peptide and amino acid uptake systems is essential .These enzymes and uptake systems work in concert and are termed the proteolytic system[7].

Uptake systems

Three different systems have been indentified for amino acid uptake. The first couples amino acid transport to a proton motive force (PMF). The second means of amino acid transport is an exchange system where downhill influx of a precursor is coupled to downhill efflux of a product. The third method of amino acid transport is a phoshate - bond linked system where hydrolysis of a high energy phosphate intermediate such a ATP is coupled to solute translocation across the membrane.

Three different modes of peptide [4, 5 or 6 amino acids] utilization have been proposed. The first model envisages the coupling of peptide uptake and hydrolysis by a transmembrane peptidase which results in release of free amino acids into the cell. The second model proposes that the peptide is cleaved extracellularly by a peptidase and the liberated amino acids are subsequently taken up by membrane located amino acid carriers. The third model, which seems most probable, presents a two step process where peptides are transported into the cell via specific transport systems and are hydrolysed in the cellular cytoplasm by peptidases[7].

Proteolytic enzymes

The proteolytic enzymes of starter bacteria are considered to consist of two functionally distinct classes of enzymes - proteinases, which catalyse the hydrolysis of protein molecules, and peptidases, which catalyse the degradation of the smaller peptides produced by proteinase action[10].

Proteinases

Starter bacteria generally do not secrete significant levels of proteinases into the growth medium. However some *Lc. lactis* ssp. *cremoris* strains produced free extracellular proteinases, in addition or not to cell-wall associated proteinase[10].

The proteinases primary responsible for the extracellular proteins are bound to the cell wall. The proteinase activity can be partially or wholly released from this side by incubation in Ca^{2+} - free buffer, or by use of lysozyme or phage lysin treatment[10]. In general these enzymes appear to be high Mr proteins (80-140 KDa), to have pH optima around 5.5 - 6.5, to be activated or stabilized by Ca^{2+} and to be inhibited by serine proteinase inhibitors (PMSF, DFP)[7].

Two main types of proteinase activity, PI and PIII, were distinguished. PI degrades β-casein with only a very slow hydrolysis of a-casein while PIII degrades β-casein in a manner different to PI-type in addition to α- and κ-casein. In addition a third category of enzyme is present in the lactococci, a naturally occuring hybrid of the PI and PIII types, which degrades β-casein in a manner similar to the PI enzyme but it also hydrolyses α-casein in a manner somewhat different to PIII proteinases[7].

It has been reported intracellular proteinase activities. Some of them only weakly hydrolyse caseins and more rapidly break down shorter peptides[12]. However since cross-contamination of cell fractions could have occured the true intracellular status of these enzymes is quenstionable[7].

Peptidases

Much work focused on specificities and cellular location of starter peptidases. However, this work has suffered from the experimental procedures used for enzyme (endopeptidase) activity and cell fractionation. Despite this, there is now sound evidence for the existence of intracellular, cell membrane and cell wall bound peptidases, the majority of which indicate intracellular location[7,12].

The principal peptidases in the starter bacteria appear to be exopeptidases which catalyse cleavage of one or two amino acids from the free N-terminal of the peptide chain. Exopeptidase activity is exemplified by amino - , di- and tripeptidases. Endopeptidases in contrast can cleave a large peptide at some point, within the peptide, removed from the carboxyl or amino terminal end. In this respect a proteinase can be regarded as an endopeptidase[7]. However starter proteinases can be distinguished in that they can hydrolyze casein molecules while starter endopeptidases hydrolyse small peptides (3-4 kDa).

Since β-casein has a high proline content its hydrolysis by the cell wall proteinases leads to proline-rich oligopeptides. Five types of exopeptidase are known which cleave peptide bonds involving proline (these bonds can be hydrolysed only by proline-specific peptidases). These are aminopeptidase P (proline aminopeptidase, x....Pro....y....), proline iminopeptidase (prolyl aminopeptidase, (Pro... x .....), proline iminodipeptidase

(prolyl dipeptidase, prolinase, Pro... x), imidodipeptidase (proline dipeptidase, prolidase, x.... Pro) and dipeptidylamino peptidase (x....Pro.....y.....)[7,13].

The observation that proteinase-negative (Prt-) cells grow at the same initial rate as the parent Prt+ cells confirms that proteinase in not important for growth in milk at low cell densities (<10^8 cfu/ml). It is of interest to note that while Prt- variants are deficient in cell wall-bound proteinase. These cells contain peptidase activities and peptide transport systems which appear to be similar to those in the parent cells. Prt- variants reach only 10-25% of the maximum cell density attained by Prt+ organisms in milk cultures, which is consistent with the cell density of which protein becomes an important nitrogen source[9].

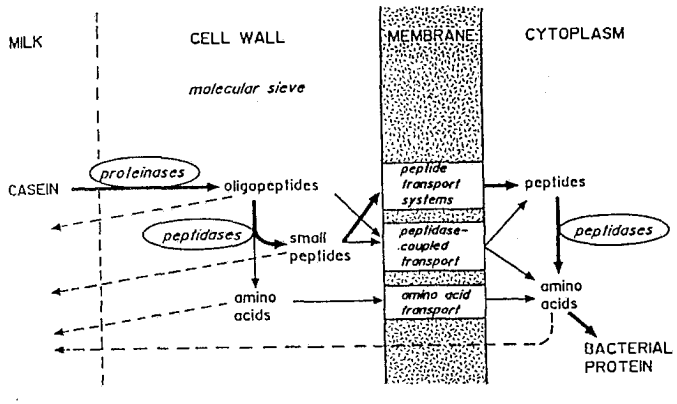

FIG.3. *Location of proteolytic enzymes and utilization of casein for growth of lactococci in milk.*

The concentration of proteolysis products in the medium at the cell surface will depend upon the balance between the local rate of production of these nutrients and the rate of diffusion away from the cell surface. If diffusion is the more rapid process then at low cell densities the low proteinase level would be ineffective since the concentration of proteolysis products is likely to be insufficient to saturate peptidases and/or uptake systems. Most lactococci, and *Lb. delbruckii* ssp *bulgaricus* grow exponentially in milk which means that proteinase activity must begin to function effectively in supplying proteolysis products before the concenration of the low molecular weight nitrogen initially present becomes rate limiting. Those strains of lactococci which do not grow exponentially in milk, but change to a slower rate at

~25% of the maximum cell density, may have a limiting proteolytic activity. The fact that addition of peptides to milk invariably increases the growth rate suggests that some step in the supply of nitrogen is rate limiting with all starter bacterial[9].

Recent experiments with lactococcal strains showed that overproduction of cell envelope-located or secreted proteinase resulted in a 20% higher specific growth and acidification rate in milk. These results indicate that the growth of lactococci in milk is limited by the caseinolytic activity of the proteinase[14].

Subsequently proteolysis is unlikely to be as important as the efficacy with which peptidases and membrane transport systems can utilize those peptides containing essential amino acids.

There is no evidence that peptides per se can be incorporated directly into protein so that peptidases must catalyse complete peptide hydrolysis. The proteinase and peptidase systems of starter bacteria therefore both play vital roles for growth in milk by producing from milk protein the essential amino which would otherwise limit growth[9].

A general scheme for utilization of casein for growth of lactic acid bacteria in milk is presented in Fig.3. Additional extracellular endopeptidase(s) activity may improve this scheme. However, although different endopeptidases have been studied in lactococci, their cellular locations are still not clear[15-18].

LIPOLYTIC ACTIVITIES

Lactic acid bacteria are only weakly lipolytic when compared with such activity by many groups of bacteria[19].

Intracellular and extracellular lipases have been reported for lactococci and lactobacilli but the experimental methods to differentiate the locations were not infallible.

In general, the lipase activity of cell suspension is considered to be extracellular and the activity of cell - free extracts as intracellular.

The majority of studies have cited lipase activities in cell-free extract[8,19-22]. On the other hand *Lb.* casei exhibited both intracellular and extracellular lipase activities [19].

Lipase and esterase activities have been detected in cell-free extracts of numerous *Lactococcus* and *Lactobacillus* species[8,19].

A preference for liberation of shorten-chain fatty acids has been observed for lactococci, and lactobacilli. In contrast, it has been reported that long chain fatty acids

(C16:0 and C18:1) accumulated in greatest quantities when lipases from *Lb. casei* were incubate with milk fat[19].

It has been found that lactococci and lactobacilli cells derived from the logarithmic phase needed the shortest incubation time to cause a colour change in milk fat stained with Victoria blue or Nile blue [degree of lipolysis]. Similarly the esterase activity of cell-free extracts from cells of lactococci have been observed late in the logarithmic growth phase[19].

MIXED CULTURES

Mesophilic species

When mixed-strain starters include aroma production such as *Leuc. lactis* and *Lc. lactis* ssp. *diacetylactis* rates and extent of aroma production vary.

Cultures containing *Lc. lactis* ssp. *diacetylactis* begin to metabolize citrate as soon as growth begins and lactic acid is produced. However, cultures containing leuconostocs show a lag in citrate utilization and unlike the *Lactococcus* may not dissimilate all the available citrate. Thus the rate of diacetyl production will differ depending on starter composition [3].

Production of diacetyl by the leuconostocs is favoured by low pH and combination of these bacteria with *Lc. lactis* ssp. *cremoris* and/or *Lc. lactis* ssp. *lactis*, which lower pH quite rapidly is therefore an advantage[6].

In all types of mixed culture the level of diacetyl declines once all the citrate is utilised as a result of increased synthesis of diacetyl reductase. Prompt cooling to 2°C prevents this reduction and if cooling is carried out just before citrate utilization is complete the synthesis of diacetyl reductase will remain repressed[3].

Thermophilic species

The best documented example of associative growth is that of *Str., salivarius* ssp. *thermophilus* and *Lb. delbruckii* ssp. *bulgaricus*. These organisms have an interaction in milk which is mutually favourable but not interdependent [i.e., proto-cooperative rather than symbiotic growth][3].

In mixed culture the rate of acid production and usually the liberated tyrosine (index of proteolysis) are greater than the sum of the two single cultures growing under the same conditions[3,23].

Lactobacilli are highly proteolytic and *Str. salivarius* ssp. *thermophilus* is less proteolytic. The streptococcus benefits by using small peptides liberated from casein by proteolytic enzymes of the lactobacillus. Actively growing streptococci in turn

release formate as an end metabolite which stimulates the lactobacillus [it is possible that formate promotes purine synthesis and cell division]. The streptococcus also releases CO_2 from urea catabolism which further stimulates growth of the lactobacillus [3,6].

TEMPERATURE AND pH OF FERMENTATION

The optimum temperature for growth of mesophilic starters lie between 25 and 30°C. At 30°C the lactococci have mean generation time in milk of 60-70 min and grow to a maximum cell density of 0.5 mg dry weight of bacteria per ml. In complex broth media the same organisms have doubling times of 35-40min. Growth is limited as a result of low pH [4.5].

Commercial milk cultures of the cheese starter strains are generally prepared of slightly sub-optimal temperatures [22-25°C] in order to balance high cell numbers against over-acidification. Single strain starter cultures grown in separated milk at 25°C reach maximum cell numbers at pH 4.65 and this value (corresponding to about 0.7% lactic acid) is usually taken as the optimum for good subsequent acid development in cheese vats. If cultures are allowed to develop more acidity, their lag phase, on subculture to cheesemilk, is lengthened, presumably due to damage to cells by low pH and lactic acid.

During some cheesemaking processes [e.g. Cheddar] the starter lactococci are required to produce lactic acid at temperatures of up to 40°C. At such superoptimal temperatures, growth and acid production become uncoupled, especially in *Lc. lactis* ssp. *cremoris*, which is more temperature sensitive than *Lc. lactis* ssp. *lactis* [6].

The thermophilic starters, *Str. salivarius* ssp. *thermophilus* and the lactobacilli, are more acid tolerant and will reduce the pH to 4.1 in the case of *Str. salivarius* ssp. *thermophilus* and to 3.8 in the case of *Lb. delbruckii* ssp. *bulgaricus* when grown in milk at 42°C.

Molar growth yields for a number of lactobacilli may be temperature - dependent. For example, those of *Lb. lactis* and *Lb. delbruckii* ssp. *bulgaricus* are lower when grown at 40°C than at 37°C [3 moles ATP per mole of glucose at 40°C and 2 at 37°C][6].

Although the pH of the medium or extracellular pH indirectly influences cell growth and metabolism, it is the intracellular or cytoplasmic pH that ultimately has the greater effect on cellular metabolism. Several metabolic activities in starter acid bacteria, for example, have been reported to be regulated by the intracellular pH, including amino acid and peptide transport systems[24].

It has been observed that rapid growth of lactococci and streptococci in media containing excess lactose did not occur when the intracellular pH was reduced below a critical pH of 5.0[24], and that growth and lactate production are limited by undissociated lactic acid in cultures of *Lb. helvericus*, whereas the pH value of the medium had only an indirect effect[25].

ΠΕΡΙΛΗΨΗ

ΓΑΛΑΚΤΙΚΑ ΒΑΚΤΗΡΙΑ: ΦΥΣΙΟΛΟΓΙΑ ΚΑΙ ΑΝΑΠΤΥΞΗ

Τα γαλακτικά βακτήρια - *Lactobacillus, Lactococcus, Leuconostoc, Pediococcus* και *streptococcus salivarius ssp thermophilus*, διακρίνονται σε ομοζυμωτικά και ετεροζυμωτικά.

Τα lactococcus χρησιμοποιούν την λακτόζη μέσω ενός συστήματος φωσφοτρανσφεράσης και μεταβολίζουν και την γλυκόζη και την γαλακτόζη ενώ τα *Str.salivarius ssp. thermophilus* και *Lb.delbruckii ssp bulgaricus* εισάγουν στο κύτταρο την λακτόζη με μιά περμεάση και δεν μεταβολίζουν την απελευθερούμενη γαλακτόζη.

Το *Lactococcus lactis ssp diacetylactis* και τα leuconostocs μεταβολίζουν τα κιτρικά και παράγουν ενώσεις αρώματος, διακετύλιο και ακετοΐνη.

Για την ανάπτυξη των οξυγαλακτικών βακτηρίων στο γάλα σε υψηλές πυκνότητες κυττάρων η καζεΐνη είναι απαραίτητη πηγή αζώτου. Η ανάπτυξή τους δε στο γάλα περιορίζεται απο την καζεϊνολυτική δράση των πρωτεϊνασών κυτταρικού τοιχώματος.

Τα οξυγαλακτικά βακτήρια έχουν συστήματα εισαγωγής στο κύτταρο αμινοξέων και πεπτιδίων τα οποία συνδυάζονται με τις πεπτιδάσες αυτών των βακτηρίων (κυτταρικών τοιχωμάτων,μεμβανών και κυρίως ενδοκυτταρικά) για την ανάπτυξή τους στο γάλα.

Τα οξυγαλακτικά βακτήρια είναι ασθενώς λιπολυτικά. Λιπολυτικές και εστερασικές δραστικότητες έχουν ανιχνευθεί σε κυτταρικά εκχυλίσματα πολλών ειδών των γενών *Lactococcus* και *Lactobacillus*, ενώ επίσης έχουν αναφερθεί και εξωκυτταρικές λιπάσες.

Στις μικτές καθαρές καλλιέργειες (starters) όπως των *Str. salivarius ssp. thermophilus* και *Lb.delbruckii ssp bulgaricus*, οι μικροοργανισμοί έχουν θετικές αλληλεπιδράσεις.

Η ανάπτυξη των μεσόφιλων οξυγαλακτικών starters στο γάλα περιορίζεται σε pH 4,5 ενώ οι θερμόφιλοι είναι πιο οξεάντοχοι και μειώνουν το pH σε 4,1-3,8 (pH μέσου

ανάπτυξης). Όμως το ενδοκυτταρικό pH φαίνεται να έχει μεγαλύτερη επίδραση στον κυτταρικό μεταβολισμό απ' ότι στο pH του μέσου.

REFERENCES

1. Aguilar, A., In: *LAB research and industrial application in the agro-food industries.* Caen France (1991).

2. Schleifer, K.H., *FEMS Microbiology Reviews*, **46**, 201 (1987).

3. Marshall, V.M., *FEMS Microbiology Reviews*, **46**, 327 (1987).

4. Garvie, E.I., In: *Advances in the microbiology and biochemistry of cheese and fermented milk*, Elsevier Applied Science Publishers Ltd., London and New York (1984).

5. Schleifer, K.H. In: *LAB research and industrial application in the agro-food industries.* Caen France (1991).

6. Marshall, V.M.E. and Law, B.A. In: *Advances in the microbiology and biochemistry of cheese and fermented milk*, Elsevier Applied Science Publishers Ltd., London and New York (1984).

7. Law, J.M. *Biochemistry and genetics of the proteolytic system in Lactococcus* . Ph.D. Thesis. University College Cork, Ireland (1991).

8. Olson, N.F. *FEMS Microbiology Revies*, **87**, 131 (1990).

9. Thomas, T.D. and Mills, O.E. *Netherlands Milk Dairy Journal*, **35**, 255 (1981).

10. Thomas, T.D. and Pritchard, G.G. *FEMS Microbiology Reviews*, **46**, 245 (1987).

11. Smid, E.J., Poolman, B. and Konings, W.V. 1991. *Applied and Environmental Microbiology* , **57(9)**, 2447 (1991).

12. Gripon, J.-C. Monnet, V., Lamberet, G. and Desmazeaud, M.J. In: *Food Enzymology*, V.1. Elsevier Science Publishers Ltd . London (1991).

13. Khalid, N.M. and Marth, E.H.*Journal Dairy Science*, **73**, 2669 (1990).

14. Bruinenberg, P.G., Vos, P. and De Vis, W.W. *Applied and Environmental Microbiology* , **58(1)**, 78 (1992).

15. Exerkate, F.A. *Applied and Environmental Microbiology*, **47(1)**, 177 (1984) .

16. Yan, T-R., Azuma, N., Kaminogawa, S. and Yamauchi, K. *Applied Environmental Microbiology* , **53(10)**, 2296 (1987).

17. Yan, T-R., Azuma, N.Kaminogawa, S., and Yamauchi, K., *European Journal Biochemistry* , **54**, 259 (1987).

18. Tan, P.S.T., Ros, K.M. and Konings, W.N. *Applied and Environmental Microbiology*, **57(12)**, 3593 (1991).

19. Kamaly, K.M. and Marth, E.M. *Journal Dairy Science*, **72**, 1945 (1989).

20. Singh, A., Srinivasan, R.A. and Dudani, A.T. *Milchwissenchaft* , **28(3)**, 164 (1973).
21. El Soda, M., Abd El Wahab, H., Ezzat, N., Desmazeand, M.J. and Ismail, A. *Le Lait*, **66(4)**, 431 (1986).
22. El Soda, M., Korayem, M. and Ezzat, N. *Milchwissenchaft* , **41(6)**, 353 (1986).
23. Rajagopa,, S.N. and Sandine, W.E. *Journal Dairy Science*, **73**, 894 (1990).
24. Nannen, N.L. and Hutkins, R.W., *Journal Dairy Science*, **74**, 741 (1990).
25. Gatje, G. and Gottschalk, G. 1991. *Applied Microbiology Biotechnology*, **34**, 446 (1991).

Chimica Chronica, New Series, 23, 155-168 (1994)

PREPARATION AND PROPERTIES OF MANGANESE (II) AND MANGANESE (III) COMPLEXES POSSESSING LIGANDS WITH CARBOXYLATE AND PHENOLIC / PHENOXIDE GROUPS

A.L.PETROU [1*] and S.P.PERLEPES [2]

1. *Laboratory of Inorganic Chemistry, University of Athens, Panepistimiopolis, Kouponia, Athens 15701, Greece.*
2. *Department of Chemistry, University of Patras, Patras, Greece.*

(Received March 22 ,1994)

SUMMARY

Trinuclear complexes of hydrocaffeic and caffeic acids with manganese (II) have been prepared and studied. The proposed Mn_3^{II} - core geometry, is supported by various spectroscopic (diffuse reflectance, i.r.), magnetic, thermogravimetric and potentiometric data. Ferulic acid forms an oligonuclear complex the structure of which involves coordination of both carboxylate (monodentate) and deprotonated phenolic (phenoxide) oxygen (terminal or bridging) groups.

Key words : hydrocaffeic , caffeic , ferulic acid complexes , Mn_3 - core geometry , oligonuclear complex

INTRODUCTION

Recent interest in manganese chemistry has been motivated by a variety of reasons. The main ones are (i) the identification of Mn-containing enzymes [1-5], and (ii)

* Author to whom correspondence should be addressed.

the propensity of higher nuclearity Mn clusters to display large spin ground states[6-8].The former reason has stimulated intense research to understand the coordination chemistry of Mn in the intermediate oxidation-state range (II-IV) and nuclearity 2-4 with mainly O- based biologically - relevant donor groups(oxo, carboxylato , phenoxo etc...), followed by assessment of physical and spectroscopic properties with a goal to gaining insights into the nature and mode of action of the biological Mn sites. The latter reason has led to a search for preparative methodology to higher nuclearity ($\geq$6) Mn compounds and a desire to understand the factors that lead to large ground-state spin values in these and lower nuclearity species.

We have been investigating the coordination chemistry of the biologically- important mixed carboxylate/ phenoxide ligands 3,4- dihydroxyphenylpropionic acid (dihydrocaffeic acid , hydcafH_3) *(1)*, trans - 3-(3,4- dihydroxyphenyl) propenoic acid (caffeic acid , cafH_3)*(2)* and 3-(4-hydroxy-3-methoxyphenyl) propenoic acid (ferulic acid, ferH_2) *(3)*, with first- row transition metals:

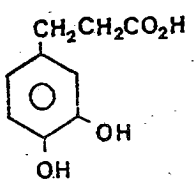

(1)

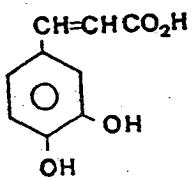

(2)

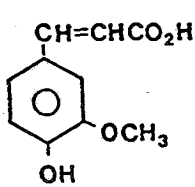

(3)

Our work to date has concentrated on vanadium [9], iron[10], cobalt [10], nickel [10], copper[10] and zinc [11]. Herein are described the results of our investigation with manganese. Prior reports of the synthesis and properties of manganese complexes with ligands simultaneously containing carboxylate and phenolic functionalities are few. Christou et al. have reported two remarkable manganese complexes with salicylic acid

($salH_2$).The nonanuclear complex [$Mn^{III}_8Mn^{II}O_4(O_2CPh)_8(py)_4(sal)_4(salH)_2$] [12] (py=pyridine) contains two recognizable $[Mn_4O_2]^{8+}$ units held together via the intermediacy of an $Mn^{II}(sal)_4$ bridging unit. The anion of $[Mn^{II}(EtOH)_4]$ $[Mn^{III}_2(sal)_4(py)_2]$ [13] consists of two Mn^{III} atoms bridged by two μ -phenoxo oxygen atoms from salicylate groups whose carboxylates are also bound to the metal . The cation consists of a Mn(II) atom which possesses four EtOH and two trans oxygen ligands, the latter belonging to salicylate carboxylate groups in the anion.

EXPERIMENTAL

The chemicals used were commercially- available products of Fluka and Merck. Their purity was checked by mass spectra:m/e of the molecular ions 182(calcd. 182.2), 180(calcd. 180.2), 194(calcd. 194.2) for hydrocaffeic, caffeic and ferulic acids, respectively. Their sodium salts $hydcafH_2Na.H_2O$, $cafH_2Na.H_2O$ and $ferHNa.H_2O$ have been prepared and characterised as before[10]. For the preparation of the complexes, to solutions of the ligands (0.01 mole) in 90% MeOH solutions of KOH (0.01 mole) in 90%MeOH were added dropwise with stirring . To the clear solutions so obtained, solutions of $MnCl_2.4H_2O$ (0.005 mole) in 90% MeOH were gradually added, until a final ratio of Mn: acid ligand :KOH of 1:2:2 were obtained. A broun solution with a broun solid resulted in the case of $hydcafH_3$, a deep broun solid in the case of $cafH_3$ and a beige solid in the case of $ferH_2$. After filtration, the prepared compounds were washed with MeOH and dried over P_4O_{10} for several days. The Mn contents were analysed after titration with EDTA [14]. The K contents

were determined with (ion-selective) Potassium Electrode. Elemental analyses, physicochemical and spectroscopic measurements were carried out by published methods [15]. Magnetic susceptibilities in the solid state were determined at room temperature (24^0C) by the Faraday method using a Cahn- Ventron RM- 2 balance. Mercuric tetrathiocyanate cobaltate (II) was used as standard. The magnetic susceptibilities were corrected for diamagnetic ligand contribution.

RESULTS AND DISCUSSION

Preparative data, elemental analyses, and molar conductivities of the three complexes are reported in TABLE I. After some preliminary experimentation , the procedure described in the experimental section has been found to give consistently pure products; we have by no means explored all possible combinations of solvents and reagent ratios and, consequently, do not claim these procedures to have been optimized. We have noticed that small changes to the ligand: OH^- ratios have noticeable effects on the identity of the products or their yields. Analytical data necessitate a manganese (III) oxidation level for *(6)*, which could easily be rationalized as arising from a redox reaction involving atmospheric oxygen , a common occurrence in manganese (II) chemistry. The formulae of *(4)* and *(5)* establish them as being manganese (II) species. The colour changes during the reactions of $hydcafH_3$ and $cafH_3$ with manganese (II) in the presence of alkali and the rather low yields of *(4)* and *(5)* indicate that firstly manganese (III) species form in solution. Since the phenolic ligands employed are readily oxidizable, in addition to be good metal- binding ligands , it seems possible that a second redox reaction takes place leading to manganese (II) . The ability of manganese (III) to oxidize phenolic substrates is well - known and the use of manganese (III) complexes for such oxidations is common in organic chemistry [16]. Consequently, we refrain from attempting to rationalize with a

TABLE I.Preparative data, colours, analytical results and molar conductivities of the complexes.

Complex	Yield[a] %	Colour	Found (Calcd.) % Mn	C	H	K	Cl	Λ^{b}_{M}(Scm^2mol^{-1}) DMSO	MeOH
(4) $[Mn_3(hydcafH_2)_6(H_2O)_6]$. 6KCl	50	broun	9. 06 (9.12)	35.35(35.90)	3.12(3.69)	12.80(12.98)	10.96(11.77)	149.5	492.3
(5) $[Mn_3(cafH_2)_6(H_2O)_6]$. 6KCl	65	deep broun	9.08 (9.18)	36.87(36.13)	3.19(3.04)	12.76(13.06)	11.34(11.85)	133.3	442.2
(6) $KMn(fer)_2 . H_2O$. MeOH	55	beige	10.60 (10.39)	48.34(47.72)	4.98(4.20)	6.95(7.40)		29.4	103.6

a) Based on the metal.

b) Molar conductivities for ca. 10^{-3}mol .dm^{-3} solutions .

balanced equation what is obviously a complex reaction system; suffice it to say that complexes *(4)* and *(5)* must be the thermodynamically governed products of their reaction mixtures. Why only ferulic acid stabilizes manganese (III) is rather difficult to rationalize . Several suggestions are possible, e.g. , the presence of only one - OH group in $ferH_2$, the domination of fer^{-2} rather than $ferH^-$ in the reaction mixture , etc., but all are highly speculative. In the absence of a suitably discriminating spectroscopic handle to monitor solution species , we have not pursued this matter further.

The molar conductivities of *(4)* and *(5)* are only due to the contained KCl and the molar conductivity of *(6)* being rather low indicates large size of the manganese-containing ion [17]. In a nitrogen atmosphere the three complexes are decomposed (t.g./ d.t.g. ,thermogravimetric / differential thermogravimetric analysis). Their thermal decomposition is shown in FIG. 1.

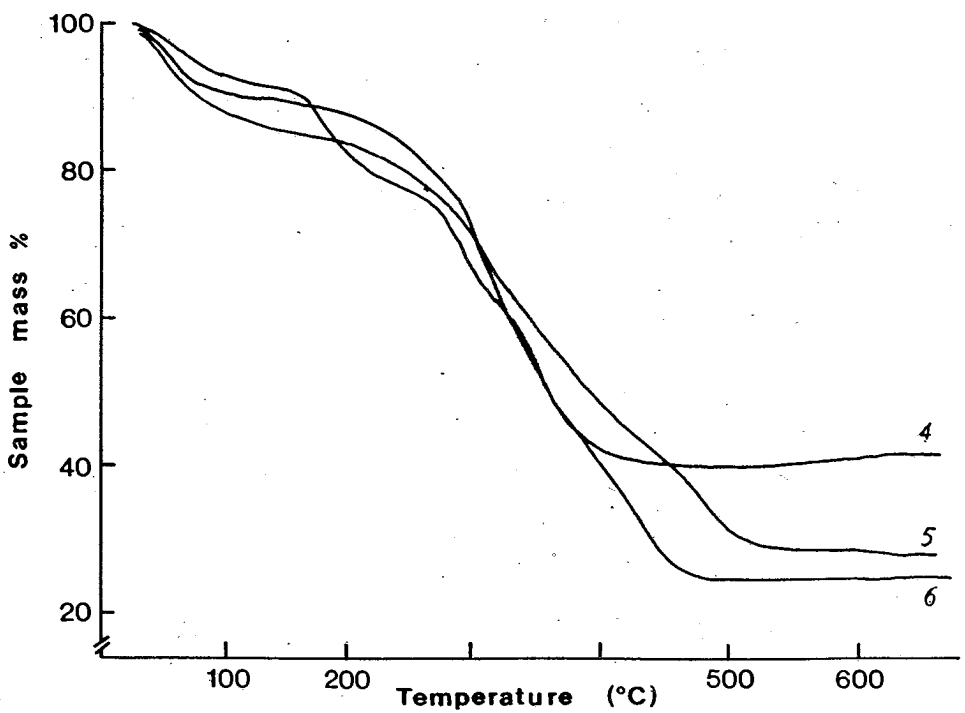

FIG.1. : *Thermogravimetric curves of the complexes.*

For complex *(4)* the measurements are consistent with a ~ 6% of the sample mass release of water at 40- 75 ^{0}C . For complex *(5)* 6% of the sample mass is removed between 45- 100 ^{0}C . For complex *(6)* methanol is removed at 30- 87 ^{0}C (6% of the sample mass) and water in a following step at 87- 150 ^{0}C (3.4% of the sample mass). The low temperature of methanol loss indicates that this is lattice held.

Titration curves for deprotonation and coordination reactions in a MeOH: H_2O 9:1 solution are shown in FIG. 2.

The titrations for the coordination reactions were conducted in the presence of metal cation with a metal: ligand ratio of 1:2 . Precipitation of the complexes occurs at relatively low pH values (6.3, 6.1 and 5.9 for complex *(4) (5)* and *(6)* respectively) , before all of the carboxylic and phenolic protons of the ligands are ionised. The ligands are present in the form of dianions and monoanions.

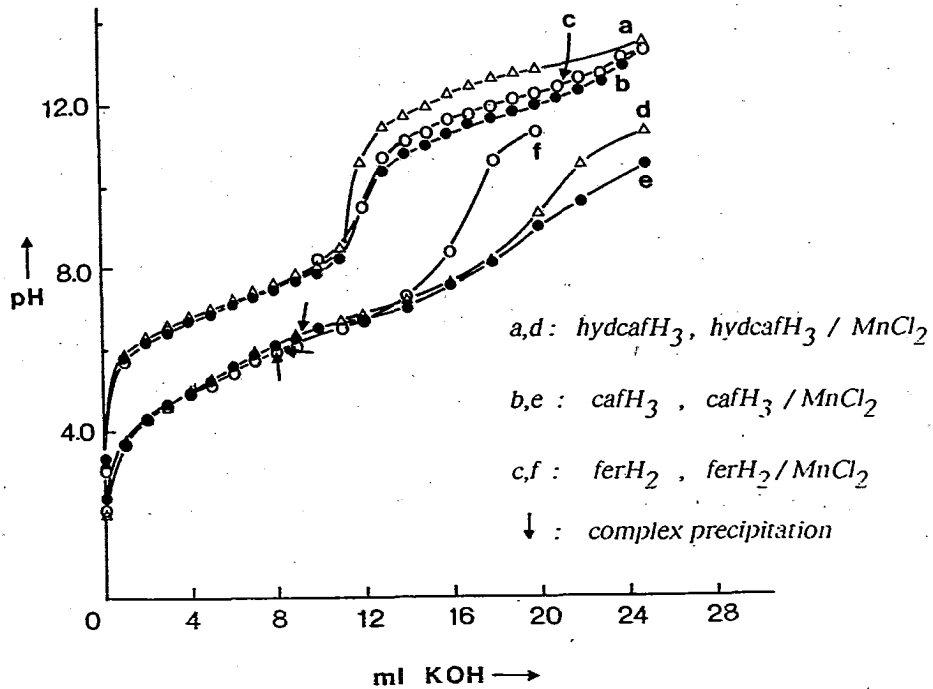

FIG. 2 .: *Titration curves of solutions of hydrocaffeic, caffeic and ferulic acids (a,b,c) and their mixtures with manganese (d,e,f).*

TABLE II gives diagnostic i.r. and far-i.r. bands. In the νOH region , the spectra of the complexes show two broad bands. The broad character of the bands indicates the existense of intense hydrogen bonding.In the spectra of *(4)*, and *(5)* the medium band below 3400 cm^{-1} is due to the presence of non-deprotonated phenolic OH groups. In*(6)* only one band is attributed to $\nu_{as}(CO_2^-)$ and to $\nu_s(CO_2^-)$, in agreement with the existence of one type of carboxylate coordination [18]. For this complex $\Delta_{complex} > \Delta_{ferHNa.H2O}$, where $\Delta=\nu_{as}(CO_2^-)-\nu_s(CO_2^-)$; this suggests that the carboxylate group of fer^{2-} is coordinated as a monodentate ligand[18]. In *(4)* and *(5)* two $\nu_{as}(CO_2^-)$ and two $\nu_s(CO_2^-)$ bands are observed, suggesting the existence of two different types of coordinated carboxylate groups[18].The higher $\nu_{as}(CO_2^-)$ band and the lower $\nu_s(CO_2^-)$ band are assigned to the stretching modes of the mono-atomic carboxylate bridge[18,19], while the other two bands are assigned to the modes of the triatomic carboxylate bridges [18]. Owing to the asymmetric bonding mode of the mono-atomic carboxylate group, a large splitting Δ (280 cm^{-1} for *(4)* , 315 cm^{-1} for *(5)*) of the $-CO_2^-$ stretching frequencies is observed [19].All complexes exhibit various ν (Mn- O) bands in the far- i.r. region.

The solid-state d-d spectra of complex *(4)* and complex *(5)* (TABLE III) can be assigned to transitions in a high- spin d^5 pseudo- octahedral stereochemistry [20]. The room- temperature effective magnetic moments of *(4)* and *(5)* are close to the spin-only value of 5.92 BM for a high- spin d^5 ion . However , from these room- temperature values it is difficult to rule out relatively weak ferromagnetic or antiferromagnetic interactions between adjacent manganese (II) atoms[21].

The solid- state electronic spectrum of *(6)* is different from those of *(4)* and *(5)* . It displays a very intense band at 375 nm and two weak bands at 470 and 580 nm. The weaker absorptions are reasonably attributed to manganese (III) d-d transitions, while the more intense band is attributable to LMCT .As can be seen in TABLE III ,

TABLE II. Characteristic i.r. bands (cm^{-1}).

Assignment	hydcafH_3	hydcafH_2Na.H_2O	cafH_3	cafH_2Na.H_2O	ferH_2	ferHNa.H_2O	*(4)*	*(5)*	*(6)*
$\nu(OH)_{,H2O}$		3600 s		3600 s		3600 s	3505 sb	3430 sb	
$\nu(OH)_{,H2O,MeOH}$									3510mb,3450mb
$\nu(OH)_{phenolic}$	3420 m	3410 m	3421 m	3420 m	3440 m	3435 m	3390 mb	3370 mb	
ν_{as} (CO_2^-)		1480 s		1468 s		1472 s	1540 s, 1430 s	1585 vs,1500m	1510s
ν_s (CO_2^-)		1320 s		1346 s		1347 s	1295m,1260m	1395m,1270m	1285m
ν(Mn- O)							515m,460m 420w	528m,485w, 415w	575s,530m, 460w

TABLE III. Ligand Field electronic spectra and solid state magnetic moments of the complexes.

Compound	Diffuse reflectance [a]				μ_{eff} / Mn [b] (BM)
	$^6A_{1g} \rightarrow {}^4T_{2g}(D)$	$^6A_{1g} \rightarrow {}^4A_{1g}, {}^4E_g(G)$	$^6A_{1g} \rightarrow {}^4T_{2g}(G)$	$^6A_{1g} \rightarrow {}^4T_{1g}(G)$	
(4)	390	415	450	577	5.68
(5)	380	400	460	570	5.56
	L M C T		d→d		
(6)	375		470 sh	580	5.10

a) in nm b) at 297 K.

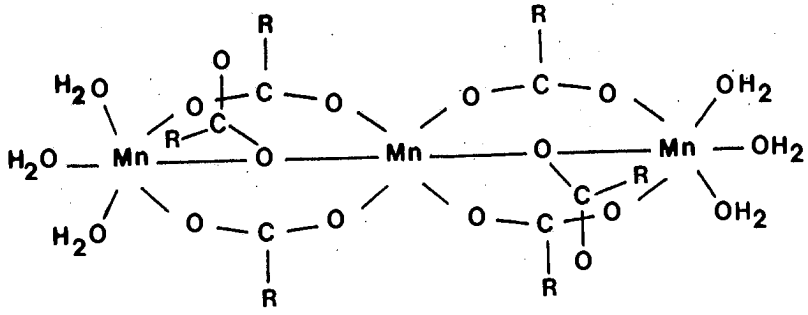

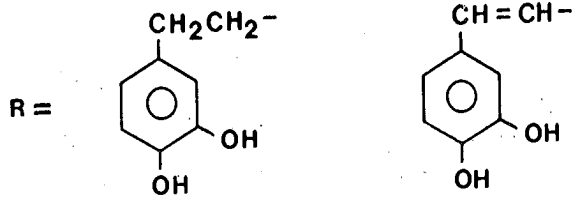

(4) (5)

FIG.3 . : *The proposed structures of the prepared complexes (4) and (5)* .

the room- temperature value of μ_{eff}/ Mn for *(6)* is 5.10 BM . This effective magnetic moment is somewhat more than would be expected for the spin- only value associated with a high- spin d^4 ion, namely 4.90 BM for four unpaired electrons (S=2). The μ_{eff} value may be indicative of an intramolecular ferromagnetic exchange interaction between high- spin manganese (III) centers in a dinuclear or oligonuclear structure [22].

From the overall study presented above , it is concluded that *(4)* and *(5)* most probably have the same trinuclear structure shown in FIG. 3 . Molecular models show that such a structure is quite feasible. However , polymeric structures based on these trimeric units (via bridging H_2O molecules, for example) can not be ruled out.The proposed Mn_3^{II} - core geometry is very rare among carboxylato- bridged trimetal complexes most of which have basic metal carboxylate [23], or other triangular structural motifs [23].The proposed core geometry has been structurally characterized only in three related manganese complexes , namely $[Mn_3^{II}(O_2(CH_3)_6(biphme)_2]$ [23], $[Mn_3^{II}(O_2(CH_3)_6(bpy)_2]$ [24] and $[Mn_3^{II}(O_2(Ph)_6(bpy)_2]$[3]. Aspects of this core geometry are also known in few other complexes [23].It is worth noting that the proposed core geometry is of great importance in Bioinorganic chemistry[23]. For *(6)* an oligonuclear structure involving coordination of both carboxylate (monodentate) and deprotonated phenolic (phenoxide) oxygen (terminal or bridging) groups is tentatively proposed.

ΠΕΡΙΛΗΨΗ

Παρασκευή και ιδιότητες συμπλόκων μαγγανίου (II) και μαγγανίου (III) με υποκαταστάτες φέροντες καρβοξυλικές , φαινολικές και ομάδες φαινοξειδίου

Εχουν παρασκευασθεί και μελετηθεί τριπυρηνικά σύμπλοκα υδροκαφεϊκού και καφεϊκού οξέος με μαγγάνιο (II). Η προτεινόμενη γεωμετρία πυρήνα- Mn_3 , υποστηρίζεται από διάφορα φασματοσκοπικά (διαχυτική ανάκλαση, υπέρυθρος

φασματοσκοπία) , μαγνητικά , θερμοσταθμικά και ποτενσιομετρικά δεδομένα. Το φερουλικό οξύ σχηματίζει ένα ολιγοπυρηνικό σύμπλοκο του Mn (III) , η δομή του οποίου περιλαμβάνει σύμπλεξη και καρβοξυλικής ομάδος (μονοσχιδής) και αποπρωτονωμένου φαινολικού οξυγόνου (φαινοξειδίου) ακραίωνή γεφυρών.

ACKNOWLEDGEMENTS

We wish to thank the University of Athens for financial support of the work.

REFERENCES

1.Wieghardt K., *Angew.Chem., Int. Ed. Engl.*, 28, 1153 (1989).

2.Vincent J.B. and Christou G., Adv. *Inorg. Chem.*, 33, 197 (1989).

3.Christou G., *Acc. Chem. Res.*, 22, 328 (1989).

4.Pecoraro V.L., *Photochem. Photobiol.*, 48, 249 (1988).

5.Dismukes G.C., *Photochem. Photobiol.*, 43, 99 (1986).

6.CaneschiA., Gatteschi D., Laugier J., Rey P.,Sessoli R., Zanchini C., *J.Am.Chem.Soc.*, 110, 2795 (1988).

7.Boyd P.D.W.,Li Q.,Vincent J.B., Folting K., Chang H.- R., Streib W.E., Huffman J.C., Christou G.and Hendrickson D.N., *J.Am. Chem. Soc.*, 110, 8537 (1988).

8.Caneschi A., Gatteschi D., Sessoli R., Barra A.L., Branel L.C. and Guillot M., *J. Am. Chem. Soc.*,113, 5873 (1991).

9.Petrou A.L., *Transition Met. Chem.* , 18 , 462, (1993).

10.a)Petrou A.L., Koromantzou M.V. and Tsangaris J.M., *Transition Met. Chem.*, 16, 48 (1991). b)Petrou A.L., Koromantzou M.V. and Tsangaris J.M., *Chimika Chronika, New Series* , 22 189 (1993).

11.Petrou A.L. and Perlepes S.P., submitted for publication .

12.Christmas C., Vincent J.B., Chang H.- R., Huffman J.C., Christou G. and Hendrickson D.N., *J.Am.Chem.Soc.*,110, 823 (1988).

13.Vincent J.B., Folting K., Huffman J.C. and Christou G., *Inorg. Chem.*, 25, 996 (1986).

14.Schwarzenbach G.and Flaschka H.(transl. revis. by H.M.N.H. Irving), Complexometric Titrations, 2nd edit. Methnan Co. Ltd. London (1957), Vogel A.I., A Textbook for Quant. Inorg. Analysis, Longmans Co. (1961).

15.a. Kabanos T.A. and Tsangaris J.M., *J.Coord. Chem.*, 13, 89 (1984).

b. Rahman A.A., Nicholls D. and Tsangaris J.M. , *J.Coord. Chem.*, 14, 327 (1986).

c.Hondrellis V., Perlepes S.P., Kabanos T.A. and Tsangaris J.M., *Synth. React.*

Inorg. Met.- Org. Chem., 83 (1988).
16.Arndt D., Manganese Compounds as Oxidizing Agents in Organic Chemistry, Open Court La Salle, 11, 1981.
17.Geary W.J., *Coord. Chem. Rev.*, 7, 81 (1971).
18.Deacon G.B.and Phillips R.J., *Coord. Chem. Rev.*, **33**, 227 (1980).
19. Costes J.- P., F.Dahan and J.- P. Laurent. *Inorg. Chem.*. **24**. 1018, (1985).
20.Lever A.B.P., Inorganic Electronic Spectroscopy, 2nd Edn., Elsevier, Amsterdam, 1984.
21.Hodgson D.J., Schwartz B.J. and Sorrell T.N., *Inorg. Chem.*, **28**, 2226 (1989).
22.Schake A.B., Schmitt E.A., Conti A.J., Streib W.E., Huffman J.C., Hendrickson D.N. and Christou G., *Inorg. Chem.*, **30**, 3192 (1991).
23.Rardin R.L., Bino A., Poganiuch P., Tolman W.B., Liu S. and Lippard S.J., *Angew. Chem., Int. Ed. Engl.*, 29, 812 (1990) and refs. therein.
24.Menage S., Vitols S.E., Bergerat P., Codjovi E., Kahn O., Girerd J.- J., Guillot M., Solans X .and Calvet T., *Inorg. Chem.*, **30**, 2666 (1991).

Abbreviations

Hydrocaffeic acid	abbr.	$hydcafH_3$
Caffeic acid	abbr.	$cafH_3$
Ferulic acid	abbr.	$ferH_2$

Chimica Chronica, New Series, 23, 169-189 (1994)

KINETICS OF POTASSIUM ADSORPTION BY ENTISOLS

(as described by two Mathematical models)

A.Dimirkou,[1] A.Ioannou[2], M.Doula[1], C.Deligianni[1]

1 National Agriculture Research Foundation of Greece, Soil Science Institute of Athens, Sof. Venizelou 1, Lycovrisi 14123, Attiki, Greece.
2 University of Athens, Department of Chemistry, Panepistimiopolis-Zografou Athens 15771, Greece.

(Received September 28, 1994)

SUMMARY

The kinetics of K-adsorption from solution to exchangeable phases were investigated in Ca-saturated samples of Entisols. Four initial K concentrations (C_o) and five different pH values were used so as to gain the experimental data. Two mathematical models, a modified Freundlich (Kuo-Lotse, 1974) and a first order equation, in their linear form, were fitted to K-adsorption data. From the first order equation we obtained the following pH and C_o-dependent form of the adsorbed amount of K in equilibrium (x_{eq}) which is of great interest for agricultural use :

$$\ln x_{eq} = -0.8513 + 5.80 \cdot 10^{-4} C_o + (0.654 - 3.00 \cdot 10^{-5} C_o)\ pH$$

For the comparison of the two models the coefficients of determination (r^2) were calculated. Kuo-Lotse equation was found to describe better K-adsorption (x) by Entisols and its Co and pH-depended form is given :

$$x = [0.0869 - 4.13 \cdot 10^{-6} C_o + (3.25 \cdot 10^{-3} + 1.78 \cdot 10^{-7} C_o)pH] \cdot C_o \cdot t^{[-0.365+3.79 \cdot 10^{-5} C_o+(0.0815-7.86 \cdot 10^{-6} C_o)pH]}$$

Key words: Kinetics, adsorption, potassium, Entisols, Kuo-Lotse model, first-order model.

Postal address of the corresponding author: A.Ioannou, 14 Thermopillon st., 15344 Pallini,Greece.

INTRODUCTION

So far, plenty of studies concerning kinetic reactions on pure clays and soils have been published. The study of K-adsorption and desorption by soils is a matter of special interest since potassium is one of the three main nutrients required by plants.

Several researchers, based on the results of their investigations substantiated the existence of three kinds of binding sites for K exchange in soils (Bolt et al., 1963; Goulding and Talibudeen, 1979). Potassium adsorption associated with external planar sites (exchangeable K) is described by rapid kinetics of exchange. Potassium which is located in interlattice exchange sites is characterised by slow kinetics while potassium adsorption from interlattice edge sites is characterised by intermediate kinetics.

Jardine and Sparks (1984) compared samples of an Evesbora soil (multireactive soil system) with pure kaolinite, montmorillonite and vermiculite, so as to be able to explain the behaviour of the complex system during K-adsorption and desorption. They applied first-order kinetics for several temperatures and found that at room temperature or lower, two rate coefficients described K adsorption. The first rate coefficient was related to a rapid reaction and the second rate coefficient was related to a slow reaction. The former reaction was ascribed to exchange sites of the soil that are readily accessible to cation exchange reactions and the latter was ascribed to exchange sites that were difficulty accessible to K exchange. Furthermore, the very good description of the kinetics using the parabolic diffusion law and the values of activation energies indicated that the rate-controlling process for K-adsorption by the soils was probably intraparticle diffusion.

Selim et al. (1976) proposed that solution-exchangeable K reactions could be described by n^{th} order kinetics and that the reaction of K-desorption is amenable to 1^{st} order kinetics. Yet, others claim that the kinetics of K-adsorption and desorption in

complex and heterogeneous soil systems conform to first-order kinetics and to the parabolic law (Sivasubramaniam and Talibudeen, 1972 ; Sparks et al., 1980a ; Sparks and Jardine, 1981). Potassium release from micaceous minerals also seems to conform to the parabolic law and is controlled by diffusion phenomena (Barshad, 1951 ; Rausell-Colom et al., 1965 ; Chute and Quirk, 1967 ; Feigenbaum et al., 1981).

The kinetics of K-adsorption is greatly affected by the type and amount of clay, the organic matter content of the soil system, the temperature and the pH. The influence of some of these factors has been investigated in the past (Brady, 1990 ; Grewal and Kanwar, 1976 ; Magdoff and Bartlett, 1980).

The purpose of this investigation was 1) to determine the applicability of Kuo-Lotse (1974) and first-order equations to describe the kinetics of K-adsorption by Entisol Xerorthent soil of Greece and 2) to investigate which of the above two equations describes better the K-adsorption kinetics with pH and initial concentrations.

MATERIALS AND METHODS

Studies were performed on a Viotia soil (Entisol Xerorthent) located in central Greece. As Entisol Xerorthent are characterised recent soils in which the horizons are not developed and with xeric moisture regime. The classification is according to the Soil Taxonomy of USDA (1975). The taxonomic classification is given in Table I. Physical and chemical properties of the soil are given in Table II. The samples were air-dried and crushed to pass a 2-mm sieve. Particle size analysis was determined by the pipette method (Kilmer and Alexander, 1949). Organic matter was determined by the Walkley-Black (1934) method. Cation exchange capacity was determined using a

$MgCl_2$ saturation with subsequent displacement by $CaCl_2$ (Okazaki et al., 1963 ; Rich, 1962). The pH measurements were obtained from a 1:2 soil water mixture. The $CaCO_3$ equivalent was determined by treatment with dilute acid and the volume of released CO_2 was measured by the Bernard Calcimeter.

Prior to initiation of the kinetic adsorption studies, subsamples of the soil were Ca-saturated using 1 N $CaCl_2$. The soil was subsequently washed with deionized water followed by washing with a 1:1 acetone-H_2O mixture until a negative test for Cl^- was obtained with $AgNO_3$. The soil was saturated with Ca, as in most mineral soils this is one of the predominant cations. Also, by first saturating with this cation, most exchangeable K was removed from the soil. The saturated sample was air-dried and crushed to pass a 2-mm sieve. Soil pH was measured on the Ca-saturated sample using a 1:2 soil/water mixture. The Cation Exchange Capacity (C.E.C.) of the Ca-saturated sample was ascertained by displacement with 1N $MgCl_2$. The quantity of Ca in solution was measured using atomic absorption spectrophotometry.

Adsorption studies were carried out using triplicate 1-gram Ca-saturated samples which were placed in 100-ml polypropylene centrifuge tubes. Fifty millilitres of KCl solution containing 246, 1177, 4731 or 6021 μg K along with twenty millilitres of buffer solution of pH 5.0, 6.0, 7.0, 8.0 or 9.0 were added to the tubes. The samples were shaken (185 cic/min) at room temperature (25°C) for 1, 10, 15, 20, 25, 30, 35, 40, 45, 50, 55, 60, 70, 80, 90, 120, 180, 240 and 1440 min, 48, 96 and 192 hours, centrifuged (4000 rpm) and K in the supernatant was determined by flame photometry. The amount of sorbed potassium was calculated from the difference between initial and final K concentrations.

Two mathematical models were applied to describe the kinetics of K-adsorption on the Entisol soil.The Kuo-Lotse (1974) equation was applied to K-adsorption as follows:

$$x = k_a C_o t^{1/m} \qquad [1]$$

$$\ln x = \ln (k_a C_o) + \frac{1}{m} \ln t$$

where x is the amount of K sorbed at time t, C_o is the initial K concentration, k_a is the rate coefficient of the reaction and m is a constant.

If $\ln(k_a C_o) = a$ and $\frac{1}{m} = b$ the equation (1) can be simplified to :

$$\ln x = a + b \ln t \qquad [2]$$

a and b can be calculated from the intercept and the slope of the plot lnx vs lnt, respectively, for all studied pH values.

Plotting k_a vs pH and 1/m vs pH we arrived at the pH-dependent form of k_a and 1/m for all studied initial concentrations of potassium. If a linear relationship between k_a and pH and between 1/m and pH is existed the calculated values of the intercepts and slopes of k_a=f(pH) and $\frac{1}{m}$=f(pH) were plotted against the initial added K concentrations resulting in the simultaneous dependence of k_a and 1/m on pH and C_o. In each step of the above process the coefficient of determination (r^2) was calculated. The substitution of k_a and 1/m in Eq.(1) by their pH and C_o-dependent forms gave the pH and C_o-dependent form of the Kuo-Lotse model.

The second model examined was the first-order kinetic model which is described as follows (Jardine and Sparks, 1984) :

$$\frac{dx}{x_{eq}} = k_b (x_{eq} - x)dx \qquad [3]$$

where x is the amount of K sorbed at time t, x_{eq} is the amount of K sorbed at equilibrium and k_b is the rate coefficient.

Integrating, with appropriate boundary conditions of $t = 0$; $x = 0$, Equation (3) becomes :

$$\ln(x_{eq} - x) = \ln x_{eq} - x_{eq}k_b t \qquad [4]$$

If $\ln x_{eq} = a$ and $-x_{eq}k_b = b$ Equation (4) becomes :

$$\ln(x_{eq} - x) = a + bt \qquad [5]$$

a and b can be calculated from the intercept and the slope of the plot $\ln(x_{eq} - x)$ vs t , respectively, for all studied pH values.

The two models were evaluated by comparing coefficients of determination (r^2) of each one. The r^2 values were determined by least square regression analysis.

Again, plotting k_b and $\ln x_{eq}$ vs pH for all initial K concentrations, we determined their pH dependent forms. Assuming a linear relationship between k_b and pH, $\ln x_{eq}$ and pH we calculated the corresponding slopes and intercepts for all initial concentrations of potassium. Plotting the values of slopes and intercepts against C_o we determined the pH and C_o-dependent forms of k_b and $\ln x_{eq}$. The coefficients of determination (r^2) were calculated for every step of the process.

RESULTS AND DISCUSSION

As shown in Fig. 1 and 2, K-adsorption on the Entisols was noninstaneous and equilibrium was reached in about 30 to 45 minutes, for all initial K concentrations and

pH values. The higher the initial K concentration, the longer it took the soil to achieve equilibrium. This noninstaneous K-adsorption is in agreement with the findings of other researchers also studied soils (Sparks et al, 1980; Jardine and Sparks, 1984). Researchers who studied pure systems such as certain found that the reaction between the soil solution and exchangeable phases of K was almost instaneous (Malcom and Kennedy, 1969).

Table I: Soil taxonomic classification and particle size distribution of the soil

Taxonomic classification	Depth (cm)	Sand (%)	Silt (%)	Clay (%)
Entisol Xerothent	0-50	45	24	31

Table II : Physical and chemical properties of the soil

Sample	Liquid limit	EC (mmhos/cm)	pH 1:2	C.E.C. (meq/100g)
Entisol Xerothent	47	$\langle 3$	8.7	15

$CaCO_3$ equiv. (%)	Organic matter (%)	Exchangeable K (meq/100g)	C.E.C. (after Ca-saturation treatment)	pH (after Ca-saturation treatment)
17.2	0.6	0.19	16.0	7.85

Entisols contain low amounts of clay and thus, K-exchange sites are limited. As a result of this, the quantity of adsorbed potassium is not large. Nevertheless, one can notice a clear increase in the amount of adsorbed K as initial K concentration and pH increased, as shown in Figs. 1 and 2.

Two models, the Kuo-Lotse approach (1974) and the first-order equation, were tested by least square regression analysis to describe K-adsorption. The experimental data were plotted according to the linear form of both equations.

K-adsorption data conformed to the Kuo-Lotse model (Eq. 2) for all initial K concentrations and pH values, as shown in Fig. 3 and 4. The coefficient of determination (r^2) was calculated for each initial concentration at all pH values (Table III).

They ranged from 0.997-0.999, indicating the excellent description of K-adsorption kinetics by this particular model.

The k_a value from the Kuo-Lotse (1974) model is exponentially related to the intercept (a) of the plot lnx vs lnt ($k_a = \frac{e^a}{C_o}$).

Plotting k_a values against pH for all initial K concentrations (Fig.5) we obtained the pH-dependent forms of k_a ($k_a = c + dpH$) (Table IV).

They all provided very high r^2 values (>0.997) with the exception of the initial concentration, 246 ppm ($r^2 = 0.909$). The plots of the intercept (c) and slope (d) of $k_a = f(pH)$ against C_o ($c = e + f \cdot C_o$ and $d = g + h \cdot C_o$) gave the pH and C_o-dependent form of k_a.

These plots had r^2 values 0.992 and 0.567, respectively. Neglecting that the latter r^2 value is very low, since the former is very high, we determined the C_o and pH-dependent form of k_a :

$$k_a = 0.0869 - 4.13 \cdot 10^{-6} C_o + (3.25 \cdot 10^{-3} + 1.78 \cdot 10^{-7} C_o) pH \cdot \qquad [6]$$

We tested the reliability of the above equation for several pH and C_o values and found that the theoretically estimated values of k_a was very close to those given by the experiment, with an error ranging from 0.1% to 3%.

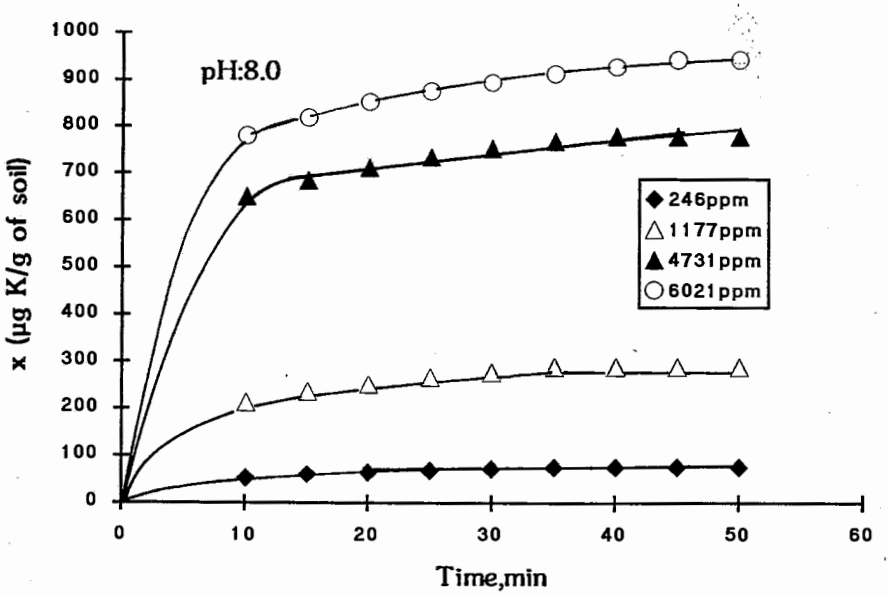

Figure 1. Potassium adsorption by Entisol Xerothent as a function of time at pH 8.0 and different initial concentrations.

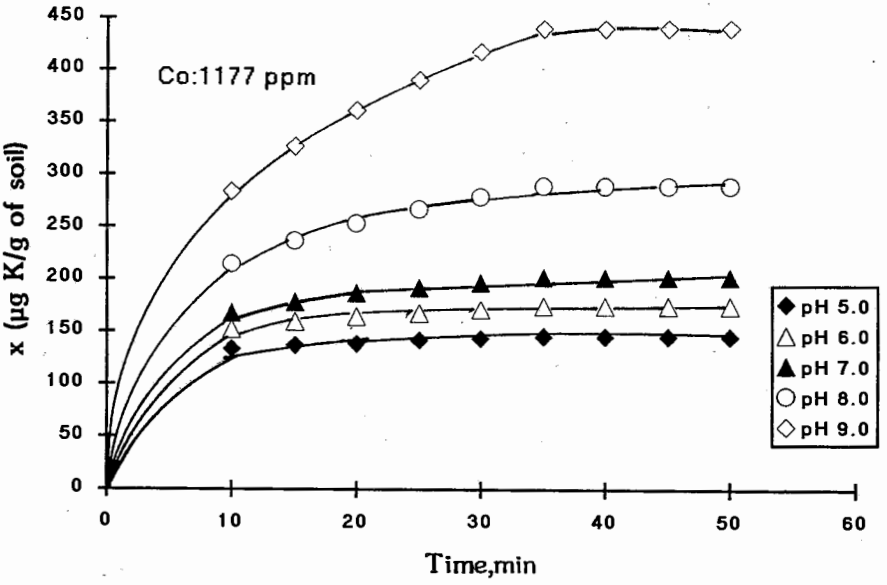

Figure 2. Potassium adsorption by Entisol Xerothent as a function of time at different pH values and initial concentration of 1177 ppm.

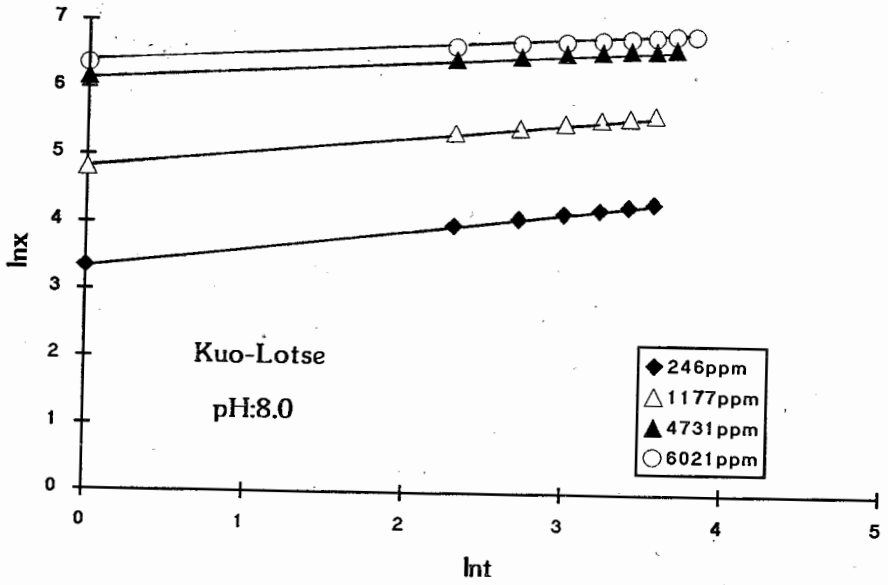

Figure 3. Kuo-Lotse kinetics for potassium adsorption by Entisol Xerothent at pH 8.0 and different initial concentrations.

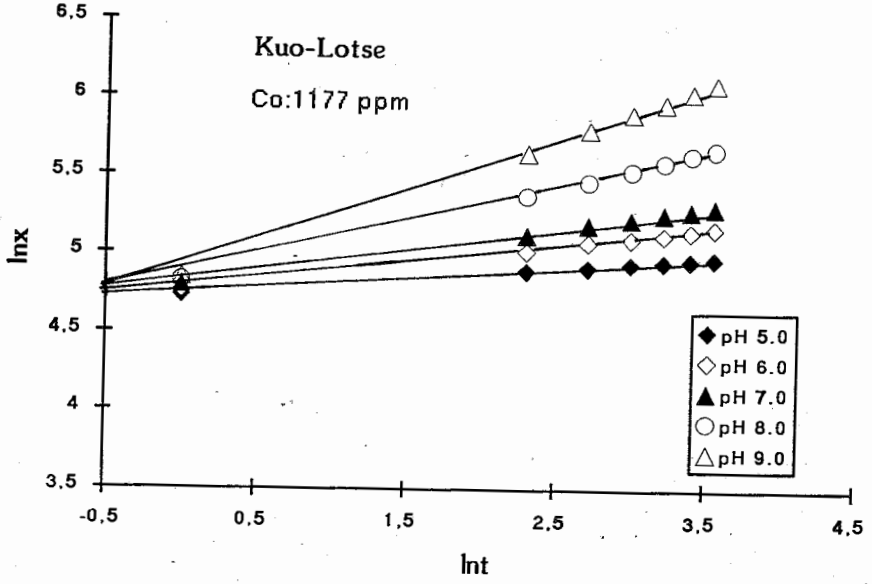

Figure 4. Kuo-Lotse kinetics for potassium adsorption by Entisol-Xerothent at different pH values.

According to Eq. (6) k_a increases with increasing pH and decreases with increasing initial K concentration.

TABLE III : Regression equations, coefficients of determination (r^2) and rate coefficients (k_a) of adsorption for Kuo-Lotse model.

C_o (ppm)	pH	a	b	r^2	k_a (min^{-1})
246	5.0	3.254	0.0709	0.999	0.10526
	6.0	3.259	0.1147	0.997	0.10578
	7.0	3.316	0.1679	0.999	0.11199
	8.0	3.369	0.2703	0.999	0.11808
	9.0	3.368	0.4080	0.996	0.11796
1177	5.0	4.734	0.0686	0.999	0.0966
	6.0	4.764	0.1128	0.999	0.0996
	7.0	4.798	0.1433	0.999	0.1030
	8.0	4.821	0.2379	0.999	0.1054
	9.0	4.847	0.3490	0.999	0.1082
4731	5.0	6.043	0.0526	0.999	0.0890
	6.0	6.088	0.0644	0.998	0.0931
	7.0	6.128	0.0848	0.999	0.0969
	8.0	6.171	0.1332	0.999	0.1012
	9.0	6.210	0.2320	0.999	0.1052
6021	5.0	6.215	0.0592	0.999	0.0831
	6.0	6.267	0.0718	0.999	0.0875
	7.0	6.321	0.0911	0.999	0.0924
	8.0	6.363	0.1282	0.999	0.0963
	9.0	6.409	0.2111	0.999	0.1009
r^2				0.999	

The latter is in agreement to Bronsted's activity rate theory. This is also shown in Table III.

Constant 1/m is the slope of the plot lnx vs lnt. The plots of 1/m vs pH for all studied C_o (Fig. 6) gave the pH-dependent form of 1/m ($\frac{1}{m}$ = i + jpH) (Table V).

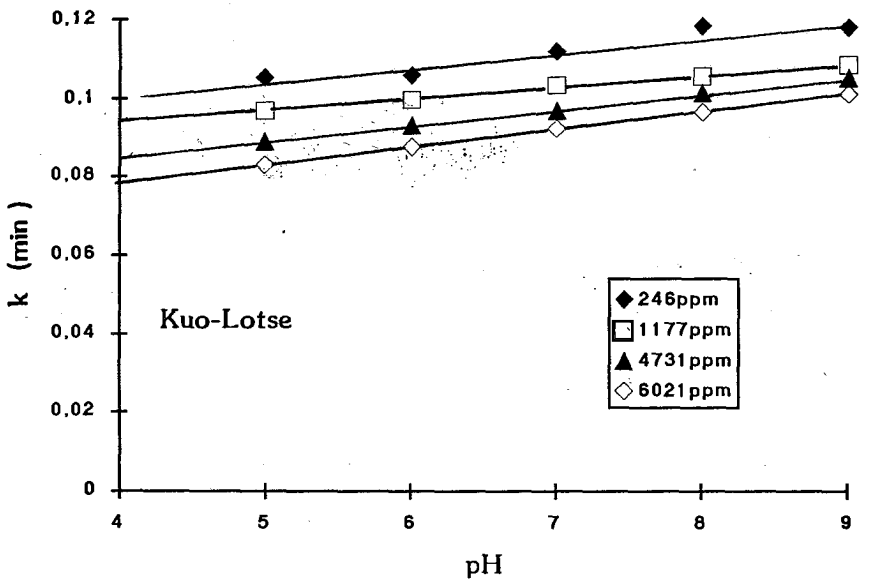

Figure 5. Rate coefficient (k_a) of Kuo-Lotse model as a function of pH at different initial concentrations.

The calculated values of r^2 ranged between 0.855-0.943 and the linearity was relatively good. Plotting the intercepts (i) and slopes (j) of the above plots against the initially added K concentration ($i = p + q \cdot C_o$ and $j = v + w \cdot C_o$) we determined the pH and C_o-dependent form of 1/m (Table V).

These two plots had r^2 values of 0.974 and 0.979, respectively. The pH and C_o-dependent form of 1/m is given :

$$\frac{1}{m} = -0.3650 + 3.79 \cdot 10^{-5} C_o + (0.0815 - 7.86 \cdot 10^{-6} C_o)pH \qquad [7]$$

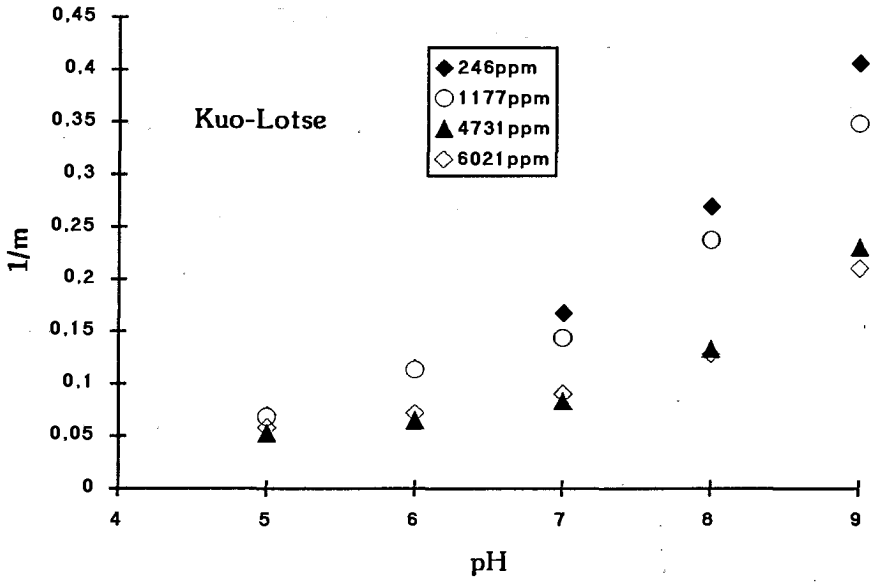

Figure 6. Constant 1/m of Kuo-Lotse model as a function of pH at different initial concentrations.

Substitution of Eqs. (6) and (7) for the k_a and 1/m values in Eq. (1) led to the final form of the Kuo-Lotse (1974) model :

$$x = [0.0869 - 4.13 \cdot 10^{-6} C_o + (3.25 \cdot 10^{-3} + 1.78 \cdot 10^{-7} C_o)pH] \cdot C_o \cdot {}_t^{[-0.365+3.79 \cdot 10^{-5} C_o + (0.0815 - 7.86 \cdot 10^{-6} C_o)pH]} \quad [8]$$

The Kuo-Lotse (1974) model was developed from the Freundlich equation taking into account the fact that the slope of the Freundlich plot is independent of reaction time. The Freundlich equation is highly empirical and so is the developed model we employed in this study. Nevertheless, despite its empirical character it was found to provide an excellent description of K-adsorption kinetics by Entisols.

TABLE IV : Regression equations and coefficients of determination for the pH and C_o-depended form of Kuo-Lotse's rate coefficient (k_a).

C_o (ppm)	k_a = c + d pH	r^2
246	$0.0854 + 3.77 \cdot 10^{-3}$ pH	0.909
1177	$0.0823 + 2.90 \cdot 10^{-3}$ pH	0.997
4731	$0.0687 + 4.05 \cdot 10^{-3}$ pH	0.999
6021	$0.0610 + 4.44 \cdot 10^{-3}$ pH	0.999
	c = e + f C_o	r^2
	$0.0869 + -4.13 \cdot 10^{-6}$ C_o	0.992
	d = g + h C_o	r^2
	$3.25 \cdot 10^{-3} + 1.78 \cdot 10^{-7}$ C_o	0.567

TABLE V : Regression equations and coefficients of determination for the pH and C_o-depended form of Kuo-Lotse's 1/m.

C_o (ppm)	$\frac{1}{m}$ = i + j pH	r^2
246	-0.3745 + 0.0830 pH	0.943
1177	-0.2978 + 0.0686 pH	0.938
4731	-0.1859 + 0.0427 pH	0.855
6021	-0.1399 + 0.0360 pH	0.869
	i = p + q C_o	r^2
	$-0.3650 + 3.79 \cdot 10^{-5}$ C_o	0.974
	j = v + w C_o	r^2
	$0.0815 + -7.86 \cdot 10^{-3}$ C_o	0.979

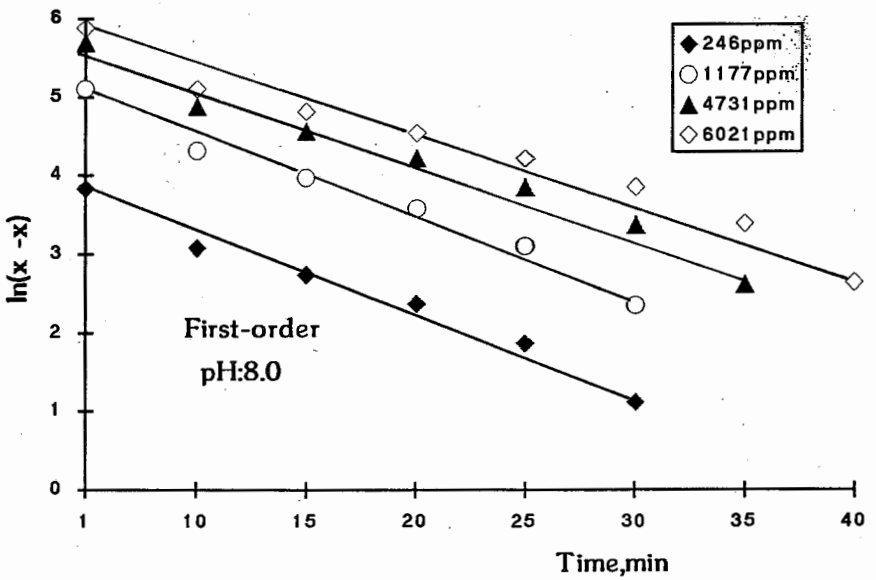

Figure 7. First-order kinetics for potassium adsorption by Entisol Xerothent at pH 8.0 and different initial concentrations.

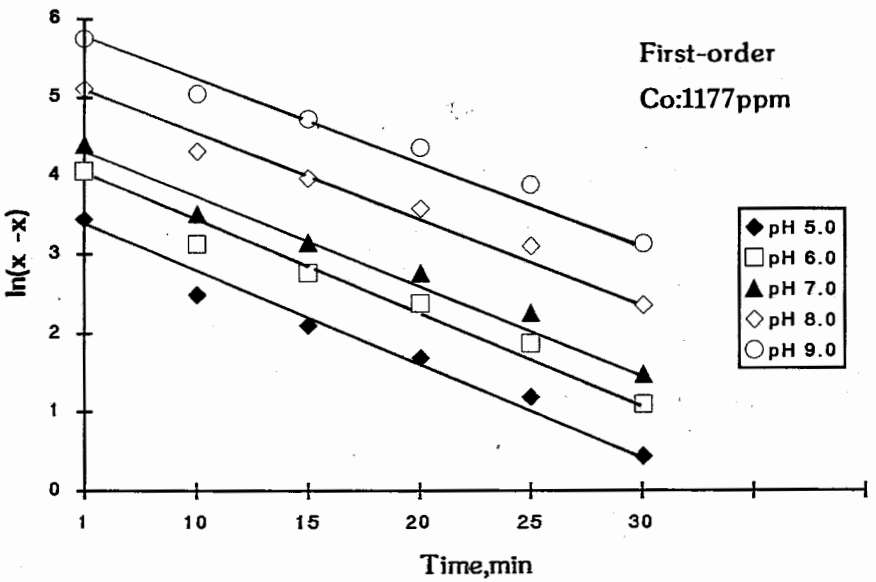

Figure 8. First-order kinetics for potassium adsorption by Entisol Xerothent at different pH values and initial concentration of 1177 ppm.

The application of the first order model (Eq. 5) to the experimental data (Fig. 7 and 8) gave r^2 values ranging between 0.912-0.996 (Table VI), indicating a relatively linear relationship between $\ln(x_{eq} - x)$ and t. Thus, this model also described K-adsorption by Entisols but not as well as the Kuo-Lotse model did.

Plotting $\ln x_{eq}$ against pH for all initially added K concentrations (Fig. 9) we derived the pH-depended form of $\ln x_{eq}$ ($\ln x_{eq} = i + jpH$) The r^2 values were greater than 0.952 (Table VII). The plots of the intercept (i) and slope (j) of $\ln x_{eq} = f(pH)$ against C_o ($i = p + q \cdot C_o$ and $j = v + w \cdot C_o$) led to the C_o and pH-dependent form of $\ln x_{eq}$. The r^2 was 0.878 and 0.929, respectively. The linearity was quite good and the final form of $\ln x_{eq}$ is :

$$\ln x_{eq} = -0.8513 + 5.798 \cdot 10^{-4} C_o + (0.6538 - 3.300 \cdot 10^{-5} C_o)pH \qquad [9]$$

Equation (9) relates the amount of K that is retained by the soil with the initial K concentration and the pH of the soil. The utility of Eq. (9) in agriculture is obvious, since it can predict the amount of K which must be added per unit weight of a soil at a specific pH so as to gain the desired K retention.

The plots of k_b vs pH (Fig. 10) gave the pH-dependent form of k_b ($k_b = c + dpH$) for each initial K concentration and relatively high r^2 values (>0.945) were obtained (Table VIII). The plots of the intercept (c) and slope (d) of $k_b = f(pH)$ vs C_o gave low r^2 values (0.613 and 0.603, respectively) which could not be accepted for the continuation of the process. Thus, we were unable to produce a C_o and pH-dependent form of k_b and therefore a C_o and pH-dependent form of the first order model.

TABLE VI : Regression equations, coefficients of determination (r^2) and rate coefficients (k_b) of adsorption for first-order model.

C_o (ppm)	pH	a	b	r^2	k_b (min^{-1})
246	5.0	2.0727	-0.11116	0.993	$3.37 \cdot 10^{-3}$
	6.0	2.6237	-0.0893	0.994	$2.29 \cdot 10^{-3}$
	7.0	3.2042	-0.08856	0.996	$1.77 \cdot 10^{-3}$
	8.0	4.0158	-0.08964	0.981	$1.18 \cdot 10^{-3}$
	9.0	4.7317	-0.07655	0.912	$6.08 \cdot 10^{-4}$
1177	5.0	3.5605	-0.09913	0.988	$6.83 \cdot 10^{-4}$
	6.0	4.1831	-0.09685	0.987	$5.53 \cdot 10^{-4}$
	7.0	4.5356	-0.09540	0.986	$4.87 \cdot 10^{-4}$
	8.0	5.2637	-0.09075	0.983	$3.14 \cdot 10^{-4}$
	9.0	5.9281	-0.08575	0.977	$1.95 \cdot 10^{-4}$
4731	5.0	4.5902	-0.08901	0.984	$1.74 \cdot 10^{-4}$
	6.0	4.8726	-0.08806	0.985	$1.57 \cdot 10^{-4}$
	7.0	5.2271	-0.08733	0.984	$1.39 \cdot 10^{-4}$
	8.0	5.8359	-0.08525	0.982	$1.09 \cdot 10^{-4}$
	9.0	6.6585	-0.08010	0.974	$6.83 \cdot 10^{-5}$
6021	5.0	4.9095	-0.07957	0.980	$1.27 \cdot 10^{-4}$
	6.0	5.1887	-0.07896	0.981	$1.14 \cdot 10^{-4}$
	7.0	5.5812	-0.08393	0.971	$1.07 \cdot 10^{-4}$
	8.0	6.0041	-0.07694	0.977	$8.15 \cdot 10^{-5}$
	9.0	6.7567	-0.07385	0.975	$5.45 \cdot 10^{-5}$
r^2				0.979	

From Table VI one can remark the decrease of k_b value as the initial K concentration increased (Bronsted's activity rate theory) but also the decrease of k_b as pH increased.

TABLE VII: Regression equations and coefficients of determination for the pH and C_o-depended form of first-order's lnx_{eq}.

C_o (ppm)	lnx_{eq} = i + j pH	r^2
246	-1.3674 + 0.6710 pH	0.994
1177	0.6231 + 0.5816 pH	0.989
4731	1.8669 + 0.5100 pH	0.952
6021	2.5312 + 0.4510 pH	0.964
	i = p + q C_o	r^2
	-0.8513 + $5.80 \cdot 10^{-4}$ C_o	0.878
	j = v + w C_o	r^2
	0.6538 + $-3.30 \cdot 10^{-5}$ C_o	0.929

TABLE VIII : Regression equations and coefficients of determination for the pH and C_o-depended form of first-order's rate coefficient (k_b).

C_o (ppm)	k_b = c + d pH	r^2
246	$6.4874 \cdot 10^{-3}$ + $-6.634 \cdot 10^{-4}$ pH	0.978
1177	$1.2939 \cdot 10^{-3}$ + $-1.215 \cdot 10^{-4}$ pH	0.993
4731	$3.1104 \cdot 10^{-4}$ + $-2.594 \cdot 10^{-5}$ pH	0.962
6021	$2.2105 \cdot 10^{-4}$ + $-1.775 \cdot 10^{-5}$ pH	0.945
	c = e + f C_o	r^2
	$4.641 \cdot 10^{-3}$ + $-8.419 \cdot 10^{-7}$ C_o	0.613
	d = g + h C_o	r^2
	$-4.697 \cdot 10^{-4}$ + $8.627 \cdot 10^{-8}$ C_o	0.603

This is unlike what we noticed in Kuo-Lotse model. This opposite behaviour could be justified taking into account the different derivation of the two rate constants.

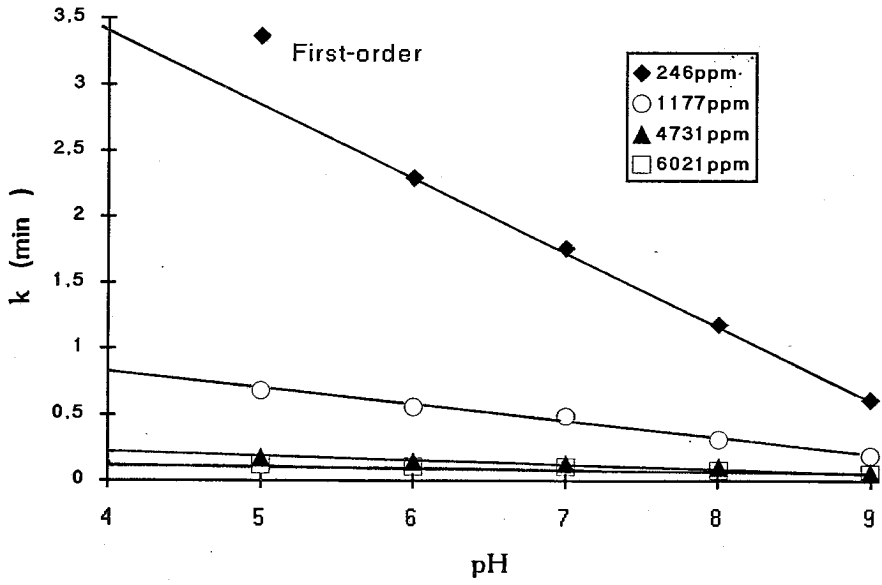

Figure 9. Rate coefficient (kb) of first-order model as a function of pH at different initial concentrations.

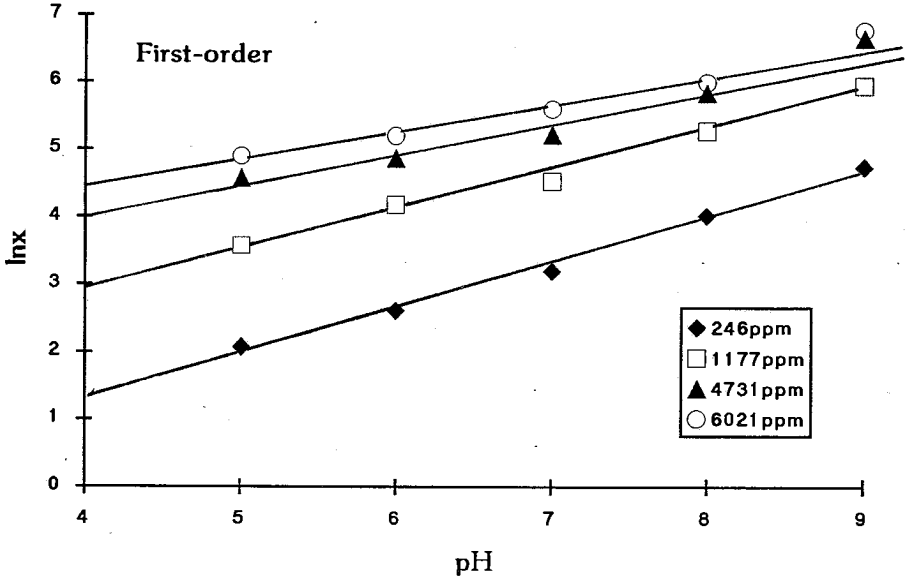

Figure 10. lnX_{eq} of first-order model as a function of pH at different initial concentrations.

CONCLUSION

The Kuo-Lotse (1974) model was preferable to the first-order equation for the description of K-adsorption kinetics by Entisols and it also provided a better conformance to the experimental data relating pH and Co changes. Its pH and C_o-depended form is :

$$x = [0.0869 - 4.13 \cdot 10^{-6} C_o + (3.25 \cdot 10^{-3} + 1.78 \cdot 10^{-7} C_o)pH] \cdot C_o \cdot {}_t^{[-0.365+3.79\cdot10^{-5} C_o+(0.0815-7.86\cdot10^{-6} C_o)pH]}$$

The rate coefficient (k_a) of the Kuo-Lotse model increased as pH increased and decreased as initial K concentration increased. Also a significant equation relating the quantity of adsorbed K amount to the soil pH and the initial amount of potassium was derived from the first-order model:

$$\ln x_{eq} = -0.8513 + 5.798\cdot10^{-4} C_o + (0.6538 - 3.300\cdot10^{-5} C_o)pH$$

This equation could be essential in agriculture.

ΠΕΡΙΛΗΨΗ

Στην παρούσα εργασία μελετήθηκε η προσρόφηση του καλίου από ασβεστωμένα εδάφη τύπου Entisol.

Χρησιμοποιήθηκαν τέσσερα διαλύματα KCl διαφορετικής συγκέντρωσης Καλίου και πέντε διαφορετικά pH. Διερευνήθηκε η προσαρμογή δύο μοντέλων, των Kuo-Lotse και κινητικής πρώτης τάξης . Από τη σύγκριση των συντελεστών γραμμικότητας των δύο μοντέλων (r^2) προέκυψε ότι το μοντέλο Kuo-Lotse είχε καλύτερη εφαρμογή.

Από την κινητική πρώτης τάξης προέκυψε η ακόλουθη εξίσωση , η οποία εκφράζει το ποσό του προσροφημένου καλίου στην ισορροπία σε σχέση με το pH και την αρχική συγκέντρωση του καλίου στο διάλυμα, η οποία παρουσιάζει μεγάλο ενδιαφέρον από γεωργική άποψη.

$$\ln x_{eq} = -0.8513 + 5.798\cdot10^{-4} C_o + (0.6538 - 3.300\cdot10^{-5} C_o)pH$$

Από το μοντέλο Kuo-Lotse προέκυψε η κάτωθι εξίσωση προσρόφησης του καλίου από το έδαφος τύπου Entisol σε συνάρτηση με το pH και την αρχική συγκέντρωση καλίου στο διάλυμα.

$$x = [0.0869 - 4.13 \cdot 10^{-6} C_o + (3.25 \cdot 10^{-3} + 1.78 \cdot 10^{-7} C_o)pH] \cdot C_o \cdot {}_t^{[-0.365+3.79\cdot10^{-5} C_o+(0.0815-7.86\cdot10^{-6} C_o)pH]}$$

REFERENCES

1. Barshad , I. 1951. Cation exchange in soils : I. Ammonium fixation and its relation to potassium fixation and to determination of ammonium exchange capacity. *Soil Sci.* **77**:463-472.

2. Bolt , G.A., M.E. Summer, and A. Kamphort. 1963. A study of the equilibria between three categories of potassium in an illitic soil. *Soil Sci. Soc. Am. Proc.* **27**:294-299.

3. Brady , N.C. 1990. *"The nature and properties of soils"* p. 374

4. Chute , J.H. and J.P. Quirk. 1967. Diffusion of potassium from mica-like minerals. *Nature (London)* **213**:1156-1157.

5. Feigenbaum , S. , R. Edelstein, and I. Shainberg. 1981. Release rate of potassium and structural cations from micas to ion exchangers in dilute solutions. *Soil Sci. Soc. Am. J.* **45**:501-506.

6. Goulding , K.W.T., and O. Talibudeen. 1979. Potassium reserves in a sandy clay soil from the Saxmundham experiment : Kinetics and equilibrium thermodynamics. *J. Soil Sci.* **30**:291-302.

7. Grewal , J.S., and J.S. Kanwar. 1976. Potassium and Ammonium Fixation in Indian Soil (Review) , New Delhi , India: *Indian Council for Agricultural Research*

8. Jardine , P.M., and D.L Sparks. 1984. Potassium-calcium exchange in a multireactive soil system : I. Kinetics. *Soil Sci. Soc. Am. J.* **48**:39-45.

9. Kilmer , V.J., and L.T. Alexander. 1949. Methods of making mechanical analyses of soils. *Soil Sci.* **68**:15-24.

10. Kuo , S., and E.G. Lotse. 1974. Kinetics of phosphate adsorption and desorption by lake sediments. *Soil Sci. Soc. Am. Proc.* **38**:50-54.

11. Magdoff , F.R., and R.J. Bartlett. 1980. Effect of liming acid soils on potassium availability. *Soil Sci.,* **129**:12-14.

12. Malcom , R.L., and V.C. Kennedy. 1969. Rate of cation exchange on clay minerals as determined by specific-ion electrode techniques. *Soil Sci. Soc. Am. Proc.* **33**:247-253.

13. Okazaki , R., H.W. Smith, and C.D. Moodie. 1963. Hydrolysis and salt-retention errors in conventional cation exchange capacity procedures. *Soil Sci.* **96**:205-209.

14. Rausell-Colom , J.A., T.R. Sweetman , L.B. Wells , and K. Norrich. 1965. Studies in the artificial weathering of mica. *p. 40-70. In Experimental Pedology, Proc. Univ., Nottingham, England. The 11th Easter School Agric. Sci.*

15. Rich , C.I. 1962. Removal of excess salt in cation-exchange capacity determinations. *Soil Sci.* **93**:87-94.

16. Selim , H.M., R.S. Mansell, and L.W. Zelazny. 1976. Modelling reactions and transport of potassium in soils. *Soil Sci.* **122**:77-84.

17. Sivasubramaniam , S., and O. Talibudeen. 1972. Potassium-aluminium exchange in acid soils : I. Kinetics. *J. Soil Sci.* **23**:163-176.

18. Soil Survey Staff (1975). Soil Taxonomy-USDA. *Agric. Handbook No 436*

19. Sparks , D.L., and P.M. Jardine. 1981. Thermodynamics of potassium exchange in soils using a kinetics approach. *Soil Sci. Soc. Am. J.* **45**:1094-1099.

20. Sparks,D.L., L.W. Zelazny, and D.C. Martens. 1980a. Kinetics of potassium exchange in a Paledult from the Coastal Plain of Virginia. *Soil Sci. Soc. Am. J.* **44**:37-40.21. Sparks, D.L, L.W. Zelazny, and D.C. Martens. 1980b. Kinetics of potassium desorption in soil using miscible displacement. *Soil Sci. Soc. Am. J.* 44:1205-1208.

Author Index (Volume 23, 1994)

Keyword Index (Volume 23) 1994

CONTENTS

October - December 1994 Volume 23 No 4

This year visit Macedonia

Macedonia

For 4,000 years* steeped in the history of Greece

Statue of Aristotle, Stagira.

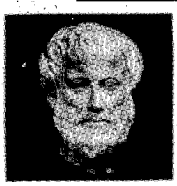

Aristotle, the tutor of Alexander the Great, was born in Stagira in Macedonia in 384 BC. Together with Plato, he is regarded as one of the greatest philosophers the world has known. Aristotle was a true academic, concerned with Physics, Astronomy, Rhetoric, Literature, Political Science and History. His teachings laid the foundation for modern scientific thought.

The White Tower of Thessaloniki.

Thessaloniki, the heart of Macedonia, is a **modern city** with 1,000,000 inhabitants. It is strategically located at the crossroads of Europe with Asia. Having spread the **Word** at Philippi, the Apostle Paul continued his teachings in Thessaloniki. Its important monuments from antiquity and byzantium up to the present, provide testimony to the role that the city has played as the second capital of Hellenism.

The Bust of Alexander the Great. Acropolis Museum. Athens.

Alexander was born in 356 BC in Pella, Macedonia, established by his father Philip II, as the centre of Hellenism. Nurtured on the thoughts of his tutor, Aristotle, he rose to fame as a brilliant military leader. He influenced the course of history, rightfully earning his title as Alexander the Great. In 335 BC he became Commander in Chief of all the Greeks. By the time of his death in 323 BC he had created an enormous empire, stretching from the shores of the Adriatic to India, and from the Caucasus Mountains to Egypt. He spread the Greek spirit far and wide among nations who worshipped him as a god.

Symbol of the Greek Macedonian Dynasty from the tomb of Philip II. Archaeological Museum. Thessaloniki.

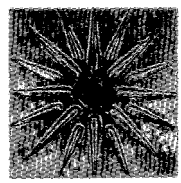

This 16 pointed star of Vergina was uncovered during the archaeological excavations at Vergina. This symbol of the Greek Macedonian Dynasty decorated the golden tomb of Philip II. The Star of Vergina, extracted from the soil of Macedonia, has since become the symbol of Hellenism.

The Olympian Aphrodite (3rd Century BC) Museum of Dion.

This statue of Aphrodite came to light during archaeological digs at the ancient sacred city of Dion. Dion, at the foot of Mt Olympus, was the most important spiritual site for the Northern Greeks, playing the same role in their lives as that of the oracle at Delphi.

St Dimitrios, detail of 7th Century Mosaic. Church of St. Dimitrios. Thessaloniki.

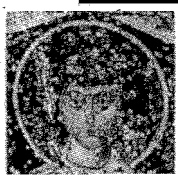

St Dimitrios, Protector of the city of Thessaloniki, was martyred in 305 AD defending Christianity. He is regarded as the Patron Saint of Thessaloniki and its saviour during difficult moments.

4.000 years: Post-Mycenaean ceramic relics found in Assiros and Mycenaean swords found in Grevena date back 4.000 years, evidence of Macedonia's role at the vortex of Greek history. Even in mythology Macedon, mythical founder of the Macedonian race, is the son of Aeolos (god of the winds). Throughout the years Macedonia contributed to the fountain of knowledge of the Ancient Greeks. In the 5th century BC Demokritos, father of Atomic Theory, lived and worked in Avdira.*

GREECE
Chosen by the Gods